PREPARATION OF DRUG-LOADED ELECTROSPUN CELLULOSE ACETATE FIBER MATS AND RELEASE-CHARACTERISTICS OF FOUR MODEL DRUGS

SANTI TUNGPRAPA

A THESIS SUBMITTED IN PARTIAL FULFILLMENT
OF THE REQUIREMENTS FOR THE DEGREE OF
DOCTOR OF PHILOSOPHY PROGRAM IN APPLIED CHEMISTRY
SCHOOL OF GRADUATE STUDIES
KING MONGKUT'S INSTITUTE OF TECHNOLOGY LADKRABANG
2008

KMITL-2008-SC-D-010-396

หัวข้อวิทยานิพนธ์	การเตรียมเส้นใยอิเล็กโตรสปันเซลลูโลสอะซิเตตที่มียาบรรจุอยู่และลักษณะการปลดปล่อยยา 4 ชนิด
นักศึกษา	นายสันติ ตั้งประภา
รหัสประจำตัว	47067502
ปริญญา	ปรัชญาดุษฎีบัณฑิต
สาขาวิชา	เคมีประยุกต์
พ.ศ.	2551
อาจารย์ที่ปรึกษาวิทยานิพนธ์	รศ.ดร. อิทธิพล แจ้งชัด
อาจารย์ที่ปรึกษาร่วมวิทยานิพนธ์	รศ.ดร. พิชญ์ ศุภผล

บทคัดย่อ

งานวิจัยนี้เป็นการศึกษาถึงผลของระบบตัวทำละลายและความเข้มข้นของสารละลายต่อรูปร่างสัณฐานวิทยาและขนาดเส้นใยอิเล็กโตรสปันของเซลลูโลสอะซิเตต สารละลายเซลลูโลสอะซิเตตถูกเตรียมโดยใช้ระบบตัวทำละลายเดี่ยว (อะซีโตน, คลอโรฟอร์ม, ไดเมทิลฟอร์มามายด์, ไดคลอโรมีเทน, เมทานอล, กรดฟอร์มิกและไพริดีน) และระบบตัวทำละลายผสม (อะซีโตน-ไดเมทิลอะเซทามายด์, คลอโรฟอร์ม-เมทานอลและไดคลอโรมีเทน-เมทานอล) พบว่าคลอโรฟอร์ม, ไดเมทิลฟอร์มามายด์, ไดคลอโรมีเทน, เมทานอล, กรดฟอร์มิกและไพริดีน (ที่ความเข้มข้น 5 เปอร์เซ็นต์โดยน้ำหนักต่อปริมาตร) สามารถละลายเซลลูโลสอะซีเตตแต่ไม่สามารถปั่นออกมาเป็นเส้นใยได้ ซึ่งในขณะที่สารละลายของเซลลูโลสอะซิเตตในอะซีโตนสามารถปั่นให้เส้นใยสั้นๆ โดยยังมีเม็ดปมอยู่ จากนั้นได้มีการปรับปรุงสารละลายโดยการผสมเมทานอลลงในคลอโรฟอร์มและไดคลอโรมีเทนที่ความเข้มข้น 5 เปอร์เซ็นต์โดยน้ำหนักต่อปริมาตร สำหรับระบบของสารละลายที่สามารถปั่นให้เส้นใยที่มีความยาวต่อเนื่องได้แก่ สารละลายที่ความเข้มข้น 16 เปอร์เซ็นต์โดยน้ำหนักต่อปริมาตรของอะซีโตน-ไดเมทิลอะเซทามายด์ ที่อัตราส่วน 1:1, 2:1 และ 3:1 โดยปริมาตรต่อปริมาตร, สารละลายที่มีความเข้มข้น 14-20 เปอร์เซ็นต์โดยน้ำหนักต่อปริมาตรของอะซีโตน-ไดเมทิลอะเซทามายด์ที่อัตราส่วน 2:1 โดยปริมาตรต่อปริมาตรและสารละลายที่มีความเข้มข้น 8-12 เปอร์เซ็นต์โดยน้ำหนักต่อปริมาตรของไดคลอโรมีเทน-เมทานอล ที่อัตราส่วน 4:1 โดยปริมาตรต่อปริมาตร

การนำเอาเส้นใยที่ได้จากกระบวนการอิเล็กโตรสปันนิ่งมาประยุกต์ใช้ในกระบวนการนำส่งและปลดปล่อยยาได้มีการศึกษากันอย่างแพร่หลายซึ่งพบว่ามีประสิทธิภาพที่ดีเมื่อเทียบกับวิธีการทั่วไป ยาในกลุ่มเอ็นแซดทั้งหมด 4 ชนิดได้แก่ นาพรอกเซน, อินโดเมทาซิน, ไอบูโปรเฟนและซูลินแดค ถูก

นำมาใช้เป็นยาต้นแบบในการศึกษา ยาเหล่านี้จะผสมอยู่ภายในเส้นใยเซลลูโลสอะซิเตตซึ่งถูกเตรียมขึ้นโดยใช้ระบบของตัวทำละลายอะซีโตน-ไดเมทิลอะเซทามายด์ที่อัตราส่วน 2:1 โดยปริมาตรต่อปริมาตร โดยลักษณะสัณฐานวิทยาและสมบัติทางความร้อนของเส้นใยที่เตรียมได้จะถูกตรวจสอบ ลักษณะการปลดปล่อยยาในเส้นใยเซลลูโลสอะซิเตตที่มียาบรรจุอยู่จะถูกทำการทดสอบ เพื่อทำการเปรียบเทียบกับการปลดปล่อยยาที่เตรียมในลักษณะเป็นฟิล์มบาง การทดสอบการปลดปล่อยยาโดยวิธีการจุ่มพบว่านาพรอกเซนที่อยู่ในเส้นใยจะถูกปลดปล่อยออกมาอย่างรวดเร็วในระยะเวลาสั้นๆ และมีปริมาณยาที่ปลดปล่อยออกมาทั้งหมดหลัง 24 ชั่วโมงประมาณ 95 เปอร์เซ็นต์ ส่วนการปลดปล่อยของยาอินโดเมทาซิน, ไอบูโปรเฟนและซูลินแดคจะมีลักษณะที่ค่อยๆปล่อยออกมาต่อเนื่อง โดยมีปริมาณยาที่ปลดปล่อยออกมาทั้งหมดประมาณ 79, 81 และ 78 เปอร์เซ็นต์ตามลำดับ ทั้งนี้จากการทดลองพบว่าการปลดปล่อยของยาจากเส้นใยจะให้ประสิทธิภาพดีกว่าการปลดปล่อยยาจากฟิล์ม อีกทั้งได้ทำการศึกษาลักษณะการปลดปล่อยยา 3 วิธี โดยใช้เส้นใยที่มียาอินโดเมทาซินเป็นต้นแบบ ได้แก่วิธี (1) แบบเติมสารละลายบัฟเฟอร์, (2) แบบไม่เติมสารละลายบัฟเฟอร์และ (3) แบบจุ่มโดยเปลี่ยนสารละลายบัฟเฟอร์ใหม่ไปเรื่อยๆ ปริมาณยาทั้งหมดที่ปลดปล่อยออกมาจากเส้นใยที่มีอินโดเมทาซินอยู่ที่ประมาณ 75, 66 และ 51 เปอร์เซ็นต์ สำหรับวิธีที่ (1), (2) และ (3) ตามลำดับ

สุดท้ายเป็นการศึกษาจลศาสตร์ในการปลดปล่อยยาเพื่อเปรียบเทียบความเร็วในการปลดปล่อยของยาแต่ละชนิด โดยค่าคงที่อัตราเร็วของยาที่อยู่ในเส้นใยจะมีค่าอยู่ระหว่าง 0.0254 และ 0.0845 (นาที)$^{-0.5}$ ส่วนค่าคงที่อัตราเร็วของยาที่อยู่ในฟิล์มจะมีค่าอยู่ระหว่าง 0.0213 และ 0.0383 (นาที)$^{-0.5}$

Thesis Title	Preparation of drug-loaded electrospun cellulose acetate fiber mats and released-characteristics of four model-drugs
Student	Mr. Santi Tungprapa
Student ID.	47067502
Degree	Doctor of Philosophy
Program	Applied Chemistry
Year	2008
Thesis Advisor	Assoc. Prof. Dr. Ittipol Jangchud
Thesis Co-advisor	Assoc. Prof. Dr. Pitt Supaphol

ABSTRACT

In this work, effects of solvent system and solution concentration on the morphological appearance and/or size of electrospun cellulose acetate (CA) products were thoroughly investigated. Cellulose acetate solutions were prepared in a range of single solvent systems (acetone, chloroform, *N, N*-dimethylformamide (DMF), dichloromethane (DCM), methanol (MeOH), formic acid, and pyridine) and in a variety of mixed-solvent systems (acetone-DMAc, chloroform-MeOH, and DCM-MeOH). Chloroform, DMF, DCM, MeOH, formic acid, and pyridine were able to dissolve CA (at 5% (w/v)), but electrospinning of these solutions produced mainly discrete beads. In contrast, electrospinning of the solution of CA in acetone produced short and beaded fibers. At the same solution concentration of 5% (w/v) electrospinning of the CA solutions was improved by addition of MeOH to either chloroform or DCM. For all the solvent systems investigated smooth fibers were obtained from 16% (w/v) CA solutions in 1:1, 2:1, and 3:1 (v/v) acetone-DMAc, 14-20 % (w/v) CA solutions in 2:1 (v/v) acetone-DMAc, and 8-12% (w/v) CA solutions in 4:1 (v/v) DCM-MeOH. Use of drug-loaded polymeric

ultrafine fibers as controlled release systems was widely studied due to their advantages over conventional methods of drug administration. Four types of non-steroidal anti-inflammatory drugs (NSAIDs), i.e., naproxen (NAP), indomethacin (IND), ibuprofen (IBU), and sulindac (SUL), were incorporated in the electrospun CA fiber mats. In this study, drug-loaded cellulose acetate fiber mats were prepared by electrospinning technique using acetone-DMAc (2:1 v/v) as the mixed solvent system. Morphological and thermal properties of the neat and the drug-loaded electrospun fiber mats were investigated. Comparative study of the drug-loaded electrospun fiber mats and drug-loaded solvent cast films was also studied. In the total immersion method, NAP-loaded as-spun CA fiber mat exhibited a burst release characteristic and the maximum release of NAP after 24 hr was around 95%. Release of IND, IBU, and SUL from the electrospun CA fiber mats was relatively smooth, with the maximum release of the drugs being about 79, 81, and 78%, respectively. At any given immersion time point, the amount of the drugs released from the drug-loaded electrospun CA fiber mats was greater than that from the corresponding as-cast films. In addition, the release characteristics of IND-drug loaded as-spun fiber mats were investigated. Three methods of release study, i.e., (1) with the addition of fresh medium, (2) without the addition of fresh medium, and (3) with sequential dipping in fresh medium, were carried out. The total amount of the drug released from the IND-loaded as-spun CA fiber mats was about 75, 66, and 51% for Method (1), (2), and (3), respectively. Lastly, study the release kinetics of model drugs from drug-loaded as-spun CA fiber mats and as-cast CA films were characterized. Apparently, the rate parameter k for all of the drug-loaded as-spun CA mats ranged between 0.0254 and 0.0845 $min^{-0.5}$, which that for all of the drug-loaded as-cast CA films ranged between 0.0213 and 0.0383 $min^{-0.5}$.

ACKNOWLEDGMENTS

Appreciation is expressed to those who have made contributions to this dissertation. First the author would like to sincerely express highly gratefulness to his advisor, Assoc. Prof. Dr. Ittipol Jangchud, and co-advisor, Assoc. Prof. Dr. Pitt Supaphol from The Petroleum and Petrochemical College, Chulalongkorn University for giving their invaluable knowledge, meaningful guidance, kind and constructive critism, consistent inspiration and encouragement throughout this research.

In addition, he would also grateful to thank to Asst. Prof. Dr. Punnama Siriphannon, Asst. Prof. Dr. Pathavut Monvisade, and Assoc. Prof. Dr. Taweechai Amornsakchai, members of the thesis committees for their invaluable comments and suggestions.

He would like to express the greatest gratitude to Asst. Prof. Dr. Chidchanok Meechaisue, lecturer at Ramkhamhaeng University, for her guidance and support. He gratefully acknowledges all faculty members and all staffs of Scientific Instrument Service Center, Faculty of Science, King Mongkut's Institute of Technology Ladkrabang for their knowledge and assistance. Moreover he would like to give his special thanks to all members in polymer science graduate students for their kind assistance, continual encouragement and wonderful friendship.

Unforgettable thanks go to Department of Chemistry, Faculty of Science, Mahanakorn University of Technology for laboratory site and utilities equipment, thanks for generous suggestions from Dr. Pravit Singtothong, Dean of the Department.

Finally, he wishes to express his deep gratitude to his family for their unconditioned love, understanding and very supportive during all these years he spent for his Ph.D. study.

TABLE OF CONTENTS

TABLE OF CONTENTS (continued)

TABLE OF CONTENTS (continued)

TABLE OF CONTENTS (continued)

TABLE OF CONTENTS (continued)

LIST OF TABLES

LIST OF FIGURES

LIST OF FIGURES (continued)

LIST OF FIGURES (continued)

LIST OF FIGURES (continued)

LIST OF FIGURES (continued)

ABBREVIATIONS

CA	Cellulose acetate
NAP	Naproxen
IND	Indomethacin
IBU	Ibuprofen
SUL	Sulindac
NSAID	Non-steroidal anti-inflammatory drug
DMF	*N, N*-dimethylformamide
DMAc	*N, N*-dimethylacetamide
DCM	Dichloromethane
DMSO	Dimethylsulfoxide
MW	Molecular weight
SEM	Scanning electron microscope
DSC	Differential scanning calorimeter
TGA	Thermogravimetric analysis
^{1}H-NMR	^{1}H-Nuclear magnetic resonance

LIST OF SYMBOLS

DC	Direct current
T_m	Melting temperature
M	Weight of sample after submersion in the testing solution
M_i	Initial weight of the sample in its dry state
M_d	Weight of the sample after submersion in the testing solution in its dry state
M_r	Weight of a model drugs that were released from the sample
M_t	Accumulation amount of drugs released at an arbitrary time t
M_∞	Accumulation amount of drugs released at an infinite time
n	Characteristic exponent
k	Rate parameter
r^2	Correlation coefficient

Chapter 1

Introduction

1.1 Rationale

In the second half of the 20th century, the use of polymers in our daily life has grown tremendously. Polymers are used in different forms and for a wide range of applications. Noticeable among these are the synthetic and regenerated polymers that have found applications not only in the textile and apparel sector but also in numerous industrial usages like tire cords, reinforcing and structural agents, barrier films, food and packaging industry, automotive parts, etc. The process of making fibers from polymers generally involves spinning, wherein the polymer is extruded through a spinneret to form fibers under suitable shear rates and temperatures. This conventional fiber formation process is generally followed by drawing that involves the plastic stretching of the as-spun material to increase its strength and modulus. Depending on whether the polymer is in the molten state or in solution, the process is likewise termed as melt-spinning or solution spinning respectively. Typical average diameters obtained by these conventional spinning methods are about 10 μm and higher [1].

Over the last ten years, a novel technique has been re-explored to generate polymeric fibers in the submicron range. This technique, termed as electrospinning, produces filaments that are in a diameter range one or two orders of magnitude smaller than those obtained from the conventional melt-spinning and solution-spinning processes. Electrospinning is, therefore, a unique process because it can generate submicron polymeric fibers. Typically, electrospun fibers have a diameter as low as 50 - 100 nm.

To understand the fundamental principle underlying the process of electrospinning, consider a spherically charged droplet of a low molecular weight conducting liquid that is held in vacuum. As shown in Figure 1.1a), the droplet is under the influence of two forces, i.e., 1) the disintegrative electrostatic repulsive force

and 2) the surface tension that strives to hold the droplet within a spherical shape. At equilibrium, the two forces completely balance each other, as is depicted by:

$$\frac{1}{8\pi\varepsilon_0}\frac{Q^2}{R^2}=8\pi\sigma_s R$$

where Q is the electrostatic charge on the surface of the droplet, R is the radius of the droplet, ε_o is the dielectric permeability of vacuum and σ_s is the surface tension coefficient.

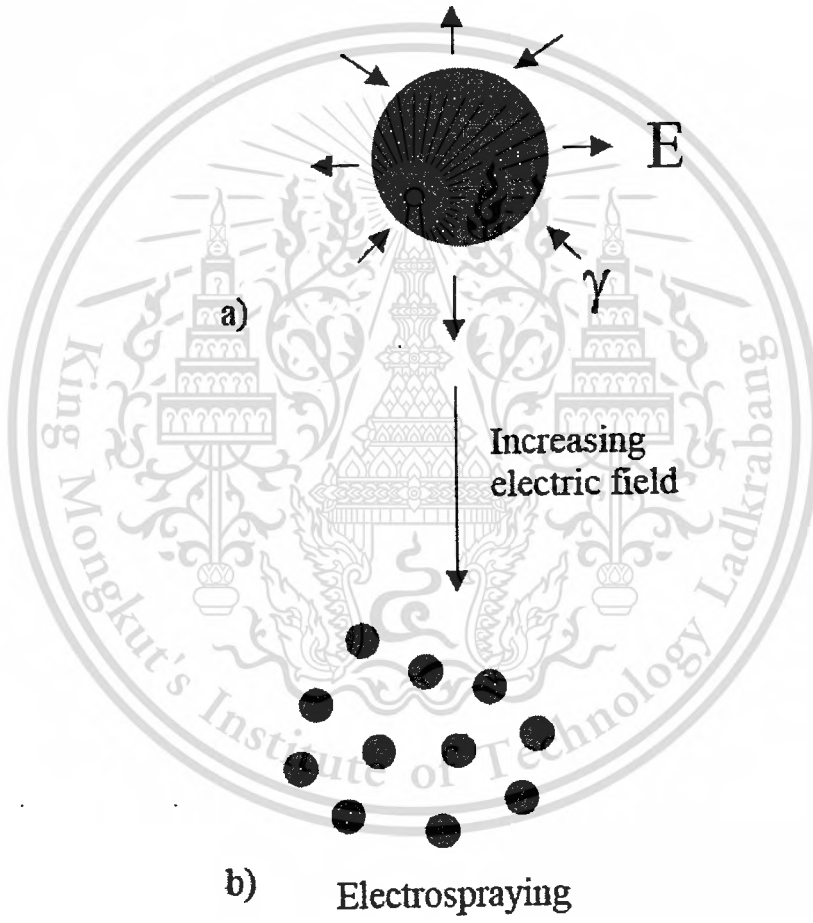

Figure 1.1 Phenomena of Electrospraying: when the electrostatic repulsive forces overcome the surface tension of the liquid, the droplet (1.1a) disintegrates into smaller droplets (1.1b)

With increasing electric field strength, the charge on the surface of the droplet increases until it reaches a critical point when the electrostatic repulsive force

overcomes the surface tension. When this happens then the droplet disintegrates and leads to the formation of smaller droplets (Fig. 1.1b). This process is termed as electrospraying and has been utilized extensively for automotive spray painting.

If this concept is extended to a solution of high molecular weight polymer solution that has sufficient chain entanglements, then instead of the formation of the droplets, a steady jet is formed that later solidifies in a polymer filament. Thus, the fundamental principle underlying the fiber formation by electrospinning can be stated as follows: a high electric potential is applied to a polymer solution (or melt) suspended from the end of the spinneret that imparts an electrostatic charge to the polymer solution. At low electric potentials, the disintegrative electrostatic repulsive forces that primarily reside on the liquid surface are balanced by the surface tension. At high electric potentials, the electrostatic repulsive force at the surface of the fluid overcomes the surface tension that results in the ejection of a charged jet. The jet extends in a straight line for a certain distance, and then bends and follows a looping and spiraling path [2]. The electrostatic repulsion forces can elongate the jet to several thousand times leading to the formation of very thin jet. When the solvent evaporates, solidified polymer filaments are collected on a grounded target (or a winder) in the form of a non-woven fabric. The small diameter provides a large surface to volume ratio that makes these electrospun fabrics interesting candidates for a number of applications including membranes [3], tissue scaffolding and other biomedical applications [4-7], reinforcement in composites [8], and nano-electronics [9].

During the last two decades, significant advances have been made in the development of biocompatible and biodegradable materials for biomedical applications, and in the case of the latter category, industrial applications, as well. In the biomedical field, the goal is to develop and characterize artificial materials or, in other words, "spare parts" for use in the human body to measure, restore, and improve physiologic function, and enhance survival and quality of life. Typically, inorganic (metals, ceramics, and glasses) and polymeric (synthetic and natural) materials have

been used for such items as artificial heart-valves, (polymeric or carbon-based), synthetic blood-vessels, artificial hips (metallic or ceramic), medical adhesives, sutures, dental composites, and polymers for controlled slow drug delivery. The development of new biocompatible materials includes considerations that go beyond nontoxicity to bioactivity as it relates to interacting with and, in time, being integrated into the biological environment as well as other tailored properties depending on the specific "*in vivo*" application.

One area of intense research activity has been the use of biocompatible polymers for controlled drug delivery. It has evolved from the need for prolonged and better control of drug administration. The goal of the controlled release devices is to maintain the drug in the desired therapeutic range with just a single dose. Localized delivery of the drug to a particular body compartment lowers the systemic drug level, reduces the need for follow-up care, preserves medications that are rapidly destroyed by the body, and increases patient comfort and/or improves compliance. In general, release rates are determined by the design of the system and are nearly independent of environmental conditions.

Providing control over the drug delivery can be the most important factor at times when traditional oral or injectable drug formulations cannot be used. These include situations requiring the slow release of water-soluble drugs, the fast release of low-solubility drugs, drug delivery to specific sites, drug delivery using nanoparticulate systems, delivery of two or more agents with the same formulation, and systems based on carriers that can dissolve or degrade and be readily eliminated. The ideal drug delivery system should be inert, biocompatible, mechanically strong, comfortable for the patient, capable of achieving high drug loading, safe from accidental release, simple to administer and remove, and easy to fabricate and sterilize. Research activity on the electrospinning of nanofibers has been successful in spinning submicron range fibers from different polymeric solutions and melts. Electrospun fiber mats due to their high functional characteristics find application as drug carriers

for the drug delivery system. Controlled delivery of drugs at a defined rate over a definite period of treatment is possible with biocompatible delivery matrices of either biodegradable polymer.

This work can be divided into two main experimental parts. The first part was the electrospinning of celiulose acetate. In this part, the effect of solvent and polymer concentration on morphological appearance of as-spun fibers was thoroughly investigated, using scanning electron microscopy (SEM). The spinning solutions were prepared in either a single solvent or in mixed-solvent systems. Mixtures of solvents can generate a series of solvent systems with wide-ranging solution properties for identifying suitable ones for efficient electrospinning. The second part was to study controlled release characteristic, the obtained fibers of selected solvent system, using four types of non-steroidal anti-inflammatory drugs (NSAIDs), i.e., naproxen, indomethacin, ibuprofen, and sulindac as the model drugs.

In the following sections, a review of the literature was provided that discussed the early attempts at electrospinning, the process of fiber formation, was proposed to describe the electrospinning process and the applications of these electrospun submicron fibers.

1.2 Objectives

The objectives of this research work were:

1. To prepare electrospun cellulose acetate fibers from single solvent and mixed solvent systems

2. To investigate the effects of solvent system and solution concentration on morphological appearance of electrospun cellulose acetate fiber mats

3. To investigate the potential use of the as-spun cellulose acetate fiber mats as controlled release vehicles

1.3 Scopes of Study

1. Literature reviews of the theory and publication involved in this research.

2. To study factors affecting the electrospinning process of electrospun cellulose acetate products such as concentration of polymer solution, the effects of solvent system and changing the composition of the mixed solvent system.

3. To compare the release characteristics of four types of NSAIDs from the drug-loaded electrospun cellulose acetate fiber mats and drug-loaded as-cast films.

4. To compare the release characteristic of the drug from the drug-loaded electrospun CA fiber mats by 3 methods of the release assay, i.e., with and without the addition of fresh medium and with sequential dipping in fresh medium.

5. To study the release kinetics of model drugs from drug-loaded as-spun CA fiber mats and as-cast CA films.

1.4 Expected Results

1. Appropriate conditions in preparing cellulose acetate ultrafine fibers with electrospinning technique can be obtained.

2. Electrospun cellulose acetate fiber mats can be used for medical applications.

3. Knowledge gained in the work can be applied with other electrospun fibers.

Chapter 2

Theories and Literature Reviews

2.1 Literature Reviews

The electrical forces on free charges residing on the surface of a polymeric liquid are primarily responsible for driving the electrospinning process. In conventional spinning processes like melt or solution spinning, the fiber is subjected to tensile, rheological, gravitational, inertial and aerodynamic forces. The action of these forces has been described in detail by Ziabicki [10]. In electrospinning, the tensile force is provided by the repulsion of like charges on the surface of the polymer jet. The principle of electrospinning finds similarities to electrostatic spraying. In fact, the electrostatic spray literature provides many insights into the electrospinning process and will be discussed in the next section.

2.1.1 Historical Background

The behavior of electrically driven jets and the stability of electrically charged liquid drops have been of interest for many years. In 1745, Bose [11] created an aerosol spray by applying a high potential to a liquid at the end of a glass capillary tube. Lord Raleigh [12] also studied the instabilities that occur in electrically charged liquid droplets. He calculated the maximum amount of charge that a drop of liquid can maintain before the electrical forces overcome the surface tension of the drop and led to the creation of a jet. Zeleny [13] studied the role of the surface instability in electrical discharges from charged droplets. His findings showed that the theoretical relations for instability were satisfied when the discharge of the jet began. Vonnegut and Neubauer [14] generated uniform streams of highly charged droplets with diameters around 0.1 mm. Their experiments proved that monodisperse aerosols with a particle radius of a micron or less could be produced from the pendant droplet at the end of a pipette. In the 1960s, Taylor [15] analyzed the conditions at the point of a

droplet that was deformed by an electric field in a conical geometry. He identified the critical electrical potential for an electrostatic formation of a cone of liquid (now known as a Taylor cone) at the end of a capillary tube. The conducting drop was supposed to be surrounded by air and suspended in a stable position from the capillary tube. By examining a range of low molecular weight fluids, Taylor concluded that the conical interface between air and the fluid was stable at the semi-angle conical angle of 49.3°. However, it was shown that conductivity and viscosity both play an important role in the electrostatic atomization process which then influence the equilibrium angle and other aspects of the process [16]. Taylor cones are considered to be important to electrospinning as they define the onset of extensional velocity gradients in the fiber formation process.

2.1.2 Reviews of Early Attempts on Electrospinning

There is a precedent for the application of electrostatic atomization or spraying to polymeric solutions in the patent and academic literature. The electrospinning of fibers dates back to 1938 when Formhals [17] invented the electrostatic apparatus. As shown in Figure 2.1, the spinning solution was discharged using a high electric field from an electrode of negative polarity. The fine filaments were attracted towards the movable electrode that was at a positive polarity. A stripping device facilitated the removal of fibers in the form of a fibrous sliver. A major drawback of such a setup was the difficulty to remove the fine fibers that adhered to the moving parts of the collecting belts, drums, wheels etc. Formhals formed fibers from a solution of cellulose acetate in ethylene glycol at a potential difference of 57 kV.

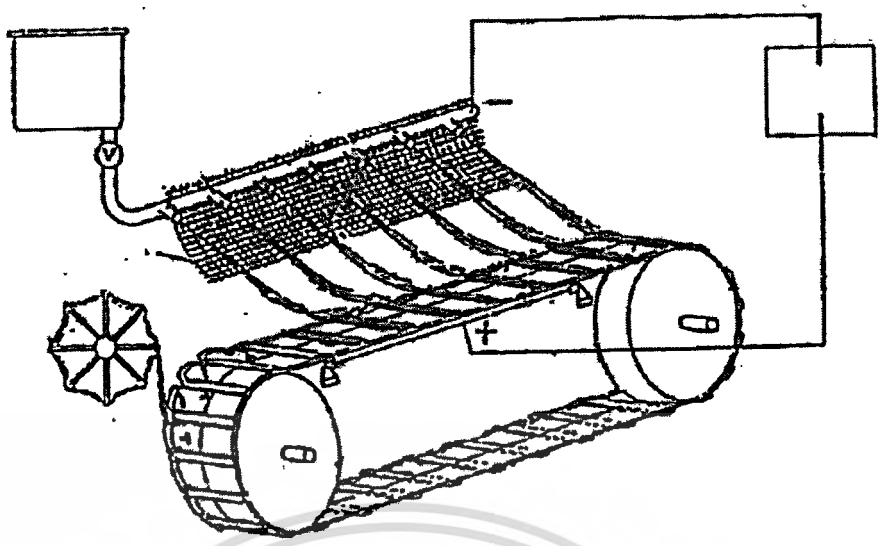

Figure 2.1 Schematic of Formhals's electrospinnig setup to produce cellulose acetate fiber [17]

In 1966, Simons [18] invented a process to produce a patterned non-woven fabric by electrospinning that was collected on a segmented receiver. The segmented receiver had two sets of segments such that one of the sets was at a different potential than the other causing the preferential deposition of fibers leading to a patterned fabric that had regions of low and high fiber density. Filaments were electrospun from a solution of polyurethane in methyl ethyl ketone having a viscosity in the range of 100 to 3000 centipoises. In a different process, Isakoff [19] devised a process to prepare fibrous sheets of organic synthetic polymers in which a filamentary web of fibers were electrostatically charged before being collected on a grounded movable surface. Fibers were electrically charged after they were formed by conventional solution spinning to facilitate their passage in a controlled trajectory.

Utilizing a different geometry of the electrospinning apparatus, Fine et. al. [20] electrospun a thermoplastic elastomer where a cup-like apparatus contained the charged polymer solution that rotated about its vertical axis. The centrifugal forces pushed the polymer solution to the edge of the cup and into the ambient air. The

presence of an electrical field caused the formation of a jet that was attracted to a grounded movable aluminum screen that was driven slowly around the rollers in the form of a belt. The combined action of electrostatic and centrifugal forces led to the formation of high strength fibrous sheets.

Instead of placing the polymer solution in a cup, Guignard [21, 22] utilized another movable belt that carried the charged molten polymer. Here, two movable belts were used, as shown in Figure 2.2. As one of the belts, which carried the charged molten polymer, approached the grounded belt, formation of several jets from the surface of the exposed melt took place. These jets traveled towards the grounded collector belt and got deposited in the form of short filaments on the grounded belt.

In a different study, Martin et al. [23, 24] extended the concepts of single component electrospinning to electrospin a mat of organic fibers from a liquid containing a 'plurality of components' from a single nozzle/syringe. They were also able to electrospin polymeric solutions having different compositions (blends) simultaneously from multiple nozzles/syringes. Collectors were either a stationary metal screen or a movable belt. The patent claimed the mat to be composed of fibers of a high molecular weight thermoplastic polymer based either on a fluorinated hydrocarbon, a silicone or an urea/formaldehyde. The resulting mats were flexible, non-absorbent, porous, and hydrophobic. These were suggested to be used as a wound dressing and as a lining for a prosthetic device.

In 1982, Bornat [25] conducted simultaneous electrospinning by using several nozzles /syringes to form fibers. As shown in Figure 2.3, the syringes were filled with the polymer solution and placed a certain distance from the collector that was in the form of a long metallic cylinder. The syringes were kept at a ground potential whereas an electrical potential of - 50 kV was applied to the collector. The electrostatic forces caused the formation of jets that were attracted towards the rotating collector. Solidified polymer filaments of poly(tetrafluoroethylene) and poly(ethylene oxide) (electrospun simultaneously) were wound on the rotating collector in this fashion to

form a tubular product. The tubular products were suggested to find applications as synthetic blood vessels and urinary ducts.

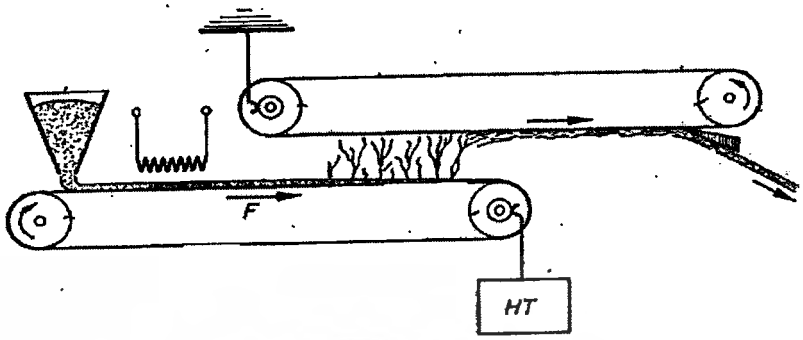

Figure 2.2 Schematic of Guignard's electrospinning setup [21, 22]

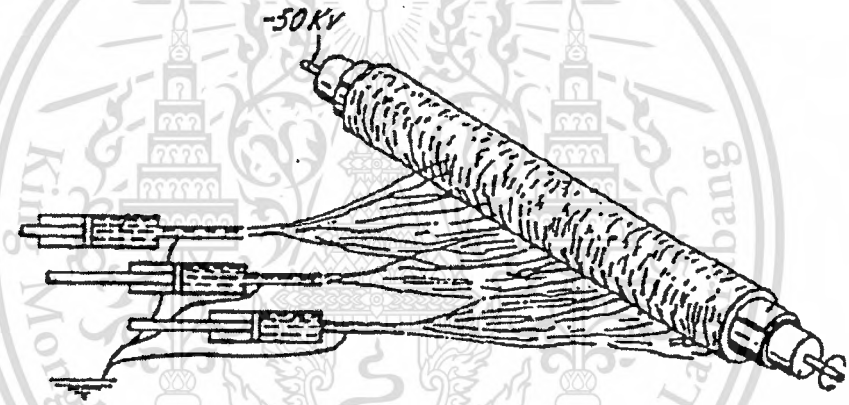

Figure 2.3 Schematic of Bornat's electrospinning setup [25]

Utilizing a slightly different approach, Simm et al. [26] were able to fabricate a composite filter based on electrospun fibers. They invented a process for the production of fiber filters in which a solution of polystyrene in methylene chloride was electrospun from an annular electrode onto two equidistant collector electrodes in the form of movable belts. The collector electrodes were already covered with a layer of cellulose fibers produced by conventional spinning methods. Thus, a composite filter that had electrospun polystyrene fibers on top of a layer of cellulose fleece was fabricated.

In 2000, Scardino et al. [27] patented a process to make a hybrid/composite yarn. The electrospun fibers having diameters ranging from 0.4 nm to 1 nm were suctioned into an air vortex and then combined with carrier filaments (obtained from conventional spinning techniques) to form nonwoven or linear (yarns) assemblies. The yarns were later utilized for weaving, braiding or knitting fabrics. Utilizing the similar approach to make composite fibrous mats, Zarkoob et al. [28] patented a process to produce silk nanofibers and silk nanofiber composites utilizing electrospinning. The electrospinning principles utilized were very similar to those mentioned above with some differences in the engineering details of the apparatus.

In a detailed study, Baumgarten [29] studied the relationships between fiber diameter, jet length, solution viscosity, flow rate of the solution and the composition of the surrounding gas. He investigated the electrospinning of acrylic nanofibers where fibers less than a micron in diameter were reported. In 1981, Lorrondo and Manley [30-32] not only studied the effect of some of the parameters on fiber formation but also conducted some characterization studies on fibers of poly(ethylene) and poly(propylene) that were electrospun from the melt. The electrospun fibers were characterized by x-ray diffraction and mechanical testing. When the applied electric field was increased, the diffraction rings became arcs, thereby indicating the increasing alignment of the crystalline phase along the fiber axis. The fiber diameter was observed to decrease with increasing melt temperature and a qualitative correlation between the fiber diameter and viscosity was established.

After a brief gap of a decade and a half, Reneker and his coworkers revived interest in electrospinning. In 1995, Doshi and Reneker [33] studied the effect of several process parameters on fiber formation of poly(ethylene oxide) (PEO) fibers. Ever since then, many polymers have been electrospun and various aspects that better characterize the electrospinning process have been studied in great details. In the following sections, several of these aspects would be described.

2.1.3 Electrospinning Process Considerations

2.1.3.1 Schematic of the Electrospinning Process

Most of the studies conducted to date have electrospun polymer solutions or melts in air (ambient conditions), although a study where electrospinning was conducted in vacuum has also been reported [34]. As shown in Figure 2.4, a typical experimental setup of the electrospinning process consists of a syringe-like apparatus that contains the polymer solution. The narrow end of the syringe is connected to a capillary, e.g. glass or Teflon. A platinum electrode dipped in the polymer solution is connected to a high voltage DC supply and collector wrapped with Al foil.

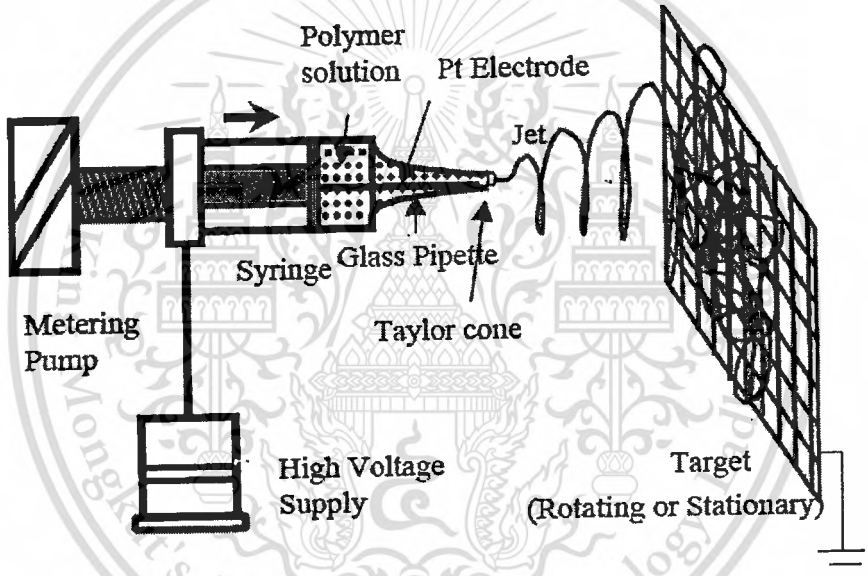

Figure 2.4 Schematic of a typical electrospinning setup

When the high voltage DC supply is turned on, the electrode imparts an electrical charge to the polymer solution. As mentioned previously, a jet is ejected from the suspended liquid meniscus at the capillary-end when the applied electric field strength overcomes the surface tension of the liquid [15]. Near the critical point, where the electric field strength is about to overcome the surface tension of the fluid, the free surface of the suspended drop changes to a Taylor cone, as described earlier. The jet is ejected from the tip of this Taylor cone as the electric field strength is increased. There are six major forces acting on an infinitesimal segment of the

charged jet. They are 1) body or gravitational forces, 2) electrostatic forces which carry the charged jet from the nozzle to the target, 3) Coulombic repulsion forces which try to push apart adjacent charged species present within the jet segment and are responsible for the stretching of the charged jet during its flight to the target, 4) viscoelastic forces which try to prevent the charged jet from being stretched, 5) surface tension which also acts against the stretching of the surface of the charged jet and 6) drag forced from the friction between the charged jet and the surrounding air. Due to the combination of these forces, the electrically charged jet travels in a straight trajectory for only a short distance before undergoing a bending instability, which results in the formation of a looping trajectory. During its flight to the collector, the charged jet thins down and, at the same time, dries out or solidifies to leave ultrafine fibers on the collective screen.

When this idea is extended to polymer solutions or melts, solidified polymer filaments are obtained on the grounded target as the jet dries. Typical operating conditions are: internal diameter of the capillary-end is usually 0.7-1 mm, flow rates of 3-10 ml/h are commonly employed at a potential drop of 5-20 kV and distances of 10-30 cm between the capillary-end and target. The target or the collector screen can be at a ground potential or be kept at a polarity opposite to that of the polymer solution. Different types, shapes and sizes of target have been utilized. Also, the target could be kept stationary or be movable. It can also be rotated about its axis to produce a mat that has a preferential alignment of fibers along a specific direction. However, the degree of molecular orientation in a fiber spun from a solution of a polymer (in particular an amorphous system) is not generally high. This is due to the high molecular mobility [10] in fibers containing solvents (chain relaxation is often faster than the time it takes for the solvent to evaporate completely from the fiber before the onset of Tg restricts any further orientation loss).

2.1.3.2 Process of Fiber Formation

The electrospinning process has three stages [2]: a) initiation of the jet and the extension of the jet along a straight line; b) the growth of a bending instability and further elongation or drawing of the jet that allows it to move in a looping and spiraling path; c) solidification of the jet into nanofibers. In the next three sections, these three stages will be described following which various mathematical models that have offered to quantify the jet behavior will be briefly outlined.

2.1.3.2.1 Initiation of the jet

In a typical electrospinning apparatus, the polymer solution is contained in a syringe or a glass capillary. One of the electrodes is dipped in the polymer solution whereas the other acts as the collector target that is kept at a certain distance from the syringe (hence, not immersed in the solution). When an electric field is applied to a polymer solution, ions in the solution aggregate around the electrode of opposite polarity. This results in the build-up of an excess of ions of oppositely charged polarity near the electrode [1]. For instance, if a positive electrode is dipped in the polymer solution, then the negative ions migrate towards the anode but the positive ions aggregate at the tip of the capillary leading to a charge build-up. Thus, the region of interest is the solution near the tip of the capillary where these excess charges aggregate at the surface of the suspended liquid/solution drop. The shape of the meniscus of the suspended polymer droplet is defined by the balance of hydrostatic pressure, electrical forces and, surface tension [35]. In weak fields, the polymer solution is held at the end of the capillary by surface tension. When the electric field increases, the meniscus elongates to form a conical configuration (Taylor Cone), until at some critical values of the electric field, surface tension can no longer balance the hydrostatic and electric forces and a thin jet is ejected from the surface of this meniscus. This ejected jet travels toward the nearest electrode of opposite polarity, or electrical ground. It is believed that excess charge is essentially static with respect to

the moving coordinate system of the jet [36]. This means that the electrospinning jet can be essentially thought of as a string of charged elements connected by a viscoelastic medium, with one end fixed at a point of origin and the other end free.

Doshi and Reneker [33] were able to measure the jet diameter as a function of distance from the apex of the cone by laser light diffraction. For a 4 wt % PEO solution in water electrospun at a electric field strength of 0.4 kV/cm, the jet diameter was observed to decrease with increasing distance. The jet diameter decreased by a factor of 5 (from 90 μm to about 18 μm) at a distance of 10 mm from the tip of the cone. Taking the solvent (water) evaporation into account, this indicated a large amount of stretching of polymer chains in the jet. With the aid of high-speed photography, Fong and Reneker [2] measured jet diameters in the range of 20-100 μm for a 3 wt% PEO solution in water electrospun at electric field strength of 0.5 kV/cm. The polymer solution was electrospun through a hole of 300 μm in the bottom of a metal spoon. It was found that when the semi-vertex conical angle was 22.5°, the electric force was high enough to overcome both the surface tension and viscoelastic forces and as a result, a jet was ejected. After the initiation of the jet, the conical protrusion relaxed to a steady rounded shape in a few milliseconds. At times, the shape of the conical protrusion and jet current pulsated even though the applied field strength was constant. A steady current was associated with the cone that had a constant shape.

2.1.3.2.2 Growth of the Bending Instability and Further Elongation of the Jet

In a detailed study [36], Reneker and coworkers observed the path of the jet. After initiation, the jet traveled in a straight line for some distance (typically 2-3 cm). It was hypothesized that an electrically driven instability triggered by the perturbations of the lateral position and lateral velocity of the jet caused it to follow a bending, winding, spiraling and looping path in three dimensions. As shown in Figure 2.5, high-speed photographs taken at 2000 frames per second demonstrated that the jet in

each loop became longer and thinner as the loop diameter and circumference increased. After some time, the segments of the thinner smoothly curved loop developed a new instability similar to, but at a comparatively smaller scale, than the first. The new bending instabilities continued to grow in a similar fashion that caused the jet to spiral around the path of the first loop. The process of promoting the bending instability repeated in a self-similar manner as the polymer jet dried into a solidified filament. These were collected on the target that was kept at an attractive potential.

Rutledge et al. [37] also confirmed these observations by utilizing similar high-speed photography experiments. The bending instability of the rapidly moving jet was referred to as the 'whipping jet', where each self-similar repetition of bending instability, as described by Reneker and coworkers has been termed as a 'whipping' process. The spatial dimensions of the whipping periodicity was found to be significantly greater than the radius of the jet, so that when the jet is observed with a naked eye (30-40 frames/second) the jet appears to be splaying into multiple filaments, a hypothesis that was widely accepted before high-speed photography was utilized to fully characterize the behavior of the electrospun jet.

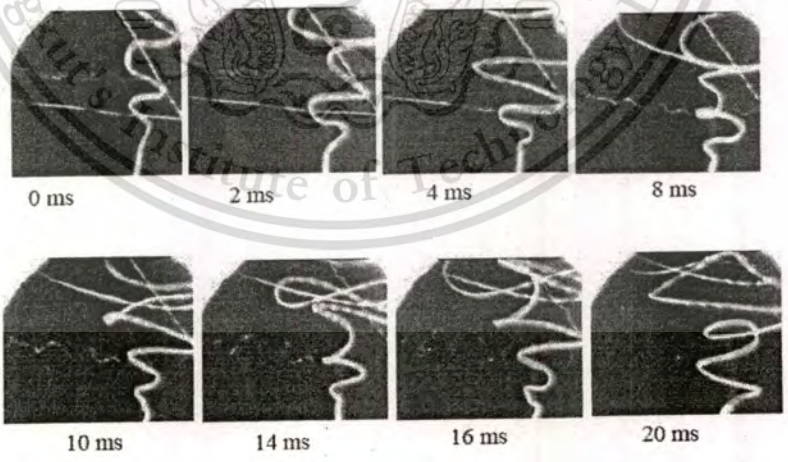

Figure 2.5 High speed photographic results on electrospun 6 wt % PEO (400,000 MW) in 60 % Water: 40 % Ethanol and 1 kV/cm. The jet initiation is at the bottom right of every frame [36]

Recently, it was shown that the electrically driven bending instability in the electrospinning of polycaprolactone resulted in the contact and merging of segments in different loops of the jet when it was in flight [38]. These contacts limited the lateral expansion of the jet path and led to the formation of a long, slender, slow moving and irregular network of electrically charged nanofibers having a fuzzy appearance. This 'garland' of nanofibers followed a 'curly' path until it was intercepted and collected at the target.

2.1.3.2.3 Solidification of the Jet into a Polymer Filament

As the rapidly 'whipping' jet moved towards the target maintained at an attractive potential, it continued to expand into a spiraling and looping path. This process continued until the jet became fairly thin and was intercepted by the target. As can be premised, the greater the distance the jet travels, the thinner it becomes. Thus, the distance between the capillary-end and the target is one process parameter that has direct implications on the fiber diameter. In fact, other process parameters include the flow rate, concentration, and electric field strength, to name a few. The effects of these and other system parameters will be discussed in greater detail in next section.

2.1.3.3 Effects of System and Process Parameters on Electrospun Fiber Diameter

The following system and process parameters have been noted to affect the fiber diameter [33, 39-44]:

System Parameters:

- Viscosity
- Concentration
- Net charge density (conductivity)
- Surface tension of the polymer fluid
- Molecular weight
- Molecular weight distribution

- Topology (branched, linear etc.) of the polymer

Process Parameters:

- Electric potential
- Flow rate of the polymer solution
- Distance between the capillary-end and target/collection screen
- Ambient parameters (temperature, humidity and air velocity in the chamber)
- Motion of target screen
- Internal diameter of the nozzle/capillary

As discussed earlier, an electrically driven jet of low molecular weight liquid would form droplets, a phenomenon more commonly referred as electrospraying. The formation of such droplets was reported to be due to the capillary breakup of the jet by surface tension [64]. In the case of polymer solutions, the pattern of capillary breakup is quite different. Instead of a complete breakup of the jet in response to the capillary instability, the jet between the droplets forms a nanofiber and the contraction of the radius of the jet, which is driven by surface tension, causes the remaining solution to form a bead. Fong et al. [39] observed the formation of beaded nanofibers that were electrospun from aqueous PEO (900,000 g/mol) solution at concentrations of 1-3 wt%, 21.5 cm and 15 kV. The corresponding zero shear rate viscosities of these solutions ranged from 13-527 centipoise respectively. As the concentration (and consequently the viscosity) was increased, the beads were observed to be larger, the average distances between beads were longer, the fiber diameter was larger and the shape of the beads changed from spherical to spindle-like. At concentrations higher than 4 wt % (1250 centipoise), uniform electrospun fibers were observed. In a similar study, Jaeger et al. [45] observed the surface of beads on PEO nanofibers by atomic force microscopy. The beads were reported to possess a highly ordered surface at the molecular level. Similar results, where systematic increases in concentration (and consequently viscosity) lead to the formation of uniform fibers, have been observed by other researchers as well [33, 46]. Recently, McKee et al. [47], investigated the effect

of solution rheological behavior on fiber morphology of linear and branched copolymers of poly(ethylene terephthalate-co-ethylene isopthalate) (PET-co-PEI) that were electrospun from a good solvent. In that study, investigation of the dependence of electrospun fiber diameter on concentration in addition to correlations between viscosity and concentration in different concentration regimes [48-50], i.e., dilute, semidilute unentangled and semidilute entangled, were investigated. A systematic approach to investigate electrospun fiber formation in different concentration regimes (dilute, semidilute unentangled and semidilute entangled) is very relevant to understand the process of fiber formation from a solution rheological standpoint and the effect it has on electrospinning. While some of these issues were addressed in the study by McKee [47], the author's recent work investigates and further tests the effects of scaling relationships between viscosity and concentration in different concentration regimes on fiber formation and morphological features of electrospun systems. The effects of concentration, viscosity and molecular weight on electrospun fiber formation were described in details.

To study the effect of surface tension on the formation of electrospun fibers, Fong et al. [39] added a co-solvent (ethanol) to the aqueous PEO solution to change the surface tension of the polymer solution. The surface tension was observed to decrease with the addition of ethanol. PEO solutions of 3 wt% were prepared in varying weight ratios of ethanol/water (from 0 to 0.702, by weight). The surface tension of a 3 wt% aqueous PEO solution was 76 mN/m and that of a 3 wt% PEO solution in ethanol/water: 0.702 was 51 mN/m. When these solutions were electrospun at 0.5 kV/cm, beaded fibers were observed at higher values of surface tension (>59 mN/m), whereas uniform fibers were observed to form at lower values of surface tension (<59 mN/m). It has now been established, that increasing the concentration (and consequently viscosity) and lowering the surface tension favors the formation of uniform fibers [40, 51, 52].

The effect of net charge density was also studied [39]. By adding a salt to the polymer solution, the conductivity of the solution was observed to increase. As a result the net charge density of the polymer solution increased. With increasing concentrations of NaCl in aqueous 3 wt % PEO solution electrospun at 21.5 cm and 15 kV, uniform fibers were observed to form at a net charge density of 3 Coulomb/liter of higher. The formation of beaded fibers was also studied by neutralizing the charges on the jet with ions of opposite polarity generated by a corona discharge. These ions were carried to the jet by flowing air. It was found that increasing the number of neutralizing ions that intercepted the electrospun jet, more beaded fibers were formed. The electrical forces on the jet were reduced by a neutralizing charge, so that the jet behavior gradually became that of an uncharged jet, and as a result beads were observed to form. The effects of neutralizing ions were consistent with the results produced by the addition of a salt to the aqueous PEO solution. Both show that the net charge density carried by the moving jet tends to resist the formation of beads. Thus, the higher the net charge density carried by the jet, the more likely that a smooth fiber can be formed.

Hsieh et al. [52] studied the effect of the nature of the collecting target on the fiber morphology and fiber packing. Fibers collected on paper were found to have smooth surfaces and more uniform sizes than those collected on a water surface. However, the fibers collected on the water surface were found to be densely packed. Electrically conductive targets, such as Al foil and water, favor a tightly packed and thick membrane structure, whereas, a loosely packed fibrous network structure was observed to form on a nonconductive target, like paper. The overall pore volume was higher in electrospun mats collected on paper than those collected on water. Also, the pores in the mats collected on Al foil and paper were better interconnected in the planar directions than those collected on the water surface. By utilizing a novel approach, Kameoka and coworkers [53-55] devised a method to achieve a controlled deposition of oriented polymeric nanofibers. This method used a metallic micron tip

that was dipped in the polymer solution to gather a droplet as a source material. Subsequent application of the voltage to this tip led to the formation of jet that was deposited on a rotating counter electrode. This resulted in the collection of oriented nanofibers that were suggested to be integrated with microfabricated structures.

Zong et al. [56] studied the effect of feed rate on fiber diameter, where the polymer solution was contained in a syringe such that the plunger was pushed by a metering pump. Observations of fibers electrospun from 25 wt% poly(D,L-lactic acid) (PDLA) solution in DMF at 0.8 kV/cm indicated that the fiber diameter increased with increasing flow rate as might be expected. Potassium dihydrogen phosphate (KH_2PO_4) at a concentration of 1 wt % was added to the solution to increase the conductivity. With increasing electric potential, the jet velocity was observed to increase significantly and the solution was removed from the capillary-end more quickly. As a result the volume of the Taylor cone at the capillary end was observed to become smaller. At higher voltages (< 25 kV), the Taylor cone disappeared completely and the jet was found to initiate directly from a region inside the capillary. In the case where polymer solution was kept in a glass capillary (or in other words, the polymer solution was not forced through the capillary-end by a plunger) Larrondo and Manley [30] determined that doubling the applied electric field decreased the fiber diameter by roughly 50%. However, Baumgarten [29] showed that the diameter of the jet reached a minimum after an initial increase in field strength and then became much larger with increasing electric fields. This was caused by the feed rate of the polymer solution through the capillary, and illustrated one of the complexities of the electrospinning process, i.e., increasing the electric field not only increased the electrostatic stress, thereby creating smaller fibers, but it also drew more material out of the capillary. Utilizing a similar glass capillary apparatus instead of the syringe, Doshi [33] conducted some investigations where he plotted the jet diameter at different positions along the jet to verify both of these relationships. It was shown that increasing the electric field resulted in an increased spinning rate. At the capillary orifice, there was

a threefold increase in the jet diameter with less than a twofold increase in applied voltage. Demir et al. [40] found a power-law dependence between the flow rate and electric voltage based on their measurements conducted on polyurethaneurea fibers that were electrospun from a solution of 21 wt % in dimethylformamide (DMF).

The effect of another key process parameter, namely the distance between the capillary-end and the target has also been studied extensively by several workers [29, 30, 33, 51, 70]. At low separation distances between the capillary-end and the target, wet fibers were collected, primarily due to the presence of significant amounts of residual solvent in the fibers. As the separation distance is increased, the time for the solvent to evaporate increased, and as a result, dry solid fibers were collected at the target. Also, with increasing distance between the capillary-end and the target, the jet underwent a larger amount of electrically driven bending or 'whipping' instability. Consequently, the amount of stretching or elongation of the jet increased and as a result the fiber diameter was observed to decrease.

At a given capillary-end to target distance, polymer filaments electrospun from solutions in high vapor pressure solvents tend to dry faster than those electrospun from low vapor pressure solvents because of an increased evaporation rate. The evaporation rate of the solvent introduces distinct morphological features on the electrospun fibers. Lastly, another parameter that affects the fiber diameter is the temperature of the polymeric fluid. This is especially critical for electrospinning from polymer melts [57]. Larrondo and Manley [30-32] observed that the fiber diameter deceased with increasing melt temperature. Given the inverse relationship between melt temperature and viscosity, they were able to draw a qualitative correlation between diameter and viscosity, i.e., fiber diameter increased with increasing viscosity of the melt. However, no quantitative relationships between fiber diameter and viscosity were reported.

Fiber diameter increased with increasing flow rate and concentration (viscosity) of the polymer solution and was observed to decrease with increasing separation distance between the capillary-end and the target. The fiber diameter also

displayed a slight decrease with increasing electric field strength. These results were summarized in Figure 2.6, where generalized trends are shown.

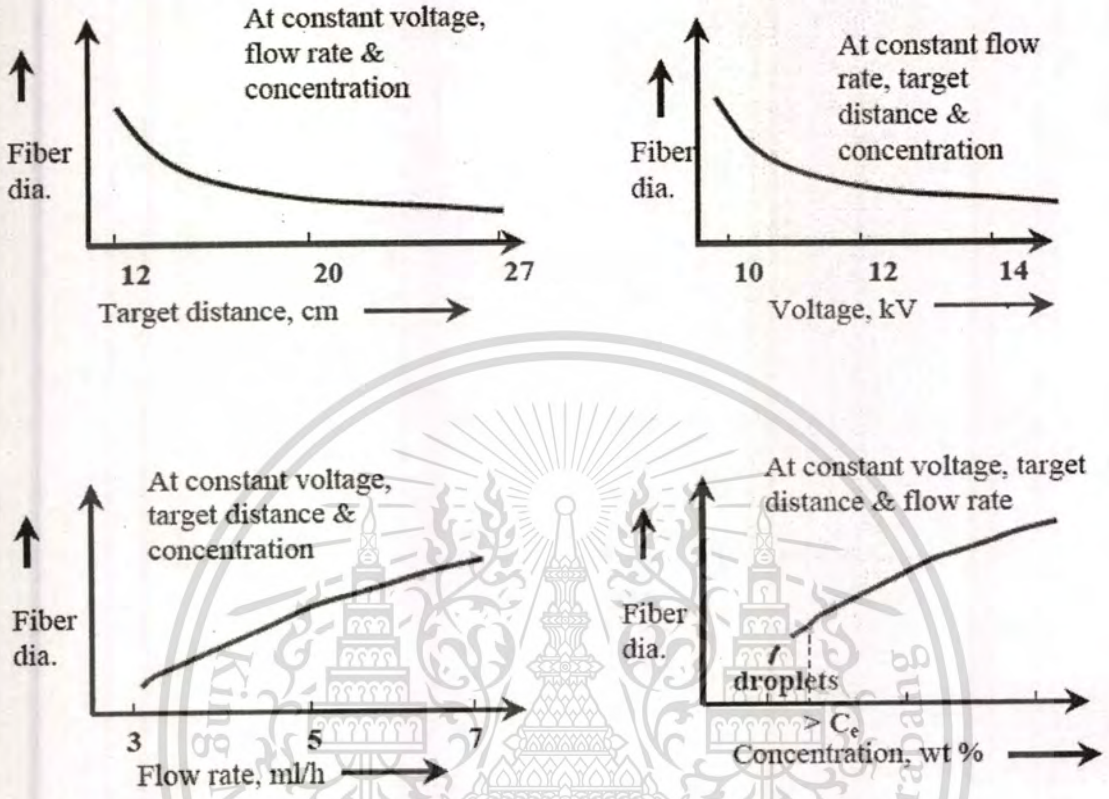

Figure 2.6 Generalized trends of the variation of electrospun fiber diameter with different parameters

2.1.3.4 Applications of Electrospun nanofibers

By virtue of their high aspect ratio (high surface area), the electrospun fibers have been suggested to find applications in a number of areas. These applications have been grouped into four main areas/subtopics, i.e., optical, electronic and high performance applications; composites; protective clothing and filtration applications; and biomedical applications. In the following subsections, each of these subtopics would be discussed briefly.

2.1.3.4.1 Electrospun Nanofibers for Composite Applications

Electrospun poly(benzimidazole) (PBI) nanofibers of diameter ca. 300 nm [2, 58] were used as reinforcing fibers in polymer matrix composites. The epoxy matrix

composites reinforced with PBI nanofibers had higher tensile modulus, fracture toughness and fracture energy. The fracture toughness and the fracture energy of the composites depended on the relative direction of the majority of nanofibers in the fabric (the winding direction) and the crack. If the crack was transverse to the winding direction of the fabric in the composites, fracture toughness and the fracture energy were found to be higher than for those samples in which the crack was along the winding direction.

In composite applications, if there is a refractive index difference between the reinforcing fibers and the matrix, then the resulting composite becomes opaque or non-transparent due to light scattering. One possible way of circumventing this limitation is to use fibers with a diameter significantly lower than the wavelength of visible light (400-700nm). In view of this consideration, Bergshoef and Vancso [59] electrospun smooth fibers of nylon-6,4 with diameters in the range of 30-200 nm from solutions in formic acid. The fibers were then incorporated in a matrix of commercially available two-component phenolic epoxy resin (Epo-plast). The composite films obtained by fiber reinforcement were fully transparent. Visible light was found to transmit over the complete range of wavelengths in the visible spectrum (400–700 nm), as was observed by spectroscopy and visible inspection.

In a different study, Fong et al. [60] were able to reformulate exfoliated montmorillonite-nylon 6 (NLS) nanocomposites by electrospinning. Fibers and nanofibers of NLS nanocomposite (diameters between 100 and 500 nm) were electrospun from solution and, collected as non-woven fabrics, or as aligned yarns. The electrospinning process resulted in highly aligned montmorillonite layers (normal to fiber axis) and nylon 6 crystallites (parallel to fiber axis).

2.1.3.4.2 Electrospun Nanofibers for Protective Clothing and Filtration Applications

Gibson et al. [61] studied the transport properties of elastomeric electrospun mats that were suggested to be utilized in protective clothing applications.

Performance measurements on electrospun mats compared favorably well with the transport properties of textiles and membranes currently used in protective clothing systems. The electrospun layers presented minimal impedance to moisture vapor diffusion required for evaporative cooling. When stretched in biaxial tension to strain levels of 100%, porous elastomeric nanofiber membranes were significantly affected in terms of their convective gas flow properties because of the opening of the interfiber pores, as might be anticipated. However, the water vapor diffusion properties remained unchanged. Experimental measurements and calculations showed that electrospun fiber mats were extremely efficient at trapping aerosol particles. The high filtration density was concluded to be a direct result of the sub-micron size high specific surface fibers generated by electrospinning process. Electrospun nanofiber coatings were applied directly to a polyurethane foam containing activated carbon, which is used as a component in military chemical protective clothing systems [62]. The airflow resistance and aerosol filtration properties correlated with the electrospun coating add on weight. Aerosol particle penetration through the foam layer was eliminated by minuscule levels of nylon electrospun nanofibers sprayed on to the surface of the foam. It was suggested that the electrospun fibers be sprayed directly onto a 3D screen form obtained by 3D body scanning to form custom-fit seamless clothing [63].

In addition to the clothing applications, nanofibers are also finding uses as filters to remove particles and droplets that are smaller than 100 nm from liquids or gases [64]. They have also been considered for the absorption of noxious molecules, since their surface area is so large and their surface chemistry can be tailored to be selective to many kinds of substances [2]. Furthermore, the author found that electrospun mats retain electrical charges up to a period of 200 hr after electrospinning. As electrical charges directly affect the filtration efficiency, the author conducted an investigation where the effect of decaying surface charges on filtration efficiency of

electrospun mats of polyacrylonitrile and polystyrene in different geometrical constructions (including a bicomponent fiber spinning approach) were investigated.

2.1.3.4.3 Electrospun Nanofibers for Biomedical Applications

The application of electrospun fibers for biomaterial applications was reported as early as 1977, when Martin et al. [23] utilized fibrillar mats for wound dressings and vascular prosthetics. It was noted that polymer concentration required for electrospinning depended upon the molecular weight of the polymer, with lower molecular weights requiring higher concentrations. Sub-micron electrospun fibers of poly(glycolic acid) [65], poly(lactic-co- glycolic acid) (PLA/PGA), poly(lactic acid) (PLA) and poly(ethylene-co-vinyl acetate) (PEVA) have been electrospun from solutions in HFIP, methylene chloride or chloroform. As PLA, PGA, PEVA and PLA/PGA are biodegradable materials, the electrospun mats from these polymers have been suggested to find applications as tissue scaffolds. Collagen nanofibers were electrospun from a solution in HFIP [66] to form fibers with a diameter of 100 nm. Aortic muscle cells were then plated out *in-vitro* onto different formulations of electrospun collagen mat. Microscopic examination of the cultures revealed that the scaffolds were densely populated with smooth muscle cells, within 7 days. Cross sectional analysis indicated that electrospun collagen promoted extensive cellular infiltration into the fibrillar network. Smooth muscle cells were observed deep within the matrix and fully enmeshed within the fibrils of the electrospun collagen. In another study, Li et al. [67], seeded BALB/c C7 mouse fibroblast cells on electrospun fibrous mats of poly(D,L-lactide-co-glycolide) (PLGA) with fibers ranging from 500-800 nm in diameter. The in-vitro studies indicated that the mouse fibroblasts adhered and spread on the surface of the PLGA fiber network and had started to migrate through the pores and to grow under layers of the fiber in network at day 3. These fibroblasts interacted and integrated well with the surrounding fibers. Scanning Electron Microscopy (SEM) showed that the development of cell growth was guided by the fiber architecture. Cells grew in the direction of fiber orientation, forming a

three dimensional and multi-cellular network according to the architecture of the nanofibrous structure. It was concluded that the electrospun structure of PLGA featured a morphological similarity to the extra cellular matrix (ECM) of natural tissue, which is characterized by a wide range of pore diameter distribution, high porosity, and effective mechanical properties. Yoshimoto et al. [68] also produced microporous, non-woven poly(ε-caprolactone) (PCL) scaffolds by electrospinning that were seeded with Mesenchymal stem cells (MSCs) derived from the bone marrow of neonatal rats. The cell-polymer constructs, which were cultured with osteogenic supplements under dynamic culture conditions for up to 4 weeks, maintained the size and shape of the original scaffolds. Penetration of the cells and abundant extra cellular matrix was observed in the cell-polymer constructs after 1 week. SEM studies indicated that the surfaces of the cell-polymer constructs were covered with cell multilayers after 4 weeks. In addition, mineralization and type I collagen were observed after 4 weeks suggesting that electrospun PCL could serve as a potential candidate for bone tissue engineering. Xu and coworkers [69, 70] observed good biocompatibility of electrospun scaffolds of poly(L-lactide-co-e-caprolactone) (PLLA-CL) when in vitro cultures of muscle, endothelial and human coronary artery smooth muscle cells proliferated and migrated along the axis of nanofibers.

Kenawy et al. [71] explored the potential of PLA and PEVA electrospun fiber mats as drug delivery vehicles. Tetracycline hydrochloride was used as a model drug. The fibers were electrospun from chloroform solutions containing a small amount of methanol to stabilize the drug. In vitro release of tetracycline hydrochloride was followed by UV-Vis spectroscopy. It was found that electrospun PEVA and 50/50 blend of PLA/PEVA mats gave relatively smooth release of the drug for 5 days. When compared to the drug release from a cast film, it was found that the total percent of the drug released from the electrospun mats was greater. This was attributed to the much lower surface area of the cast films. Zong et al. [56] also found similar results regarding the total percent in-vitro release of Mefoxin from porous PDLA electrospun

membranes. In addition, the loading efficiency, defined as the released amount by the initial loading amount, of Mefoxin in PDLA was found to be around 90%. By utilizing a novel approach, Sanders et al. [72] conducted electrospinning of a biocompatible polymer, poly(ethylene-co-vinyl acetate) (EVA) from a solution containing dispersed aqueous domains to produce EVA fibers containing aqueous micro reservoirs. The osmotic swelling of these aqueous reservoirs in the electrospun fibers lead to an eventual bursting that could potentially be utilized for drug delivery applications.

In another in-vitro study, Kenawy et al. [73] investigated the antimicrobial properties of electrospun mats and compared those to bulk materials. It was found that the anti microbial properties, assessed by measuring the inhibition zone diameter against the testing strains of B. subtilis, S. choleraesuis, S. aureas and E. coli, of the electrospun fibers of poly(vinyl phenol) PVP were enhanced in comparison to the bulk materials. Poly(vinyl phenol) (PVP) was also sulfonated to enhance its antimicrobial characteristics.

Pattama Taepaiboon, Uracha Rungsardthong, and Pitt Supaphol [74] successfully incorporated and studied sustain release of four types of non-steroidal anti-inflammatory drug, i.e. sodium salicylate (free soluble in water), diclofenac sodium (sparingly soluble in water), naproxen, and indomethacin (both insoluble in water), as model drugs. The molecular weight of the model drugs played a major role on both the rate and the total amount of drugs released from the as-prepared drug-loaded electrospun PVA mats, with the rate and the total amount of the drugs released decreasing with increasing molecular weight of the drugs. The drug-loaded electrospun PVA mats exhibited much better release characteristics of the model drugs than drug-loaded as-cast films.

2.1.3.4.4 Cellulose acetate used in drug delivery system

Cellulose acetate membranes for transdermal delivery of scopolamine base were studied by Wang et al. [75]. The cellulose acetate membranes were cast with acetone as a solvent at 22 and 40 °C. Polyethylene glycol (PEG, MW 600) was used as a pore-forming agent. The *in vitro* release rates of scopolamine base as a model drug through the membranes were evaluated in phosphate buffer solution (PBS, pH 7.4) at 32 °C. They found that both PEG content and fabrication temperature affected on the properties of resultant membranes. The structures of membranes fabricated at 40 °C are more homogeneous and denser. The permeation rate of scopolamine base through the membranes fabricated at 40 °C with 10% and 20% PEG is constant over 3 days *in vitro*. PEG content should be optimized to yield membranes with good mechanical properties and provide a linear release profile of a drug.

In 2006, Zhou et al. [76] prepared chitosan/cellulose acetate multimicrospheres (CCAM) loaded with different model drugs via the method of w/o/w emulsion. Model drugs with different hydrophilicity were selected to investigate the delivery system, such as hydrophilic ranitidine hydrochloride (RT), amphoteric acetaminophen (ACP) and hydrophobic 6-mercaptopurine (6-MP). The results showed that with the increasing of hydrophobicity of drug, the holes in the appearance of microspheres became smaller and the loading efficiency increased. The CCAM system had good effect on the controlled release in vitro of all model drugs of different hydrophobicity. However, the release rate was affected by the hydrophobicity of model drug. It became slower with the increasing of hydrophobicity of drugs. The highest release rate was almost 60% during 48 h which was for the hydrophilic drug of RT and the release rate of hydrophobic drug (6-MP) was not more than 30% in the same time.

The interplay of phase inversion and membrane formation in the drug release characteristics of a cellulose acetate (CA) membrane-based delivery system was examined by Ma et al [77]. Drug encapsulated films were cast from solutions of naproxen (drug), CA (polymer), acetone (solvent), and water (non-solvent). The rate

of drug release was controlled by the CA membrane morphologies formed during the film casting process. The burst release effect for the high DL films can be avoided by controlling the interplay of phase inversion, drug crystallization, and membrane formation. Morphology control allows higher drug loads without bursting. They also reported that the drug release followed a diffusion controlled, non-zero order release mechanism.

2.2 Controlled Release Mechanisms

Controlled release of drugs is a very important process to achieve highest therapeutic efficiency. As a result, much research has been carried out in order to develop new controlled release systems that are more efficient and, most importantly, more cost-effective. In order to, the suitable controlled release systems should be able to administer drugs at a specified rate over a proper period of time during a treatment. To achieve such characteristics, complete understanding over either the physical or chemical properties is crucial for imparting such characteristics to controlled release vehicles of choice.

There are three primary mechanisms by which active agents can be released from a delivery system: diffusion, degradation, and swelling followed by diffusion. Any or all of these mechanisms may occur in a given release system. Diffusion occurs when a drug or other active agent passes through the polymer that forms the controlled-release device. The diffusion can occur on a macroscopic scale as through pores in the polymer matrix or on a molecular level, by passing between polymer chains. Examples of diffusion release systems are shown in Figure 2.7 and 2.8.

In Figure 2.7, a polymer and active agent have been mixed to form a homogeneous system, also referred to as a matrix system. Diffusion occurs when the drug passes from the polymer matrix into the external environment. As the release continues, its rate normally decreases with this type of system, since the active agent

has a progressively longer distance to travel and therefore requires a longer diffusion time to release.

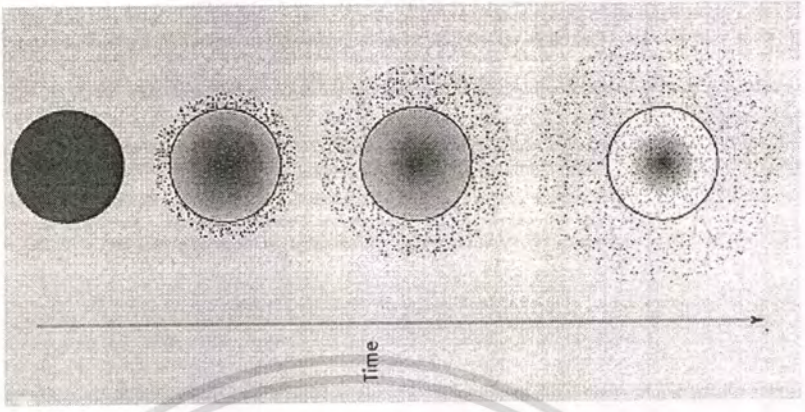

Figure 2.7 Drug delivery from a typical matrix drug delivery system

For the reservoir systems shown in Figures 2.8a and 2.8b, the drug delivery rate can remain fairly constant. In this design, a reservoir whether solid drug, dilute solution, or highly concentrated drug solution within a polymer matrix is surrounded by a film or membrane of a rate controlling material. The only structure effectively limiting the release of the drug is the polymer layer surrounding the reservoir. Since this polymer coating is essentially uniform and of a non-changing thickness, the diffusion rate of the active agent can be kept fairly stable throughout the lifetime of the delivery system.

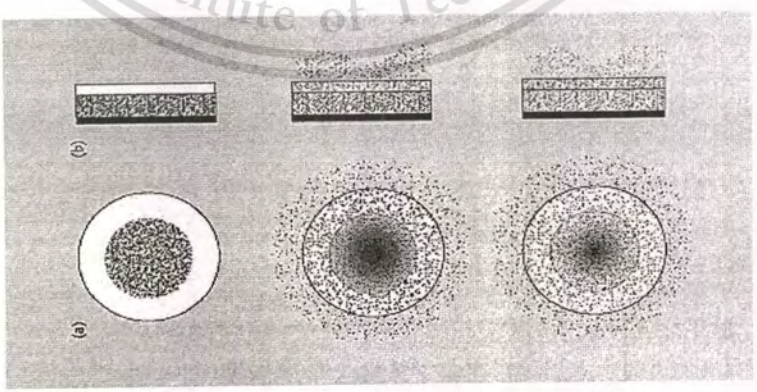

Figure 2.8 Drug delivery from typical reservoir devices: (a) implantable or oral systems, and (b) transdermal systems

The system shown in Figure 2.8a is representative of an implantable or oral reservoir delivery system, whereas the system shown in Figure 2.8b illustrates a transdermal drug delivery system, in which only one side of the device will actually be delivering the drug. Once the active agent has been released into the external environment, one might assume that any structure control over drug delivery has been relinquished. However, this is not always the case. For transdermal drug delivery, the penetration of the drug through the skin constitutes an additional series of diffusional and active transport steps, as shown schematically in Figure 2.9.

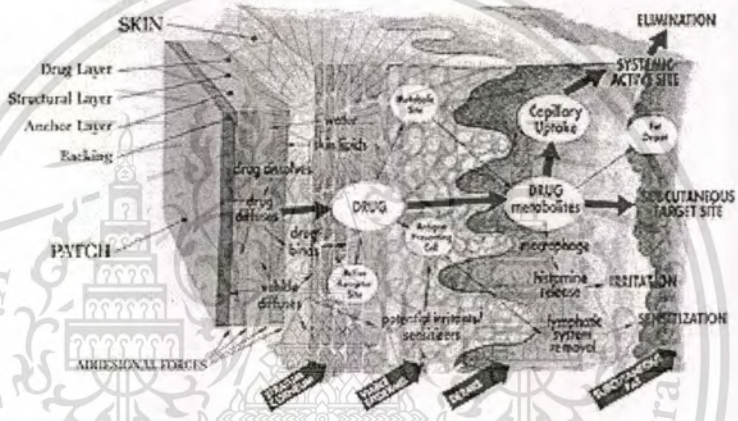

Figure 2.9 Transport processes in transdermal drug delivery

For the diffusion controlled systems described thus far, the drug delivery device is fundamentally stable in the biological environment and does not change its size either through swelling or degradation. In these systems, the combinations of polymer matrices and bioactive agents chosen must allow for the drug to diffuse through the pores or macromolecular structure of the polymer upon introduction of the delivery system into the biological environment without inducing any change in the polymer itself.

2.3 Entanglements in polymer melts and solutions

Chain entanglements in a melt are essentially the physical interlocking of polymer chains, which is a direct consequence of chain overlap. In a polymer melt, chain overlap, and hence the number of entanglements (or alternatively entanglement density), increase with polymer chain length or molecular weight.

For homogeneous solutions of a linear polymer, the well known Huggins Equation describes the solution viscosity [78]

$$\eta_{sp}(c)=[\eta]c+k_H([\eta]c)^2+..... \quad (2.1)$$

where $\eta_{sp}(c)$ is the specific viscosity, $[\eta]$ is the intrinsic viscosity, c is the polymer concentration, and k_H is the Huggins coefficient. The dimensionless product of the intrinsic viscosity and the concentration, $[\eta]c$ is referred to as the Berry number, B_e [79]. The significance of the Berry number arises from the fact that for a solution to have chain entanglements, $B_e>1$. In dilute solutions, where polymer chains do not overlap each other (see Figure 2.10a), B_e can, at best, be unity ($B_e \sim 1$). In Eq. 2.1, the intrinsic viscosity is the initial slope of the plot between specific viscosity and concentration and is related to the root-mean-squared end-to-end distance, $\langle R^2 \rangle^{1/2}$, of the linear polymer chain that has N monomers by the Fox-Flory relationship [80]:

$$[\eta] \sim \frac{\langle R^2 \rangle^{3/2}}{N} \quad (2.2)$$

In addition, the intrinsic viscosity, $[\eta]$ can also be related to the molecular weight (M) of a linear polymer by the Mark-Houwink-Sakurada equation [81]

$$[\eta] = KM^a \quad (2.3)$$

where the constants K and a depend on the polymer, solvent and temperature [82].

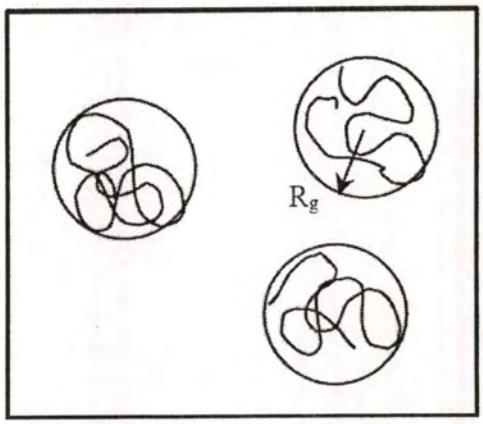

(a) Dilute, $c < c^*$

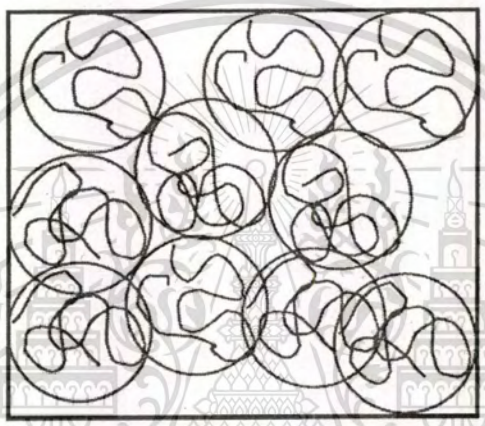

(b) Semidilute unentangled, $c^* < c < c_e$

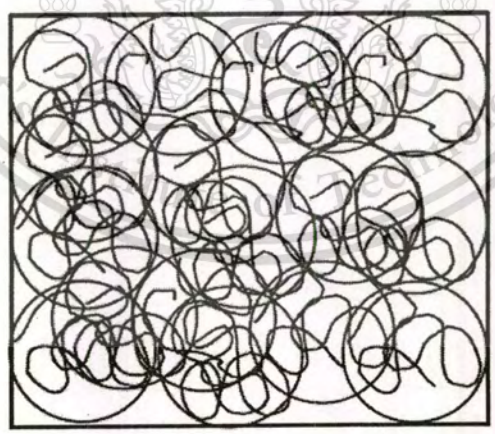

(c) Semidilute entangled, $c > c_e$

Figure 2.10 Physical representation of the three solution regimes, (a) dilute, (b) semidilute unentangled and (c) semidilute entangled

The critical chain overlap concentration, c^*, is the crossover concentration between the dilute and the semidilute concentration regimes. Physically, the critical chain overlap concentration is the point when the concentration inside a single macromolecular chain equals the solution concentration and can be expressed as

$$c^* \sim \frac{N}{\langle R^2 \rangle^{3/2}} \sim \frac{1}{[\eta]} \tag{2.4a}$$

From Eq. 2.4a, it is clear that $c^*[\eta] \sim 1$ in the dilute solution limit, thereby suggesting the criteria, $c^* \sim 1/[\eta]$, as a means of evaluating c^* (recall that this criteria is the same as that discussed above with regard to $B_e \sim 1 => c \sim 1/[\eta]$ in the dilute solution limit). Hence, the calculation of c* from chain dimensions:

$$c^* = \frac{3M}{4\pi \langle R^2 \rangle^{3/2} N_{av}} \tag{2.4b}$$

in conjunction with the criteria $c^* \sim 1/[\eta]$ are the two ways that can and have been utilized to estimate c^* (In Eq. 2.4b, N_{av} is the Avogadro number and M is the molecular weight). Furthermore, in a good solvent, the radius of gyration, R_g, is usually a better estimate of the chain dimensions than the root-mean-squared end-to-end distance, $\langle R^2 \rangle^{1/2}$ as it accounts for the hydrodynamic interactions between the polymer chains and the solvent. It is well established that the radius of gyration can be estimated from the hydrodynamic radius, R_h, (assuming non draining conditions) based on the Kirkwood- Riseman theory

$$R_g = R_h/0.875 \tag{2.5}$$

where the hydrodynamic radius can be determined by dynamic light scattering measurements.

In dilute solutions of good solvents, the solution viscosity has been measured experimentally to be proportional to the concentration, ($\eta \sim c$). This is consistent with Eq. 2.1 at very small values of c (in the dilute regime), where the higher power terms of concentration are negligible. However, for $c > c^*$ in good solvents, de Gennes

assumed a single parameter scaling in the semidilute regime to predict a power law dependence for the solution viscosity that is given by

$$\eta = \eta_s (c/c^*)^{3/(3\upsilon-1)} \qquad (2.6)$$

where η_s is the solvent viscosity and the υ is the Flory exponent (0.5 for theta solvents and 0.6 for good solvents). In good solvents, the single parameter scaling model based on the reptation model, (where the viscosity scales with molecular weight as $\eta \sim M^{3.0}$), predicts a concentration exponent of 3.75. However, experimental data [83-85] indicates a stronger dependence of viscosity on molecular weight ($\eta \sim M^{3.4}$) than that predicted by reptation theory. It has been suggested that mechanisms of relaxation other than reptation, such as contour length fluctuations, might account for this observed stronger dependence. If this stronger dependence of η on molecular weight ($\eta \sim M^{3.4}$) is taken into account, then the exponent for the concentration dependence of viscosity has been predicted to be 4.25 [86-87]. A different scaling concept, based on two parameters, was proposed by Colby et al, where an even stronger viscosity dependence on concentration was predicted ($\eta \sim c^{4.5}$) and measured experimentally ($\eta \sim c^{4.8}$) [88].

Recent work of Colby and co-workers indicates that two different power law dependences exist within the semidilute regime, such as semidilute unentangled and semidilute entangled. A physical representation of the semidilute unentangled regime is provided in Figure 2.10b, where the concentration is large enough to have some chain overlap ($c > c^*$) but not enough to cause any significant degree of entanglement. As the concentration is further increased (semidilute entangled regime, Figure 2.10c), the topological constraints induced by the larger occupied fraction of the available hydrodynamic volume in the solution, introduce chain entanglements. Furthermore, the crossover of concentration from the semidilute unentangled to semidilute entangled regime is referred to as the critical entanglement concentration, c_e. In other words, c_e, marks the distinct onset of significant chain entanglements in solution.

Returning to the discussion on scaling relationships in the two semidilute regimes, a weaker concentration exponent of 1.25 was predicted and experimental values in the range of 1.1-1.4 were reported in the semidilute unentangled regime in a good solvent. For semidilute entangled regimes, the predictions and measurements of concentration exponent are comparable to the exponents reported by de Gennes, Pearson and Colby et al. Thus, the predicted concentration exponents for the viscosity dependence in a good solvent in the semidilute regime can be summarized as:

$$\eta \sim c^{1.25} \quad \text{semidilute unentangled}$$

$$\sim c^{4.25-4.5} \quad \text{semidilute entangled}$$

2.4 Solubility parameter

Cohesive energy represents the total attractive forces within a condensed state material and can be defined as the quantity of energy needed to separate the atoms/molecules of a solid or liquid to a distance where the atoms or molecules possess no potential energy, i.e., no interactions occur between atoms or molecules. Further, cohesive energy density (CED) is the cohesive energy per unit volume. The CED for a material can be used to predict its solubility in other materials; if two components have similar values, they are likely to be soluble in each other, since interactions in one component will be similar to those in the other component. Thus, the overall energy needed to facilitate mixing of the constituents will be small, as the energy required to break the interactions within the components will be equally compensated for by the energy released due to interactions between unlike molecules. In addition, CED values can be transformed into Hildebrand solubility parameter (δ), defined as the square root of the CED,

$$\delta = (\text{CED})^{0.5} = (\Delta E_v / V_m)^{0.5}$$

where ΔE_v is the energy of vaporization and V_m the molar volume.

Solubility parameters are widely used to describe the cohesive forces within materials and have been used to describe many physical properties of a material and

predict interactions between materials. The used of solubility parameters to predict solubility/miscibility is attractive and can be applied to low molecular weight materials and polymers.

2.5 Cellulose acetate and non-steroidal anti-inflammatory drugs (NSAIDs)

2.5.1 Cellulose acetate

(CA; white powder; Mw = 30,000 g/mol; acetyl content = 39.7% (w/w))

Cellulose acetate (CA) is the acetate ester of cellulose, the primary structural component of the wall of green plants and is one of the most common biopolymers on earth. CA is prepared from cellulose by a solution process employing sulfuric acid as the catalyst with acetic anhydride in an acetic acid solvent. The acetylation reaction is heterogeneous and topochemical.

The properties of cellulose acetate are affected by the number of acetyl groups per anhydroglucose unit of cellulose and the degree of polymerization. Fewer acetyl group per anhydroglucose unit (increased hydroxyl content) increase the solubility in polar solvent and decrease moisture resistance.

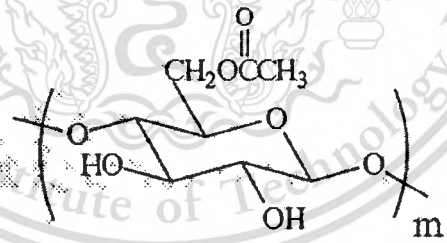

Figure 2.11 Chemical structure of cellulose acetate

2.5.2 Naproxen (NAP)

IUPAC name: 2-(6-methoxynaphthalen-2-yl)propanoic acid

Molecular formula: $C_{14}H_{14}O_3$

Molecular weight: 230.3 g/mol

Naproxen, a non-steroidal anti-inflammatory drug, is widely used to moderate pain relief in the treatment of many diseases, such as rheumatoid arthritis, osteoarthritis, degenerative joint disease, ankylosing spondylitis, acute gout and primary dismenorrea. The major clinical application on NSAIDs is their action as anti-inflammatory agents in muscle skeletal diseases.

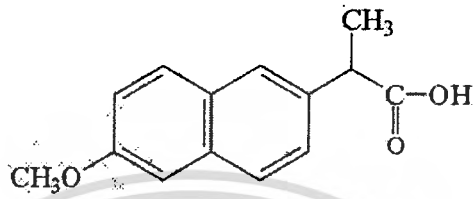

Figure 2.12 Molecular structure of Naproxen

2.5.3 Indomethacin (IND)

IUPAC name: 1-(4 - chlorobenzoyl) - 5 - methoxy - 2- methyl -1- H-indole - 3 - acetic acid

Molecular formula: $C_{19}H_{16}ClNO_4$

Molecular weight: 357.8 g/mol

Indomethacin is an indole derivative, known for its antipyretic and analgesic action. It is a nonsteroidal anti-inflammatory drug (NSAID) used in the treatment of rheumatoid arthritis and a potent inhibitor of cyclooxygenase, reducing prostaglandia synthesis, relieving pain and reducing temperature in febrific patients. The antipyretic effect is due to a resetting of the hypothalamic temperature-regulating center, whereas the anti-inflammatory and analgesic effects are due to inhibition of prostaglandin synthesis. Therapeutically, indomethacin is indicated to control pain and inflammation

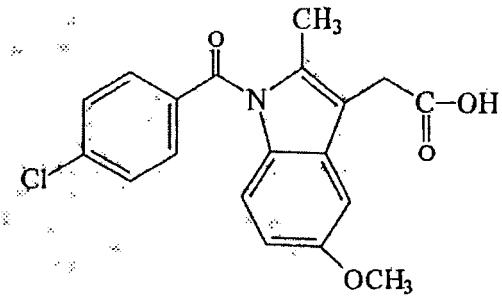

Figure 2.13 Molecular structure of Indomethacin

2.5.4 Ibuprofen (IBU)

IUPAC name: 2-[4-(2- methylpropyl)phenyl] propanoic acid

Molecular formula: $C_{13}H_{18}O_2$

Molecular weight: 206.3 g/mol

Ibuprofen belongs to a class of drugs called NSAIDs. These drugs are used for the management of mild to moderate pain, fever, and inflammation. Pain, fever, and inflammation are promoted by the release in the body of chemicals called protaglandins. Ibuprofen blocks the enzyme that makes protaglandins, (cyclooxygenase), resulting in lower levels of prostaglandins. As a consequence, inflammation, pain, and fever are reduced. The FDA approved ibuprofen in 1974.

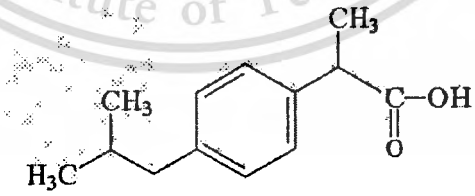

Figure 2.14 Molecular structure of Ibuprofen

2.5.5 Sulindac (SUL)

IUPAC name: 2-[6-fluoro-2-methyl -3 - [(4-methylsulfinylphenyl)methylidene]inden-1-yl]- acetic acid

Molecular formula: $C_{20}H_{17}FO_3S$

Molecular weight: 356.4 g/mol

Sulindac is a non-steroidal anti-inflammatory drug of the arylalkanoic acid class. Like other NSAIDs, it is useful in the treatment of acute or chronic inflammatory conditions. Sulindac is a prodrug, derived from sulfinylindene that is converted in the body to an active NSAID. More specifically, the agent is converted by liver enzymes to a sulfide which is excreted in the bile and then reabsorbed from the intestine. This is thought to help maintain constant blood levels with reduced gastrointestinal side effects. Some studies have shown sulindac to be relatively less irritating to the stomach than other NSAIDs except for drugs of the COX-2 inhibitor class. However, sulindac is much more likely than other NSAIDs to cause damage to the liver or pancreas.

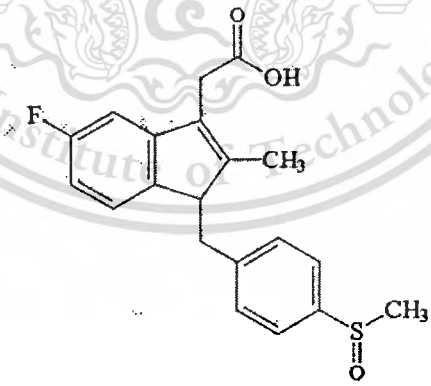

Figure 2.15 Molecular structure of Sulindac

Chapter 3

Experiment Details

3.1 Chemicals

1. Acetone (AR grade, Carlo Erba Co,Ltd)
2. Pyridine (AR grade, BDH Co,Ltd)
3. Dichloromethane (AR grade, Labscan Asia Co,Ltd)
4. Chloroform (AR grade, BDH Co,Ltd)
5. Methanol (AR grade, Labscan Asia Co,Ltd)
6. Formic acid (AR grade, Carlo Erba Co,Ltd)
7. *N, N*-Dimethylacetamide (AR grade, Labscan Asia Co,Ltd)
8. *N, N*-Dimethylformamide (AR grade, Labscan Asia Co,Ltd)
9. Sodium acetate (Ajax Chemicals)
10. Glacial acetic acid (Merck)
11. Dimethylsulfoxide (DMSO) (AR grade, Carlo Erba Co,Ltd)
12. Cellulose acetate (CA; M_w = 30,000 g/mol; acetyl content = 39.7% (w/w)) was purchased from Aldrich
13. Naproxen (Pharmasant Laboratories)
14. Indomethacin (Pharmasant Laboratories)
15. Ibuprofen (Aldrich)
16. Sulindac (Aldrich)

3.2 Equipment

1. High voltage DC power supply (model UC5-30P, Gamma High Voltage Research, USA)
2. Nozzle
3. Collector
4. Beaker

5. Aluminium foil
6. Erlenmeyer flask
7. Syringe
8. Stirrer
9. Oven
10. Shaker and water bath
11. Scanning electron microscope (SEM; JEOL JSM-6400)
12. ^{1}H-nuclear magnetic resonance spectrometer (^{1}H-NMR; Avanced DPX, Bruker)
13. Differential scanning calorimeter (DSC; Perkin Elmer DSC-7)
14. Thermogravimetric/differential thermal analyzer (TG/DTA; Perkin Elmer Pyris 1)
15. UV-spectrophotometer (Shimadzu, UV-1601)
16. Brookfield DV-III programmable viscosmeter
17. Tensiometer (CSC Sciencific)
18. Conductivity meter (Jenway 4130)
19. pH-meter (Metrohm 744)

3.3 Procedure

3.3.1 Part 1 Effect of solvent system on morphology and fiber diameter

Preparation and characterization of CA solutions

1.) The spinning solutions were prepared in either a single solvent or in mixed-solvent systems at room temperature. In the single solvents, solutions of CA in acetone, chloroform, DMF, DCM, MeOH, formic acid, and pyridine were prepared at a fixed concentration of 5% (w/v).

2.) In the mixed-solvent systems, CA was dissolved in acetone-DMAc, chloroform-MeOH, or DCM-MeOH mixtures of different composition (i.e. 16% (w/v) CA solutions in 1:1, 2:1, and 3:1 (v/v) acetone-DMAc and 5% (w/v)

CA solutions in 1:1, 3:2, 7:3, 4:1, and 9:1 (v/v) chloroform-MeOH and DCM-MeOH) and at different concentrations (i.e. 12-20% (w/v) CA solutions in 2:1 (v/v) acetone-DMAc and 2-12% (w/v) CA solutions in 4:1 (v/v) DCM-MeOH)

3.) Before electrospinning, shear viscosity, surface tension, and conductivity were measured for all the solutions.

4.) Electrospinning of the as-prepared solutions was carried out by connecting the emitting electrode of positive polarity from a high-voltage DC power supply to the solutions contained in a standard 5-ml syringe, the open end of which was attached to a blunt gauge-20 stainless steel needle (outer diameter = 0.91 mm), used as the nozzle, and the grounding electrode to a collecting screen. The applied potentials used in this work were 12 kV across a fixed collection distance of 15 cm between the tip of the nozzle and the outer surface of the screen.

5.) The morphological appearance of the as-spun materials were/was observed by use of a scanning electron microscope (SEM). Each of the fiber mat samples were mounted on the metal stubs using a double-sided adhesive tape and vacuum-coated with a thin layer of gold prior to SEM observation. Diameters of the individual fibers in the as-spun fiber mats were measured directly from the SEM images using the SemAphore® 4.0 software ($n \geq 50$).

3.3.2 Part 2 Release of model drugs from drug-loaded CA fiber mats and films

3.3.2.1 Preparation of neat and drug-loaded CA fiber mats and films

1.) A weighed amount of CA powder was dissolved in the mixed solvent of acetone: DMAc (2:1 v/v) at a fixed concentration of 16% w/v.

2.) After that, four different types of the model drugs were separately added into the CA solution under constant stirring for 4 hr prior to electrospinning. Drugs were loaded at 20 wt.% (based on the weight of CA powder).

3.) Prior to electrospinning, the as-prepared solutions were measured for their viscosity, surface tension, and conductivity, respectively.

4.) Preparation of drug-loaded electrospun fiber for the electrospinning technique

Electrospinning of the as-prepared solutions was carried out by connecting the emitting electrode of positive polarity from a high-voltage DC power supply to the solutions contained in a standard 50 mL syringe, the open end of which was attached with a gauge 20 flat-tipped stainless steel needle (outer diameter = 0.91 mm), used as a nozzle, and the grounding electrode to a home-made rotating metal drum (diameter and width ≈ 15 cm), used as the fiber-collecting device. A fixed applied electrical potential of 12 kV was applied over a fixed collection distance of 15 cm and the rotational speed of the drum was about 100 rpm. For morphological study, the collection time was about 10 min, while, for the rest of the experiments, the collection time was about 24 hr. Upon the completion of the electrospinning process, the electrospun fiber mats were removed from the collector and characterized as such.

5.) Preparation of drug-loaded CA films

The drug-loaded CA films were prepared by solution-casting technique from a CA solution having a concentration of 12% w/v (20 wt% drug-loaded) by dissolving the ingredients of drug/polymer in a mixture of acetone:DMAc (2:1). Afterwards, 12 mL of solution was poured in glass peri dish (diameter = 7 cm) and evaporated in a vacuum oven at 60 °C for 5 hr and then dried overnight at room temperature. The thickness of both the electrospun mats (for the mats that were electrospun for about 24 hr) and the as-cast films was controlled between 20 and 35 μm.

3.3.2.2 Characterization of neat and drug-loaded as-spun CA mats and as-cast CA films

1.) Morphological appearance of both neat and drug-loaded electrospun mats were observed by scanning electron microscope (SEM).

2.) The drug-loaded as-spun CA fiber and drug-loaded as-cast CA film samples before and after *in vitro* release were also observed by SEM in comparison with both morphology.

3.) A ^{1}H-nuclear magnetic resonance spectrometer was used to investigate the chemical integrity of the model drugs after electrospinning process using deuterated dimethylsulfoxide (DMSO-d_6) as a solvent.

4.) A differential scanning calorimeter (DSC) and a thermogravimetric/differential thermal analyzer (TG/DTA) were used to investigate thermal behaviors of the CA matrix, the drugs, and the drug-loaded as-spun CA mats.

5.) Degree of swelling and weight loss of both neat and drug-loaded electrospun CA mats were measured in an acetate buffer solution at 37 °C for 24 hr.

$$\text{Degree of swelling (\%)} = \frac{M - M_d}{M_d} \times 100,$$

and

$$\text{Weight loss (\%)} = \frac{M_i - M_d - M_r}{M_i - M_r} \times 100, \quad \text{where}$$

M is the weight of each sample after submersion in the buffer solution for 24 hr,

M_d is the weight of the sample after submersion in the buffer solution for 24 hr in its dry state

M_i is the initial weight of the sample in its dry state

M_r is the weight of a model drug that was released from the sample

3.3.2.3 Release of model drugs from drug-loaded as-spun CA fiber mats and as-cast CA films

3.3.2.3.1 Preparation of acetate buffer

Acetate buffer was chosen to simulate human skin pH condition of 5.5. To prepare 1000 mL of the acetate buffer solution, 150 g of sodium acetate was dissolved in about 250 mL of distilled water. Exactly 15 mL of glacial acetic acid was then

added very slowly into the aqueous sodium acetate solution. Finally, distilled water was added into the solution to fill the volume and the pH value of the solution was verified by a pH-meter.

3.3.2.3.2 Actual drug content

1.) The actual amount of drugs in the drug-loaded electrospun CA mats and as-cast CA films was quantified by dissolving the mats in 4 mL of dimethylsulfoxide (DMSO).

2.) After that, 0.5 mL of the solution was pipetted and added into 8 mL of the acetate buffer solution.

3.) Each drug-containing dilute solution was measured for the amount of drug using a UV-spectrophotometer at a wavelength of 274, 319, 232, and 327 nm for NAP, IND, IBU, and SUL, respectively (see Appendix A). These wavelength values correspond to the maximum wavelength (λ_{max}) for each drug.

4.) The amount of drug originally present in the as-spun CA mats and the as-cast CA films was back-calculated from the obtained data against a predetermined calibration curve for each model drug.

The standard calibration plot of model drug in the concentration range of 0.0025-0.05 mg/mL was used to determine the concentration of the released drug, in which the curve was linear with a relationship of absorbance (see Appendix B). The presence of DMSO in the dilute solution was proved to have no effect on the UV absorbance at the wavelengths investigated. The results were reported as averages from at least 5 measurements.

3.3.2.3.3 Drug-release assay

1.) Drug-loaded as-spun CA mats or as-cast CA films (cut into circular discs of about 2.8 cm in diameter) were accurately weighed and immersed in 40 mL of the acetate buffer solution and incubated in a shaking water bath at 37 °C.

2.) At a specified immersion period ranging between 0 and 24 hr (1440 min), 0.5 mL of the buffer solution was taken out and an equal amount of the fresh buffer solution was refilled into the cell.

3.) The amount of drugs in the withdrawn solutions was determined using the UV-spectrophotometer at the same wavelengths previously mentioned against the predetermined calibration curve for each model drug. These data were carefully calculated to determine the cumulative amount of drugs released from the samples at each specified immersion or diffusion period. The experiments were carried out in triplicate and the results were reported as average values.

4.) The release profiles of drug-loaded as-spun CA mats and as-cast CA films are plotted between accumulative amount of drug released and corresponding time.

3.3.3 Part 3 Release of indomethacin from IND-loaded CA fiber mats in various methods

3.3.3.1 Actual indomethacin content

The method of determine the actual amount of indomethacin in the IND-loaded CA fiber mats was used as the same above (3.4.2.3.2) at the wavelength of 319 nm. The actual amount of indomethacin in the IND-loaded CA fiber mat samples was back-calculated from the obtained data against a predetermined calibration curve for indomethacin (see Appendix C).

3.3.3.2 Indomethacin-release assay

The release characteristic of indomethacin from the IND-loaded electrospun CA fiber mats was investigated by 3 methods of the release assay.

Method 1 With the addition of fresh medium

IND-loaded CA electrospun fiber mats was immersed in 40 mL of the acetate buffer solution at 37 °C. At the specified immersion period ranging between 0 and 24

hr (1440 min), 0.5 mL of the buffer solution was withdrawn and after sampling, an equal amount of the fresh medium was refilled. The indomethacin release was monitored by monitoring the absorbance at a wavelength of 319 nm as a function of time. Release experiments were done in triplicate.

Method 2 Without the addition of fresh medium

The procedure and conditions for the release study in method 2 were the same as those of method 1 but after the buffer solution was withdrawn, the fresh medium buffer was not refilled in the solution at all time.

Method 3 With sequential dipping in fresh medium

IND-loaded CA electrospun fiber mats were immersed in 10 mL of the acetate buffer solution at 37 °C at the immersion time was 10 min. After that, 0.5 mL of a sample solution was withdrawn and measured for the amount of drug using a UV-spectrophotometer. The fiber sample in the first bottle was taken out from the incubation buffer and put into another bottle with 10 mL fresh buffer. The same procedure as described above was carried out in every 10 min.

3.3.4 Part 4 Release kinetics of model drugs from drug-loaded as-spun CA mats and as-cast CA films

Replotting the drug release data in the form of M_t/M_∞ versus square root of time (M_t and M_∞ represent the amount of drugs in the solution at time t and at final time) can be characterized the kinetic rate of release (k) of the model drugs from the Ritger-Peppas equation:

$$\frac{M_t}{M_\infty} = kt^n, \quad \text{for } \frac{M_t}{M_\infty} < 0.6,$$

CHAPTER 4

RESULTS AND DISCUSSION

Part 1 Effect of solvent system on morphology and fiber diameter

In this work, the electrostatic spinning or electrospinning technique was used to produce ultrafine cellulose acetate (CA) fiber mats. CA solutions were prepared in various single solvent system (i.e. acetone, *N,N*-dimethylformamide (DMF), dichloromethane, formic acid, pyridine, chloroform, and methanol) and mixed-solvent systems (i.e. acetone-DMAc, chloroform-MeOH, and DCM-MeOH). Some properties of those solvents (i.e. density, boiling point, dipole moment, dielectric constant, viscosity and surface tension) are summarized in Table 4.1 [89]. The corresponding values for water are also listed in Table 4.1 for comparison.

Table 4.1 Properties of solvents used in this work

Solvent	Density ($g.cm^{-3}$)	Boiling point (^oC)	Dipole moment (Debye)	Dielectric constant	Viscosity (mPa.s)	Surface tension ($mN.m^{-1}$)
Acetone	0.786	56.3	2.70	20.7	0.304	22.7
Chloroform	1.480	61.2	1.01	4.8	0.540	26.6
N, N-Dimethylacetamide	0.937	166.0	3.72	37.8	1.020	34.0
N, N-Dimethylformamide	0.945	153.0	3.82	37.0	0.796	36.3
Dichloromethane	1.317	39.8	1.60	8.9	0.423	27.2
Methanol	0.790	64.7	1.60	32.6	0.545	22.1
Formic acid	1.213	100.7	1.40	58.5	1.800	24.4
Pyridine	0.978	115.3	2.20	12.4	0.883	36.5
Water	0.997	100.0	1.84	78.4	0.891	72.0

4.1 Effects of solvent systems on CA electrospun fiber mats

4.1.1 Single-Solvent Systems

Acetone, chloroform, DMF, DCM, pyridine, MeOH and formic acid were chosen as solvents for dissolving CA powder. Each solution was prepared at a fixed concentration of 5% (w/v). Some of the properties i.e. shear viscosity, surface tension, and conductivity, of the CA solutions are summarized in Table 4.2. The applied electrostatic field strength was also fixed at 12 kV. The distance between needle tip and collector was kept constant at 15 cm.

Table 4.2 Shear viscosity, surface tension, and conductivity of CA solutions in a variety of single solvent systems

5% (w/v) CA solution	Shear viscosity (mPa s)	Surface tension ($mN\ m^{-1}$)	Conductivity (μS/cm)
Acetone	362	33.6	7.14
Chloroform	24.2	29.5	0.13
N, N-Dimethylformamide	137.5	32.8	1.87
Dichloromethane	28.4	31.0	2.83
Pyridine	98.8	29.1	1.17
Formic acid	58.6	30.2	4.31
Methanol	53.4	32.1	3.65

Although acetone, DMF, pyridine and formic acid dissolved CA forming a clear solution almost instantly, discrete beads were obtained on the screen collector when CA solutions in those solvents were electrospun (see Figure 4.1).

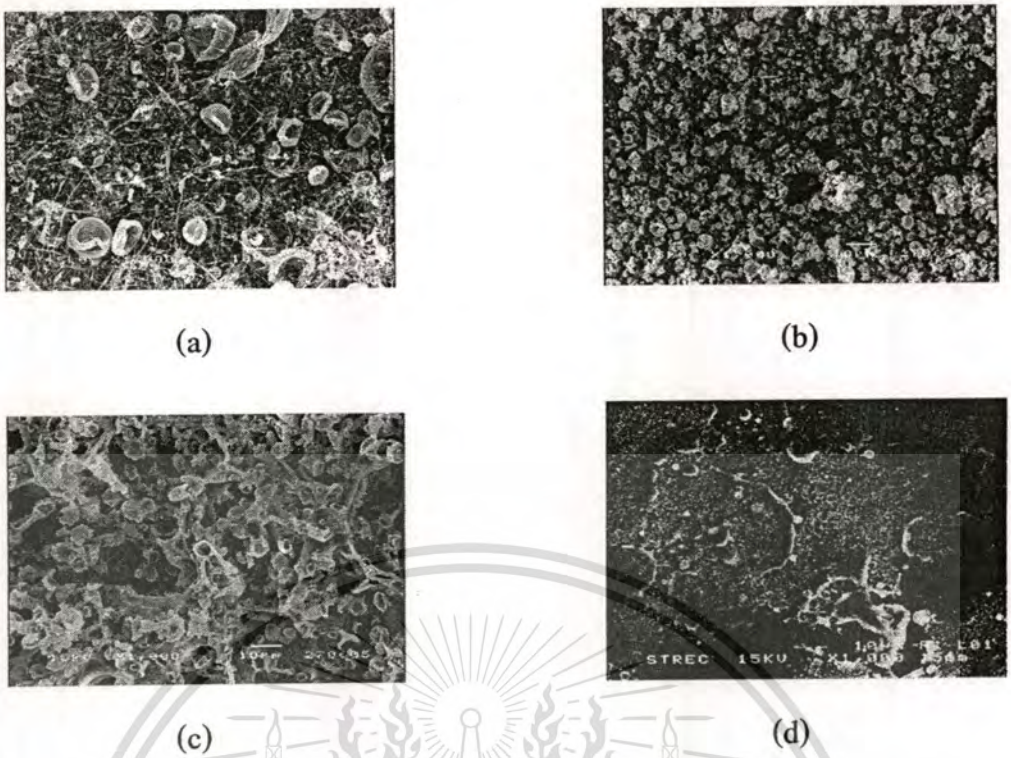

Figure 4.1 Selected SEM images of as-spun fibers from 5% (w/v) CA solution in (a) acetone, (b) formic acid, (c) pyridine, and (d) *N,N*-dimethylformamide. These fibers were electrospun under applied electrostatic field strength of 12 kV/15 cm

However, for acetone solution, small amount of short fibers were occasionally observed. Although acetone also dissolved CA forming a clear solution, but the resulting CA solution was difficult to electrospin because the solution often clogged at the tip of the nozzle. Clogging by the solution was due to the low boiling point of the solvent (56.3 °C) resulting in rapid evaporation of the solution. Similar behavior was also observed for solutions of CA in chloroform, DCM, and MeOH. Furthermore, only discrete droplets were sprayed out to form globs of CA solution on the collective screen (results were not shown).

From above resulted, electrospinning of the 5% (w/v) CA solution in acetone resulted in the formation of short and beaded fibers. Because, primarily, of the clogging problem, electrospinning of CA solutions in acetone could be improved by

addition of a co-solvent or a modifying liquid to delay the evaporation of acetone. Liu and Hsieh [52] found that addition of DMAc helped the electrospinnability of the CA solutions in acetone-water. This improved electrospinnability of the resulting CA solutions in these mixed-solvent systems could derive from the higher boiling points and dielectric constants of DMAc and water compare to those of acetone (see Table 4.1). Interestingly, addition of MeOH in chloroform and dichloromethane can improve electrospinnability and morphological appearance of as-spun CA fiber mats in the mixed solvent systems. It was found that the average diameters of the CA fiber mats could be controlled by changing the composition of the mixed solvent.

4.1.2 Mixed-Solvent Systems

Acetone and N, N-dimethylacetamide

CA solutions at a fixed concentration of 16% (w/v) were prepared in 1:1, 2:1, and 3:1 (v/v) ratio of acetone-DMAc. Some properties of the CA solutions, i.e. shear viscosity, surface tension, and conductivity, are summarized in Table 4.3. The shear viscosity of the CA solutions was expected to decrease whereas both surface tension and conductivity should, theoretically, increase with increasing acetone content in the mixed solvents. The observed decrease in shear viscosity with increasing acetone content can be explained since the shear viscosity of acetone is much less than that of DMAc. The observed slight increase in both surface tension and conductivity was unexpected since both the surface tension and the dielectric constant of acetone are lower than those of DMAc.

Figure 4.2 shows selected SEM images of the as-spun fibers electrospun from of the CA solutions in 1:1, 2:1, and 3:1 (v/v) acetone-DMAc with the applied electrostatic field strength of 12 kV/15 cm. Obviously, only smooth fibers were obtained at this concentration, despite the different compositions of the mixed solvents used. On the basis of these SEM images, the diameters of the as-spun fibers were found to increase with increasing acetone content in the mixed solvents. Specifically,

the average diameter increased from 0.16 μm for an acetone-DMAc ratio of 1:1 (v/v) to 0.32 μm for a ratio of 3:1 (v/v) (Table 4.3).

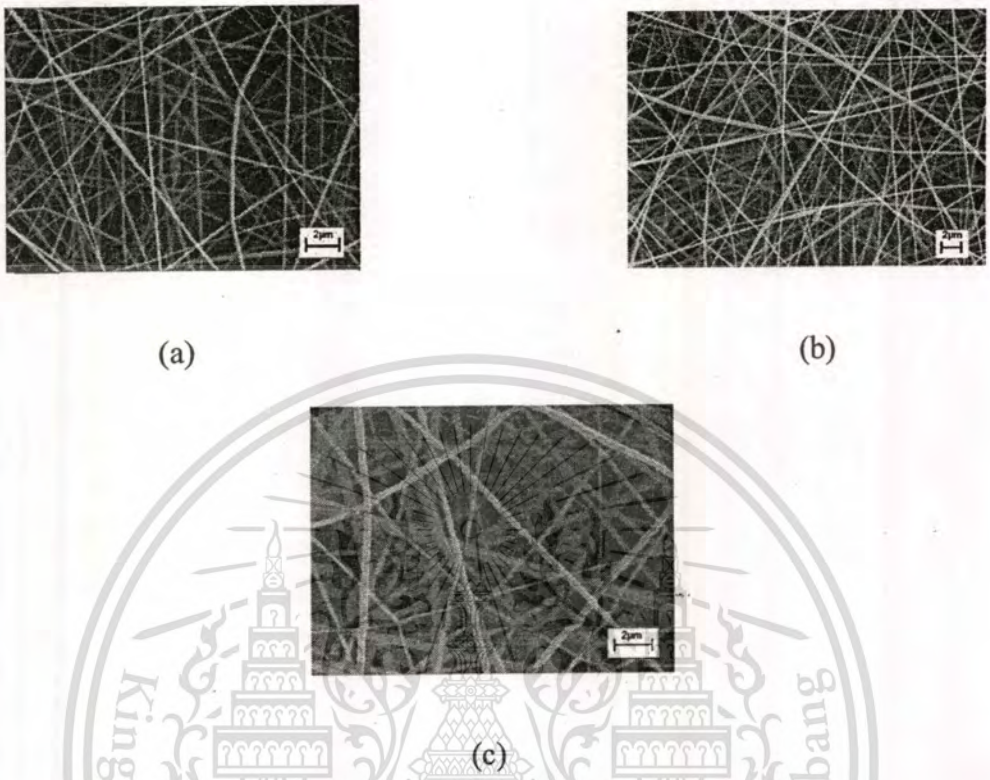

Figure 4.2 Selected SEM images of as-spun fibers from 16% (w/v) CA solutions in (a) 1:1, (b) 2:1, and (c) 3:1 (v/v) acetone-DMAc. These fibers were electrospun under applied electrostatic field strength of 12 kV/15 cm

The observed increase in fiber diameter with increasing acetone content could be because of the observed increase in the conductivity of the solutions. The increased conductivity results in increased electrostatic force on the jet, causing the jet to travel to the screen collector at a much greater speed. This, in turn, caused the onset of bending instability closer to the collector, resulting in a large reduction in the total path trajectory of the jet. This reduced path trajectory resulted in a decrease in the possibility of the jet being stretched by the Coulombic stress and the stress associated with the occurrence of the bending instability. The increased electrostatic force can also cause the mass throughput to increase which should be responsible for the

observed increase in the deposition area of the as-spun fiber mats (see Figure 4.3). Generally, higher dielectric constant and dipole moment of solvents tend to give higher electrical susceptibility of the solutions when they are subjected to an electrostatic field, which, in turn, help increase the mass throughput of the solutions from a spinneret.

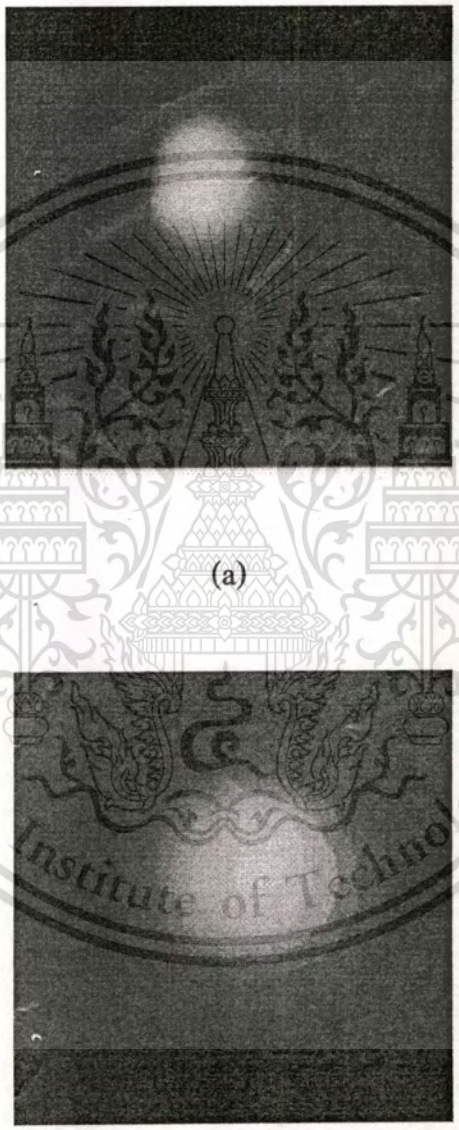

(a)

(b)

Figure 4.3 Optical images of as-spun fibers on stationary Al foils from solutions of (a) low, and (b) high electrostatic force

Table 4.3 Shear viscosity, surface tension, and conductivity of CA solutions in a variety of mixed-solvent systems, and diameters of the resulting as-spun fibers as a function of the volumetric ratio of the solvents

Sample	Ratio of mixed solvent (v/v)	Shear viscosity (mPa s)	Surface tension ($mN\ m^{-1}$)	Conductivity (μS/cm)	Fiber diameter (μm)
16% (w/v) CA solution in acetone-DMAc	1 : 1	399	30.6	5.14	0.16 ± 0.24
	2 : 1	390	29.9	5.61	0.23 ± 0.17
	3 : 1	384	32.2	6.72	0.32 ± 0.33
5% (w/v) CA solution in chloroform-MeOH	9 : 1	26.3	31.0	0.15	0.52 ± 0.23
	4 : 1	27.8	31.0	0.25	1.09 ± 0.27
	7 : 3	31.0	31.0	1.04	0.88 ± 0.26
	3 : 2	37.8	31.0	1.74	0.79 ± 0.21
	1 : 1	47.0	31.0	1.90	0.97 ± 0.37
5% (w/v) CA solution in DCM-MeOH	9 : 1	30.0	31.0	3.05	1.06 ± 0.56
	4 : 1	32.0	31.0	3.17	0.77 ± 0.22
	7 : 3	33.3	30.0	3.37	0.75 ± 0.21
	3 : 2	38.1	30.0	3.55	0.67 ± 0.19
	1 : 1	42.0	30.0	3.04	0.91 ± 0.34

Solution concentration is one of the important parameters in determining the range of concentrations from which continuous fibers can be obtained. To prepare fibers by electrospinning, proper polymer concentration and viscosity are required. To investigate the effect of solution concentration on the morphology and size of the as-spun CA fibers, CA solutions of different concentrations (12, 14, 16, 18, and 20% (w/v)) were prepared in 2:1 (v/v) acetone-DMAc. Some of the properties, i.e. shear

viscosity, surface tension, conductivity, and average fiber diameters are summarized in Table 4.4. The shear viscosity of the solutions increased regularly with increasing solution concentration; both surface tension and the conductivity should, theoretically, increase. The observed increase in shear viscosity with increasing concentration of the solutions was obviously a result of the increase in the chain entanglement.

Table 4.4 Shear viscosity, surface tension, and conductivity of CA solutions in 2:1 (v/v) acetone-DMAc and 4:1 (v/v) DCM-MeOH and diameters of the resulting as-spun fibers as a function of solution concentration

Sample	Concentration (%(w/v))	Shear viscosity (mPa s)	Surface tension ($mN\ m^{-1}$)	Conductivity (μS/cm)	Fiber diameter (μm)
2:1 (v/v) acetone-DMAc	12	155.0	28.0	4.83	0.14 ± 0.31
	14	260.0	28.3	4.81	0.19 ± 0.25
	16	390.0	29.9	5.61	0.23 ± 0.17
	18	545.0	29.7	5.51	0.33 ± 0.34
	20	928.0	30.0	5.48	0.37 ± 0.28
4:1 (v/v) DCM- MeOH	2	3.8	30.0	2.76	n/a
	4	14.5	31.0	2.55	0.48 ± 0.15
	6	49.8	31.0	3.10	0.96 ± 0.26
	8	130.0	31.0	3.26	1.10 ± 0.28
	10	297.0	32.0	3.47	1.58 ± 0.31
	12	664.0	32.0	3.22	1.23 ± 0.29

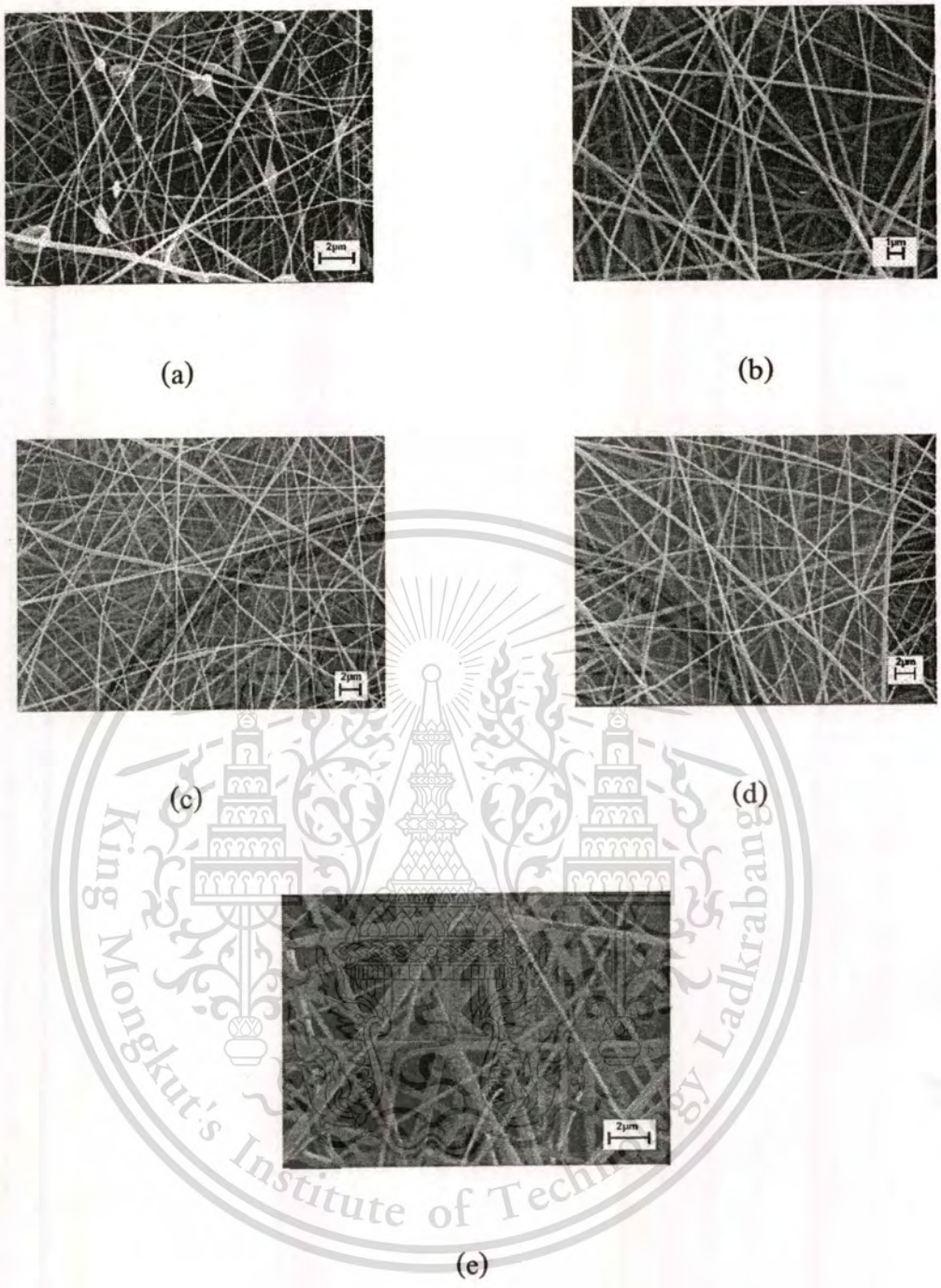

Figure 4.4 Selected SEM images of as-spun materials prepared from (a) 12, (b) 14, (c) 16, (d) 18, and (e) 20% (w/v) CA solution in 2:1 (v/v) acetone-DMAc. These fibers were electrospun under applied electrostatic field strength of 12 kV/15 cm

Figure 4.4 shows selected SEM images of the as-spun fibers after electrospinning of the CA solutions with an applied electrostatic field strength of 12 kV/15 cm. At 12% (w/v) a combination of smooth and beaded fibers was obtained. At this low concentration the low shear viscosity of the solution, hence the low viscoelastic force, was not sufficient to counter the stretching forces from both the electrostatic and Coulombic repulsion forces. Overstretching of the charged jet, as a result of these forces, resulting in partial breakup of the jet and, as a result of the surface tension, beads were formed on some of the fibers.

When the concentration of the solutions was varied between 14 and 20% (w/v), electrospinning of the solutions resulted in the formation of smooth fibers only. A result of the high viscoelastic force could counter the stretching forces, thus completely preventing partial breakup of the jet. On the basis of the SEM images shown in Figure 4.4, the diameters of the as-spun fibers increased regularly with increasing solution concentration. Specifically, the average diameter of the as-spun fibers increased from 0.14 μm when the concentration was 12% (w/v) to 0.37 μm when the concentration was 20% (w/v) (Table 4.4).

Chloroform and methanol

Because electrospinning of 5% (w/v) CA solutions in the individual solvents chloroform and MeOH produced discrete beads only, these solvents were mixed in different ratios (i.e. 9:1, 4:1, 7:3, 3:2, and 1:1 (v/v)). The mixed solvents were used to dissolve CA powder, at a fixed concentration at 5% (w/v), to prepare the spinning solutions. Some of the properties, i.e. shear viscosity, surface tension, and conductivity, of the CA solutions are summarized in Table 4.3. Evidently, the presence of MeOH caused both the shear viscosity and the conductivity of the CA solutions to increase regularly, possibly because of the different solubility of CA in these solvents and the greater dielectric constant of MeOH in comparison with that of

chloroform. Interestingly, the surface tension of the solutions was not affected by variation in the composition of the mixed solvents.

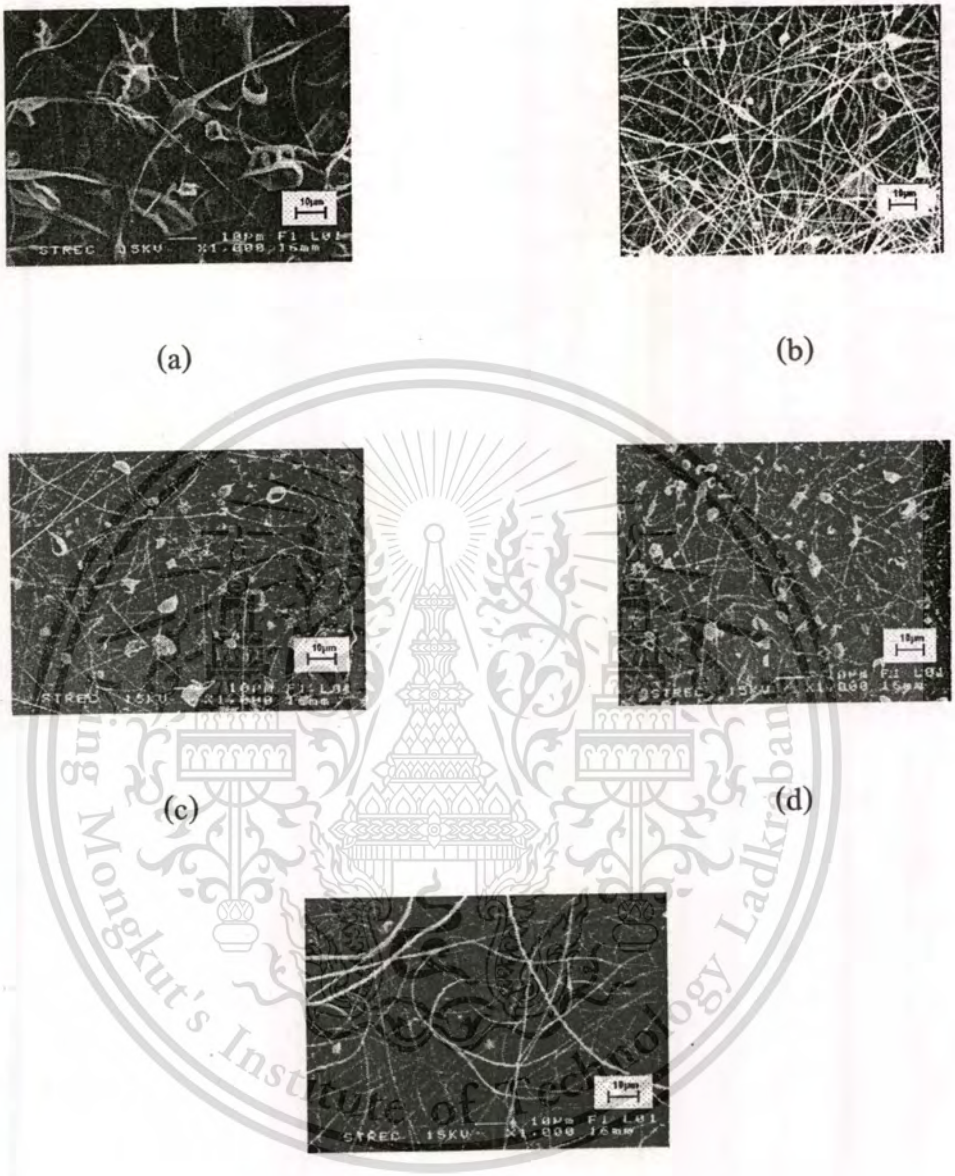

(a) (b)

(c) (d)

(e)

Figure 4.5 Selected SEM images of as-spun materials from 5% (w/v) CA solutions in (a) 9:1, (b) 4:1, (c) 7:3, (d) 3:2, and (e) 1:1 (v/v) chloroform-MeOH. These fibers were electrospun under applied electrostatic field strength of 12 kV/15 cm.

Figure 4.5 shows selected SEM images of the as-spun fibers after electrospinning of the CA solutions with an applied electrostatic field strength of 12 kV/15 cm. At a chloroform-MeOH ratio of 9:1 (v/v), discrete and very large beads with a rough surface were obtained. The rough surface was probably because rapid evaporation of chloroform (boiling point 61.2 °C, Table 4.1) caused the outer surface of the beads to "dry" first and subsequent evaporation of the solvent from inside the beads caused the skin to collapse. Increasing the MeOH content of the mixed solvents (i.e. ratios of the mixed solvent from 4:1 to 3:2 (v/v)) resulted in the formation of both beaded and smooth fibers, with the sizes of the beads decreasing with increasing MeOH content. Almost smooth fibers were obtained from the solution containing the largest amount of MeOH (i.e. solvents in the ratio 1:1 (v/v)). With regard to the size of the fibers obtained, irrespective of the composition of the mixed solvent, the average diameters of the fibers obtained (either smooth or beaded) were in the range 0.79-1.09 μm (excluding the as-spun materials from the CA solution in 9:1 (v/v) chloroform-MeOH, because of the presence of discrete beads). It should be noted that, for beaded fibers, the diameters were only measured on the fiber sections between the beads.

Dichloromethane and methanol

In the same way as for chloroform and MeOH, electrospinning of 5% (w/v) CA solutions in the individual solvents DCM and MeOH produced discrete beads only. Theses solvents were then mixed in different ratios (i.e. 9:1, 4:1, 7:3, 3:2, and 1:1 (v/v)) and used to dissolve CA powder to prepare spinning solutions at 5% (w/v). Some of the properties i.e. shear viscosity, surface tension, and conductivity, of the CA solutions are summarized in Table 4.3. Similarly to the CA solutions in chloroform-MeOH, the presence of MeOH caused both the shear viscosity and the conductivity of the CA solutions to increase regularly (except for the solution of CA in 1:1 DCM-MeOH, which had the lowest conductivity). Again, the surface tension of the solutions was not affected by variation of the composition of the mixed solvents. The observed

increase in the shear viscosity of the solutions should be a result of the greater shear viscosity of MeOH compared with that of DCM.

Electrospinning of the 5% (w/v) CA solution in DCM was impossible, because the extremely low boiling point of DCM caused the spinning solution to clog at the tip of the nozzle. Figure 4.6 shows selected SEM images of the as-spun fibers after electrospinning of the CA solutions with an applied electrostatic field strength of 12 kV/15 cm. For all ratios of the mixed solvents investigated, either beaded or smooth fibers without the presence of discrete beads were obtained. In comparison with the CA solutions in chloroform-MeOH, the amount of beads obtained was much lower, indicating better electrospinnability of the CA solutions in the current mixed-solvent system. Addition of MeOH, the boiling point of which is greater than that of DCM (Table 4.1), apparently substantially improved the electrospinnability of the resulting solutions.

With regard to the size of the fibers, irrespective of the composition of the mixed solvent the average diameters of the fibers obtained (either smooth or beaded) were in the range 0.67-1.06 μm. It is apparent from Table 4.3 that the conductivity of the solutions increased with increasing MeOH content (except for the solution of CA in 1:1 DCM-MeOH, which had the lowest conductivity) and this caused the diameters of the as-spun fibers to decrease. Although the increase in conductivity causes the jet to travel closer to the collector, before undergoing bending instability and a possible increase in mass throughput, it also causes the Coulombic stretching force to increase. While the former should cause the diameters of the as-spun fibers to increase, the latter one should be responsible for the observed decrease in the diameter of the fibers. It is postulated this is the reason for the conflicting results obtained in the literature [29].

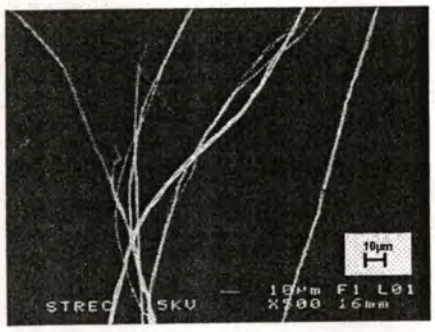

(a)

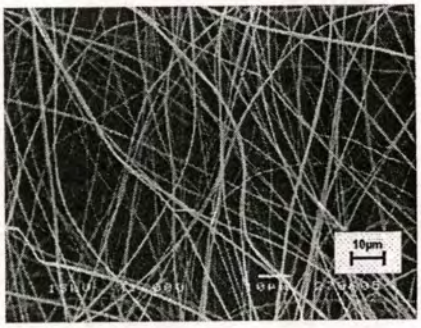

(b)

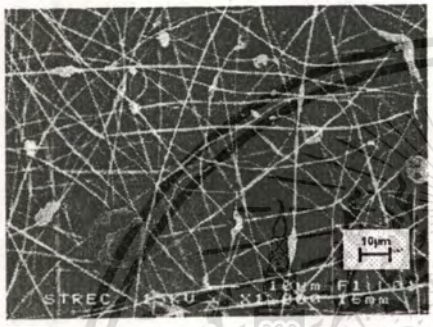

(c)

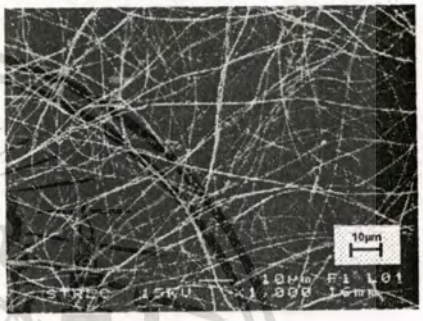

(d)

(e)

Figure 4.6 Selected SEM images of as-spun materials from 5% (w/v) CA solutions in (a) 9:1, (b) 4:1, (c) 7:3, (d) 3:2, and (e) 1:1 (v/v) DCM-MeOH. These fibers were electrospun under applied electrostatic field strength of 12 kV/15 cm

Among the different DCM-MeOH mixtures, the solution of CA in 4:1 (v/v) DCM-MeOH produced a large amount of fibers, with a smooth surface, within a fixed collection period of approximately 10 min. This particular condition was chosen for further investigation of the effect of solution concentration on morphology and/or size of the as-spun products. CA solutions in 4:1 (v/v) DCM-MeOH were then prepared at concentrations ranging from 2 to 12% (w/v). Some of the properties, i.e. shear viscosity, surface tension, and conductivity, of the CA solutions are summarized in Table 4.4. Obviously, the shear viscosity of the solutions increased regularly with increasing solution concentration, because of the increase in the chain entanglement. Similarly, the conductivity also increased slightly with increasing solution concentration, except for the solutions of concentration 4 and 12% (w/v). The reason for this is not unknown. Variation of the concentration of the solution did not seem to affect surface tension.

Electrospinning of these solutions was performed at fixed applied electrostatic field strength of 12 kV/15 cm. Figure 4.7 shows selected SEM images of the as-spun products. At 2% (w/v), discrete beads with non-uniform shape and size were obtained. The formation of discrete beads was, again, because of the low viscoelastic force (i.e. a result of the very low shear viscosity of the solution), which was not enough to counter the higher Coulombic stretching force, which later resulting in total break-up of the charged jet. At 4% (w/v) a combination of discrete beads and beaded fibers was observed. The observed increase in the shear viscosity of the solution caused the viscoelastic force to increase to a magnitude that was sufficient to prevent the total break-up of the charged jet. The presence of beads on the beaded fibers decreased significantly when the concentration of the solution increased to 6% (w/v). Total suppression of bead formation was observed when the concentration of the solution was increased to 8% (w/v), above which only smooth fibers were observed.

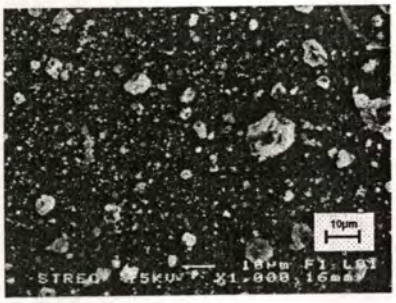

(a)

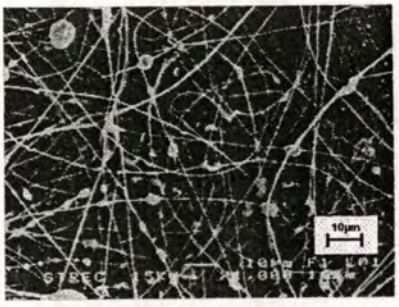

(b)

(c)

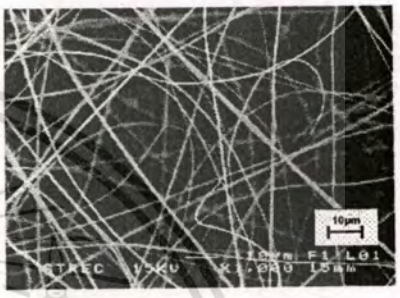

(d)

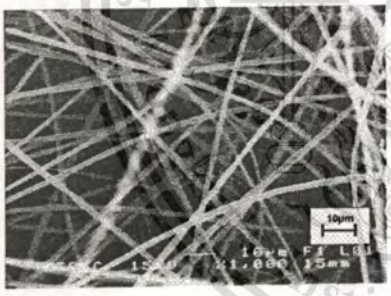

(e)

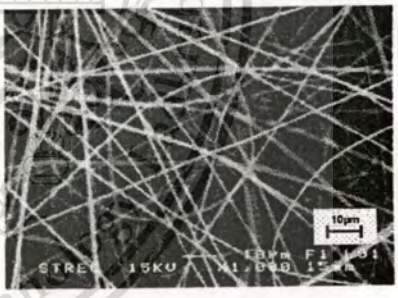

(f)

Figure 4.7 Selected SEM images of as-spun materials from (a) 2, (b) 4, (c) 6, (d) 8, (e) 10, and (f) 12% (w/v) CA solutions in 4:1 (v/v) DCM-MeOH. These fibers were electrospun under applied electrostatic field strength of 12 kV/15 cm

With regard to the size of the fibers obtained, the average diameter of the as-spun fibers increased from approximately 0.48 μm for 4% (w/v) to approximately 1.58 μm for 10% (w/v). One discrepancy was that the average diameter of the as-spun fibers from the 12% (w/v) solution was less than that of fibers from the 10% (w/v) solution. The increased concentration (i.e., increased viscoelastic force) enabled the charged jet to withstand larger Coulombic repulsion force, resulting in the observed larger diameters of the charged jet (ultimately, the as-spun fibers). The increased viscoelastic force also caused the onset for the bending instability to occur further away from the tip of the nozzle, causing the total path length that a jet segment traveled to the collector to decrease. The shorter path length decreased the probability for the charged jet to be elongated by the Coulombic repulsion force, hence the observed increase in the diameters of the fibers with increasing concentration.

The as-spun fibers from CA solutions in 4:1 (v/v) DCM-MeOH were systematically larger than those from CA solutions in 2:1 (v/v) acetone-DMAc, despite the much lower shear viscosity and conductivity of these solutions (Table 4.4). In addition, despite the much lower shear viscosity, fibers could be electrospun from CA solutions in 4:1 (v/v) DCM-MeOH in a much lower concentration range (i.e. ~ 4% (w/v) compared with ~ 12% (w/v) for CA solutions in 2:1 (v/v) acetone-DMAc).

Part 2 Release of model drugs from drug-loaded CA fiber mats and films

In this work, mats of CA ultrafine fibers were prepared by electrospinning and these electrospun fiber mats were used as carriers of drugs for total immersion drug delivery system. Four types of non-steroidal anti-inflammatory drugs (NSAIDs), i.e., naproxen (NAP), indomethacin (IND), ibuprofen (IBU), and sulindac (SUL) (all insoluble in water), were selected as "model drugs" and incorporated in the as-spun CA mats and studied their release behaviors. Table 4.5 summarizes some of the important information (i.e., molecular mass, melting temperature, solubility parameter, and pK_a) of CA and the model drugs.

Morphology and thermal property of the neat and the drug-loaded as-spun fiber mats, chemical integrity of drugs within the drug-loaded as-spun fiber mats, swelling and weight loss behavior of the neat and the drug-loaded as-spun mats in an aqueous medium, and release characteristics of the drugs from drug-loaded as-spun fiber mats were investigated by total immersion method. The main objectives of the present contribution were to fabricate electrospun mats of CA ultrafine fibers that contained either drugs, and to investigate the release characteristics of these substances from the drug-loaded as-spun CA fiber mats in comparison with those from the corresponding solution as-cast CA films.

Table 4.5 Molecular mass, melting temperature, solubility parameter, and pK_a for cellulose acetate and the model drugs

Material	Molecular mass ($g\ mol^{-1}$)	Melting temperature (^oC)	Solubility parameter $(Jcm^{-3})^{1/2}$	Water solubility (mg/L)	pK_a
Cellulose acetate	30,000	227-230	25.1	-	-
Naproxen (NAP)	230.3	153	21.0	15.9	4.15
Indomethacin (IND)	357.8	158	23.9	0.937	4.50
Ibuprofen (IBU)	206.3	75-77	19.1	49.0	4.91
Sulindac (SUL)	356.4	183	24.8	Insoluble (pH<4) , 3000 (pH ≥6)	4.70

4.2 Morphology of neat and drug-loaded as-spun CA mats

The as-prepared 16% (w/v) CA solution in acetone:DMAc (2:1 v/v) as the mixed solvent system under an electrical potential of 12 kV applied over a collection distance of 15 cm (i.e. the electrostatic field strength of 12 kV/15 cm). This concentration and solvent system were proved to be optimal conditions for

electrostatic spinning of cellulose acetate in the previous topic. Figure 4.8 shows a selected SEM image of the obtained as-spun CA fibers. Clearly, only smooth fibers were obtained. The average diameter of these fibers was about 230 ± 17 nm. Based on the uniformity of the obtained as-spun fibers, the as-prepared CA solution was used as the based solution into which four different model drugs were individually added (i.e., 20 wt.% based on the weight of CA powder). After complete dissolution of the model drugs, the resulting solutions were measured for their shear viscosity, conductivity, and surface tension as summarized in Table 4.6. For CA solutions loaded with 20 wt.% of all drugs, the addition of the drugs into the CA solutions decreases the surface tension from those of the neat CA solution as the drugs act as a plasticizer to the polymer. Incorporation of small molecules in-between the polymer chains increases the mobility and flexibility of the chains, resulting in a lowering of the surface tension. On the other hand, the addition of these drugs caused the viscosity of the resulting solutions to increase from that of the neat CA solution. For NAP- and IND-containing in CA solutions, the viscosity of the solutions increased slightly, while conductivity decreased, from those of the neat CA solution. For CA solutions loaded sulindac (SUL), it was found that the conductivity and viscosity were increased due to their chemical structures.

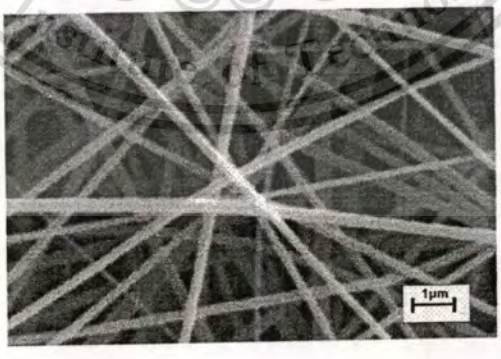

Figure 4.8 SEM image of electrospun CA fibers from CA in acetone:DMAc (2:1) solutions with 16% (w/v) concentrations and 12 kV of applied voltage. Original magnification 5000x.

These solutions were later electrospun and the selected SEM images of the drug-loaded as-spun CA fiber mats are shown in Figure 4.9. It was obvious that the addition of the drugs within the CA solution not affected significantly to the morphological appearance and size of the resulting fibers to those of the as-spun fibers from the neat CA solution. Their surfaces were smooth, uniform (no bead-and-string morphology), and oriented fibers. All these indicated that the drugs were finely incorporated into the electrospun CA fibers, with the average diameters of these fibers ranging between 263 and 297 nm (see Table 4.6).

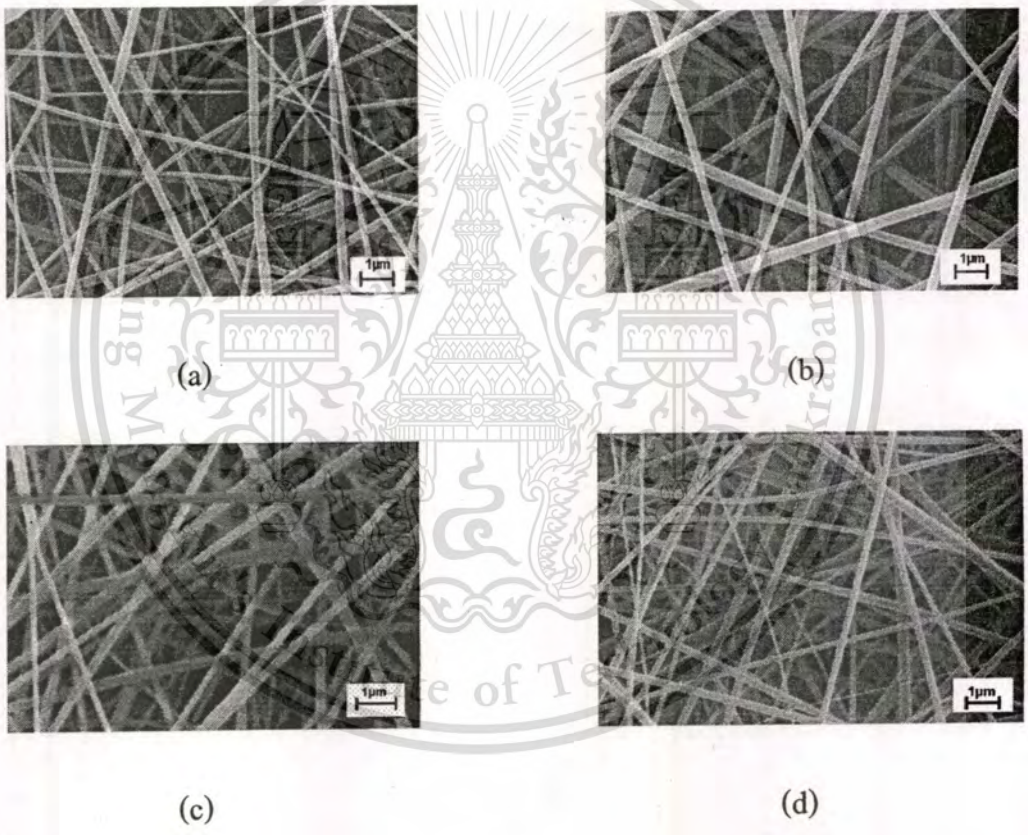

Figure 4.9 Selected SEM images (magnification = 5,000x) of drug-loaded as-spun CA fiber mats from (a) NAP, (b) IND, (c) IBU, and (d) SUL at a fixed amount of 20% by weight of CA. The electrostatic field strength was 12 kV/15 cm and the collection time was 10 min

Additionally, since neither presence of the drug crystals nor other kinds of drug aggregates was observed on the surfaces of these fibers, it was postulated that the drugs were encapsulated well within the fibers.

This was in contrast to the drug-loaded solvent-cast CA films which evidently showed the presence of either drug crystals or other kinds of drug aggregates on their surfaces (see Figure 4.10). The non-existence or the existence of the drug aggregates on the surface of the drug-loaded fibers or the drug-loaded films could also be due to the difference in the evaporation rate of the solvent during fabrication. The evaporation of the solvent from the fibers occurred in an extremely short time (i.e., during their flight to the collective device). On the other hand, the evaporation of the solvent from the films occurred in a much longer time interval. The much longer time for evaporation of the solvent from the drug-loaded as-cast CA films could be responsible for the observation of the drug aggregates on these films.

Table 4.6 Some properties of neat and drug-containing CA solutions and the average diameters of these fibers

Type of CA solution	Viscosity (mPa s)	Conductivity (μS /cm)	Surface tension ($mN\ m^{-1}$)	Fiber diameters (nm)
Neat	419 ± 1.2	5.58 ± 0.50	35.2 ± 0.20	231 ± 17
NAP-containing	431 ± 0.6	5.27 ± 0.13	32.8 ± 0.13	263 ± 19
IND-containing	426 ± 0.8	5.34 ± 0.00	33.7 ± 0.28	297 ± 14
IBU-containing	415 ± 1.5	5.16 ± 0.08	30.6 ± 0.34	279 ± 11
SUL-containing	435 ± 1.0	6.18 ± 0.11	31.5 ± 0.08	286 ± 24

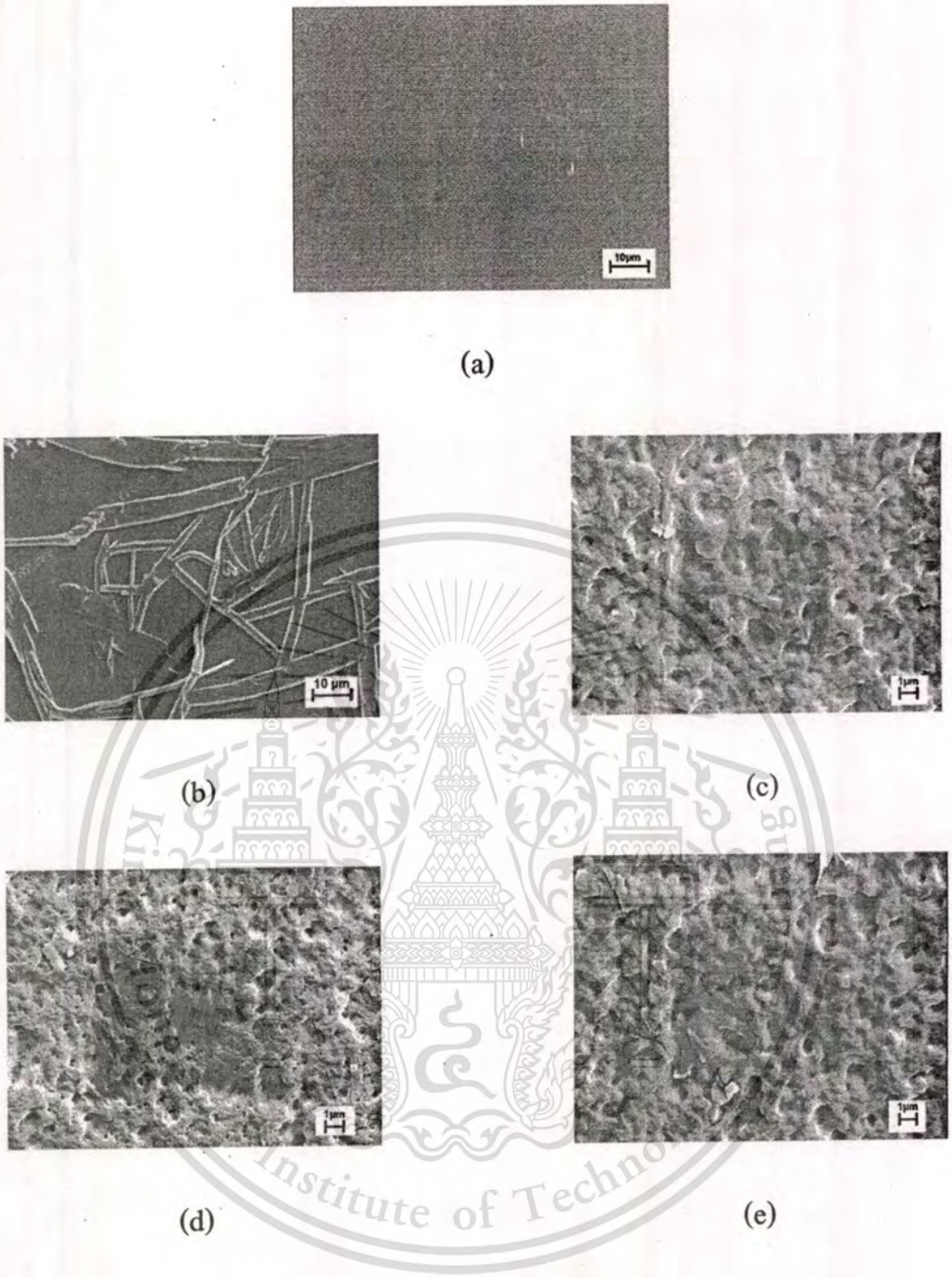

Figure 4.10 Selected SEM images (magnification = 5000x) of solvent-cast films from (a) neat 12% w/v CA solution in 2:1 v/v acetone:DMAc and the solutions containing (b) NAP, (c) IND, (d) IBU, and (e) SUL at a fixed amount of 20% by weight of CA

4.3 Chemical integrity of drugs in drug-loaded as-spun CA mats

Due to the application of a high electrical potential to the drug-containing CA solutions during the electrospinning, it is questionable whether the chemical integrity of the drugs would be intact after such a treatment. In order to verify that, drug-loaded as-spun CA fiber mats were dissolved in DMSO-d_6 and the resulting drug-containing solutions were investigated by ^{1}H-NMR. The solution from the neat as-spun CA fiber mat in DMSO-d_6 was used as an internal control. All the ^{1}H-NMR spectra along with the chemical structures of the model drugs are illustrated in Figure 4.11.

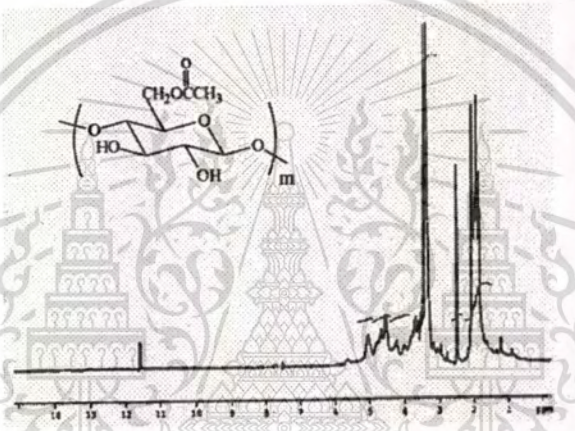

(a)

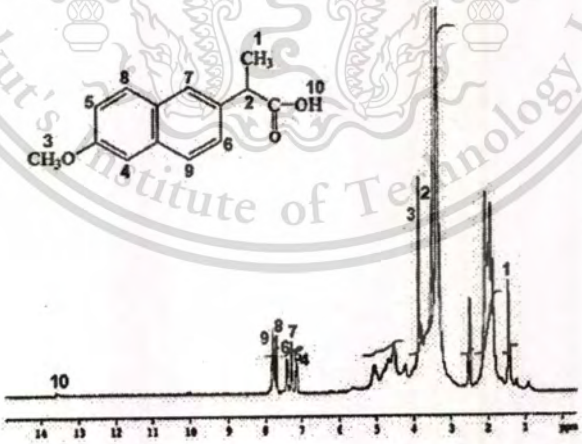

(b)

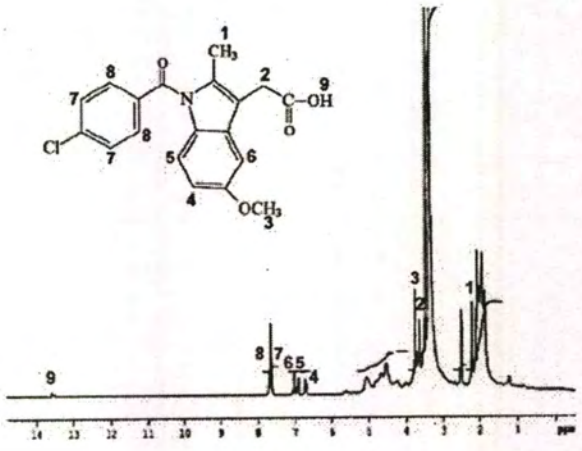

(c)

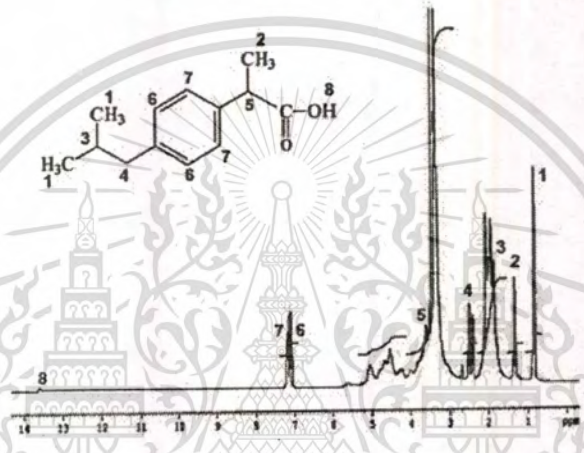

(d)

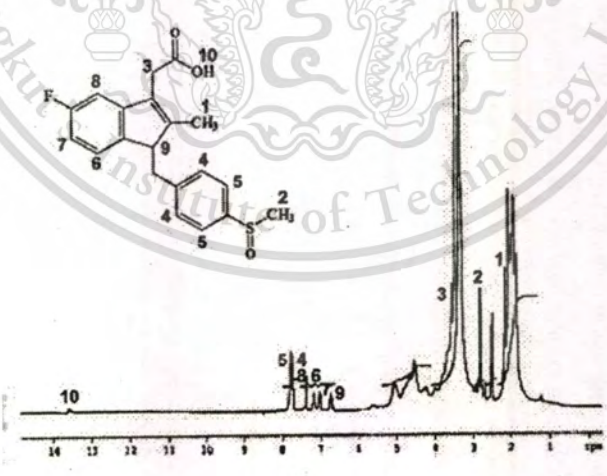

(e)

Figure 4.11 ^{1}H nuclear magnetic resonance spectra of neat and drug-loaded electrospun CA fiber mats after being dissolved in DMSO-d_6: (a) neat, (b) NAP-, (c) IND-, (d) IBU-, and (e) SUL-loaded electrospun CA fiber mats

The obtained results showed that the chemical integrity of all the model drugs was intact after the electrospinning process. The ^{1}H-NMR spectra from both pure and drug-loaded as-spun CA mats also exhibit similar characteristic peaks at the same chemical shift positions. From this results confirmed that the electrospinning process did not affect the chemical integrity of the drugs.

4.4 Thermal properties of neat and drug-loaded as-spun CA mats

The thermal properties of the neat electrospun and drug-loaded as-spun CA fiber mats were measured by DSC and TGA techniques. DSC was performed to determine the physical form of the model drugs in the non-woven nanofibrous mats as well as of the unmanipulated materials. Figure 4.12 shows DSC thermograms for the model drugs and the neat and the drug-loaded electrospun CA fiber mats. Within the temperature range investigated, all of the model drugs showed a single endothermic thermal transition, with the peak temperatures being observed at ~153, 160, 77, and 185 °C for NAP, IND, IBU, and SUL, respectively. These values corresponded to the melting transition of the model drugs (see Table 4.5). These peaks were absent or almost absent from the corresponding DSC thermograms for the drug-loaded electrospun CA fiber mats. Since neither presence of the drug crystals nor other kinds of drug aggregates was observed on the surfaces of these fibers and the chemical integrity of the drugs after electrospinning was intact, it is postulated that the absence of the melting peaks of drugs was due to the inability of the drug molecules to form crystalline aggregates within the fibers. The most likely reason was the extremely rapid evaporation of the solvent from the fibers during electrospinning, as previously mentioned.

The neat electrospun CA fiber mat exhibited two endothermic thermal transitions, with the low-temperature endotherm (i.e., 50-110 °C) corresponding to the loss of moisture coupled with a glass transition, while the higher-temperature endotherm (i.e., 215-233 °C) corresponding to the melting range of the material (see

Table 4.5). The glass transition temperature of CA was reported to occur over a wide temperature range, depending on the degree of acetyl substitution of the polymer, while the melting of CA (degree of polymerization ≈ 500-600; DS ≈ 2.4) in the form of solvent-cast film was reported to occur over a wide temperature range with the peak temperature being observed at ~ 224 °C. All of the drug-loaded electrospun CA fiber mats also exhibited a loss of moisture coupled with a glass transition over about the same temperature range as that of the neat electrospun CA fiber mat, while their melting range was either disappeared or different from that of the neat electrospun CA fiber mat.

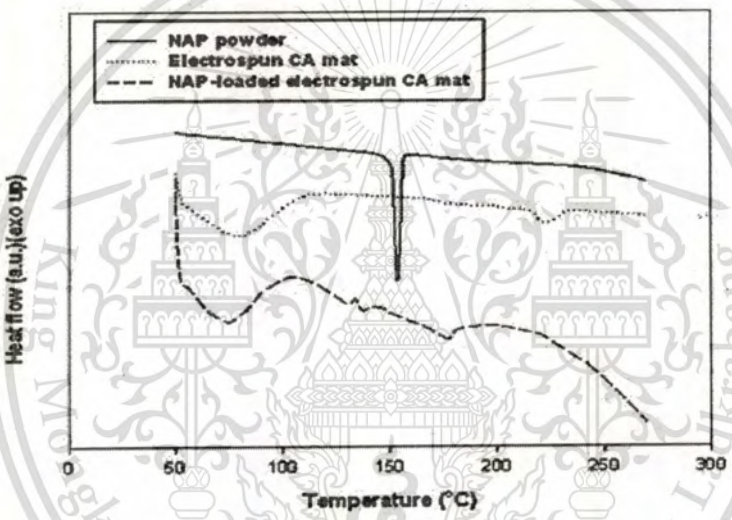

(a)

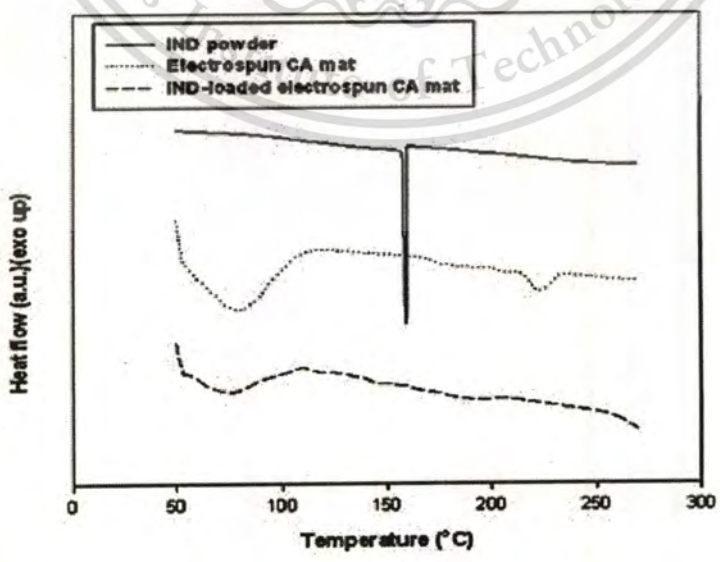

(b)

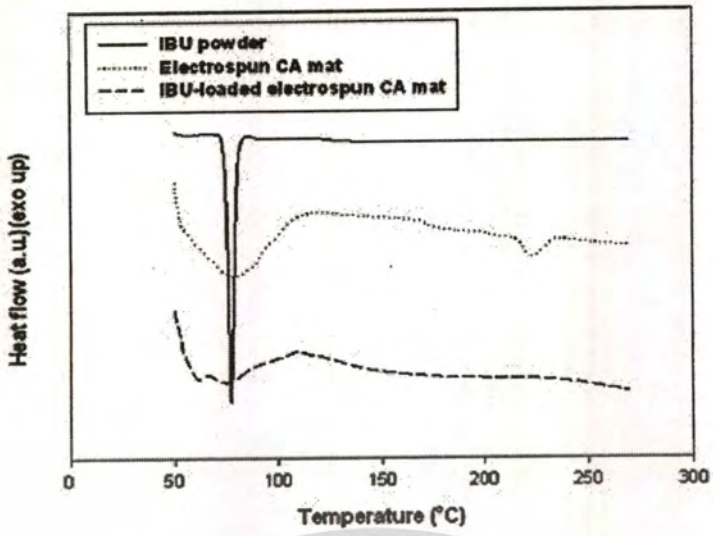

(c)

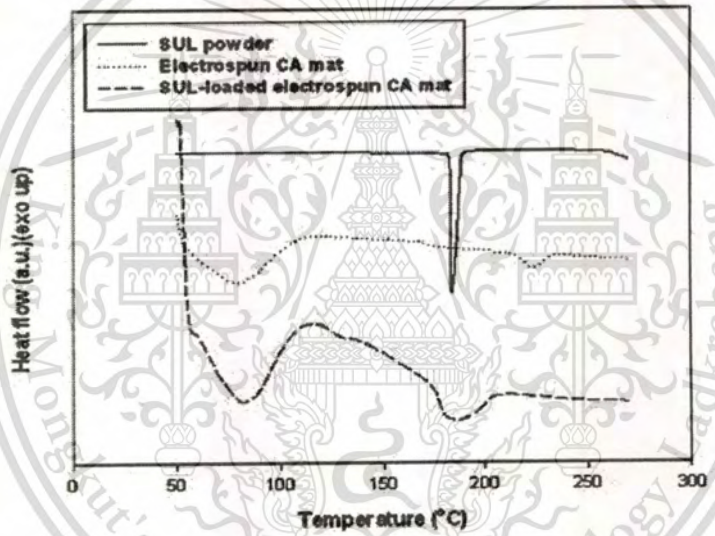

(d)

Figure 4.12 Differential scanning calorimetric thermograms of neat electrospun CA mat, pure model drugs of (a) NAP-, (b) IND-, (c) IBU-, and (d) SUL-, and corresponding drug-loaded electrospun CA fiber mats

Figure 4.13 shows TGA thermograms for the model drugs and the neat and the drug-loaded electrospun CA fiber mats. NAP, IND, and IBU exhibited one step in the loss of their mass, while SUL showed two such steps. Specifically, NAP showed the loss of its mass over the temperature range of 180-330 °C, IND over the temperature

range of 220-380 °C, IBU over the temperature range of 145-245 °C, and SUL over the temperature ranges of 230-290 and 320-550 °C. Interestingly, only SUL had the char content of about 43% at 700 °C. The neat CA fiber mat exhibited two steps in the loss of its mass, with the first covering the temperature range of 35-120 °C corresponding to the loss of moisture (about 3%) and the second covering the temperature range of 250-410 °C corresponding to the thermal degradation of the material. The char content at 700 °C for the neat CA fiber mat was about 12%.

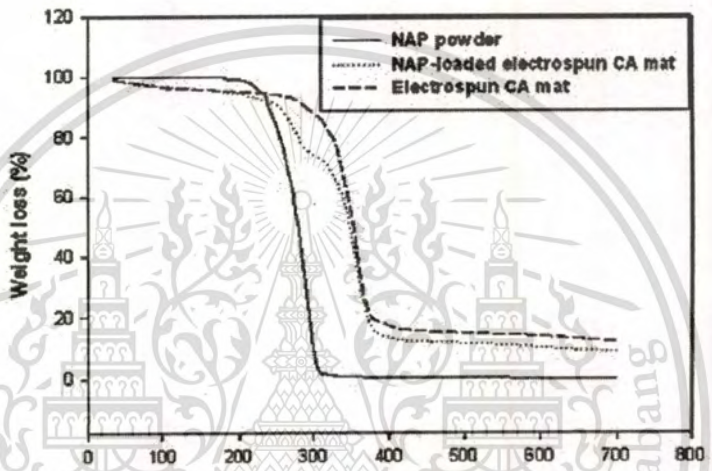

(a)

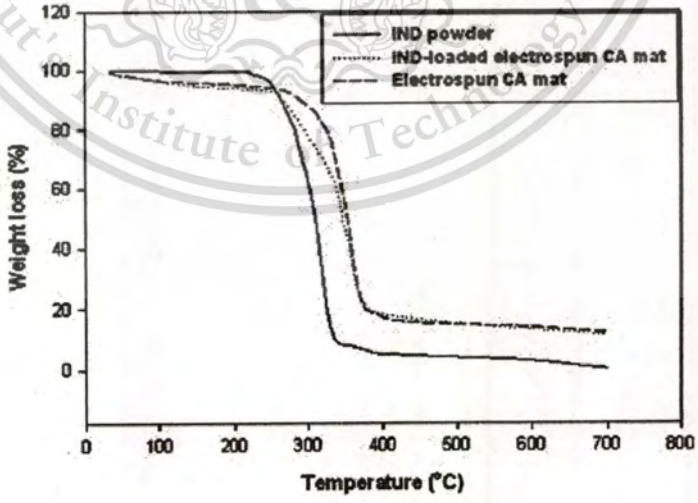

(b)

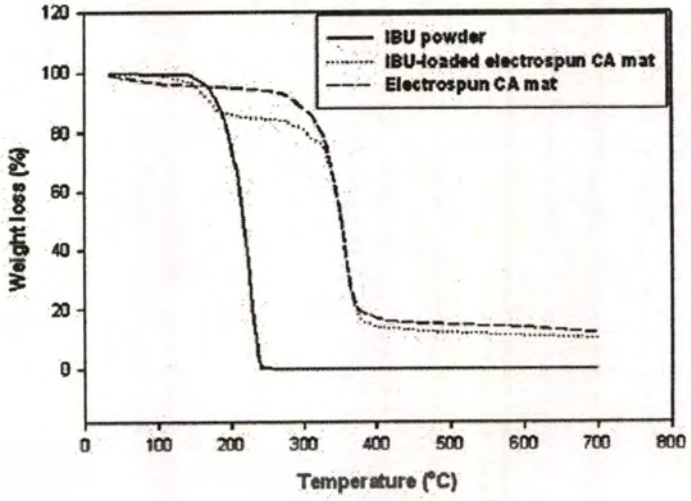

(c)

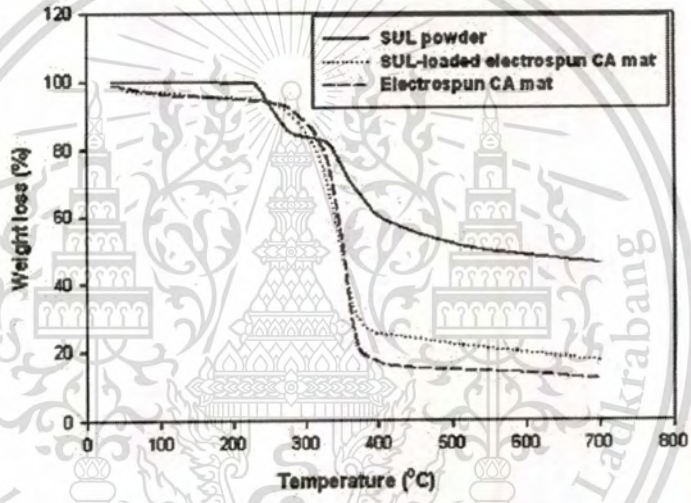

(d)

Figure 4.13 Thermogravimetric thermograms of neat electrospun CA fiber mat, pure model drugs of (a) NAP-, (b) IND-, (c) IBU-, and (d) SUL-, and corresponding drug-loaded electrospun CA fiber mats

Most of the drug-loaded electrospun CA fiber mats, except for IBU-loaded electrospun CA fiber mat, exhibited the loss of moisture over the temperature range of 35-120 °C and most of the drug-loaded electrospun CA fiber mats, except for SUL-loaded electrospun CA fiber mat, showed two more steps in the loss of their mass, obviously corresponding to the thermal degradation of the drugs and the CA matrix.

SUL-loaded electrospun CA fiber mat was the only material that showed a greater char content than that of the neat CA fiber mat, confirming the presence of the drug within the material.

4.5 Swelling behavior of neat and drug-loaded as-spun CA fiber mats and as-cast CA films

The neat and the drug-loaded electrospun CA fiber mats were further characterized to determine their swelling behavior after submersion in the acetate buffer solution at 37 °C for 24 hr (see Figure 4.14). The degree of swelling of the neat electrospun CA fiber mat was 715%. In all of the drug-loaded electrospun CA fiber mats exhibited slightly lower values of swelling (i.e., 570-630%) when compared with that of the neat electrospun CA fiber mat. On the other hand, the corresponding solvent-cast films did not swell in the testing medium solution under the experimental condition. Consequently, the large amount of water absorbed in the electrospun CA fiber mats, shown in Figure 4.14, should attribute to the amount of water that is physically absorbed in the individual fibers and the amount of water that is retained by the capillary action in the inter-fibrous pores.

Figure 4.15 shows weight loss of both the neat and the drug-loaded electrospun CA fiber mats and the corresponding solvent-cast films after submersion in the acetate buffer solution at 37 °C for 24 hr. Evidently, the percentages of weight loss for the neat fiber mats and films were low (i.e., 1.1 and 0.6%, respectively). The percentage of weight loss for the neat electrospun CA fiber mats after submersion in distilled water for 24 hr was in the range of 1.1-1.7%. Since CA is soluble in glacial acetic acid [52], it should be partially soluble in the acetate buffer solution. However, due perhaps to the high crystallinity of the neat fiber mats (as inferred from the presence of the melting endotherm for the neat electrospun CA fiber mat; see Figure 4.12) and films that limits the accessability of the buffer solution, the percentage of weight loss for both types of materials was then low.

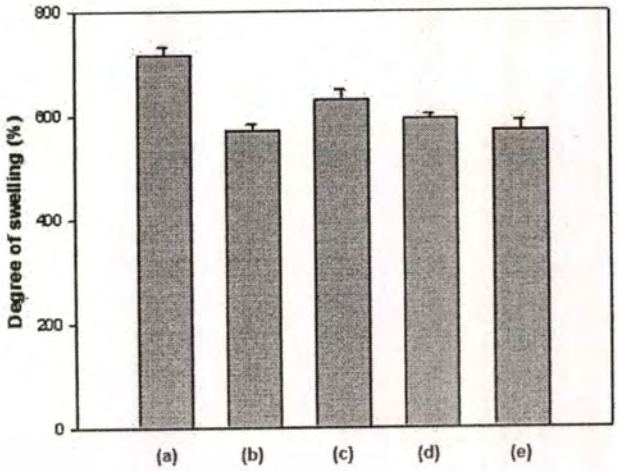

Figure 4.14 Degree of swelling (%) of (a) neat, (b) NAP-, (c) IND-, (d) IBU-, and (e) SUL-loaded electrospun CA fiber mats

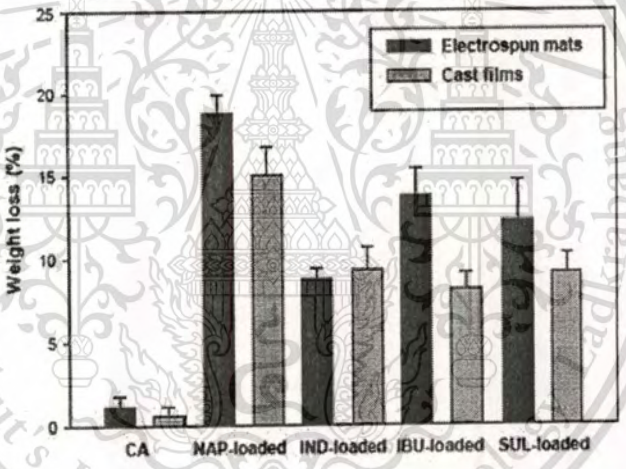

Figure 4.15 Weight loss (%) of neat and drug-loaded electrospun CA fiber mats and corresponding solvent-cast films, respectively

On the contrary, due to the suppression of the crystallization of the CA matrix in the presence of the drugs (as inferred from the absence of the melting endotherm for the drug-loaded electrospun CA fiber mats; see Figure 4.12), all of the drug-loaded fiber mats and films showed much greater weight loss than the neat materials. Generally, the fiber mat samples exhibited greater weight loss than the corresponding films, due possibly to the ability of the fiber mat samples to swell in the testing

medium. Specifically, the percentage of weight loss for NAP-loaded electrospun CA fiber mat was the greatest at 18.8%, followed by those of IBU-, SUL-, and IND-loaded electrospun CA fiber mats at 13.7, 12.2, and 8.7%, respectively, while that for NAP-loaded as-cast CA film was the greatest at 15.0%, followed by those of IND-, SUL-, and IBU-loaded as-cast CA films at 9.3, 9.1, and 8.2%, respectively. Noticeably, the weight losses of both fibers and films were due to the loss of drug molecules which were released by the aqueous solutions from inside their fibers and surface of their films.

Though not shown, the physical integrity of the neat and the drug-loaded electrospun CA fiber mats was retained (no shrinkage characteristic) after submersion in acetate buffer solution at 37 °C for 24 hr. Both the degree of swelling and the weight loss of these samples were to be discussed along with the results on the release characteristics of the model drugs from these samples in the following section.

4.6 Release of model drugs from drug-loaded as-spun CA mats and as-cast CA films

Prior to investigating the release characteristics of the model drugs from both the drug-loaded as-spun CA fiber mats and the corresponding as-cast CA films, the actual amount of the model drugs within these samples was needed to determine. Table 4.7 summarizes the actual amount of the drugs present within these samples (reported as the percentage of the initial content of the drugs loaded in both the spinning and casting solutions, i.e., 20 wt.% based on the weight of CA powder). For the drug-loaded electrospun CA fiber mats, the actual amount of the drugs within these samples was in the range of 84-93%, while, for the drug-loaded as-cast CA films, it was in the range of 81-90%.

Table 4.7 Actual amount of model drugs within drug-loaded electrospun CA mats and as-cast CA films. The original amount of the model drugs loaded in the spinning and the casting solutions was 20% based on the weight of CA.

Types of drug	Actual amount of drug based on the original amount of the drug loaded (%)	
	Drug-loaded electrospun CA mats	Drug-loaded as-cast CA films
Naproxen	91.2 ± 1.68	90.3 ± 3.43
Indomethacin	87.6 ± 3.12	86.9 ± 4.18
Ibuprofen	93.3 ± 1.43	81.4 ± 3.11
Sulindac	83.5 ± 2.47	88.6 ± 2.78

Ideally, the actual amount of the drugs present in the drug-loaded as-spun and as-cast CA films should be 100%. The discrepancy from the ideality should be due to the inhomogeneous distribution of the drugs in different areas of the fiber mats and films, which could be influenced by the fabrication techniques (e.g., the change in the local composition of the solutions during electrospinning and solvent-casting). These values were used as basis to arrive at the cumulative release of the drugs from these drug-loaded materials.

The release characteristics of the model drugs from the drug-loaded as-spun CA fiber mats and the corresponding as-cast CA films were carried out by the total immersion method, using the acetate buffer solution pH 5.5 as the transferring medium, at a controlled temperature of 37 °C. The cumulative release of the drugs (reported as the percentage of the actual amount of the drugs present within the drug-loaded samples) as a function of immersion time from the drug-loaded fiber mat and the as-cast film samples is shown in Figure 4.16. The results are shown in two ranges of the immersion time, i.e., 0-1440 and 0-120 min. At any given immersion time point, the release of the drugs from the drug-loaded electrospun CA fiber mats was greater than that from the corresponding as-cast films.

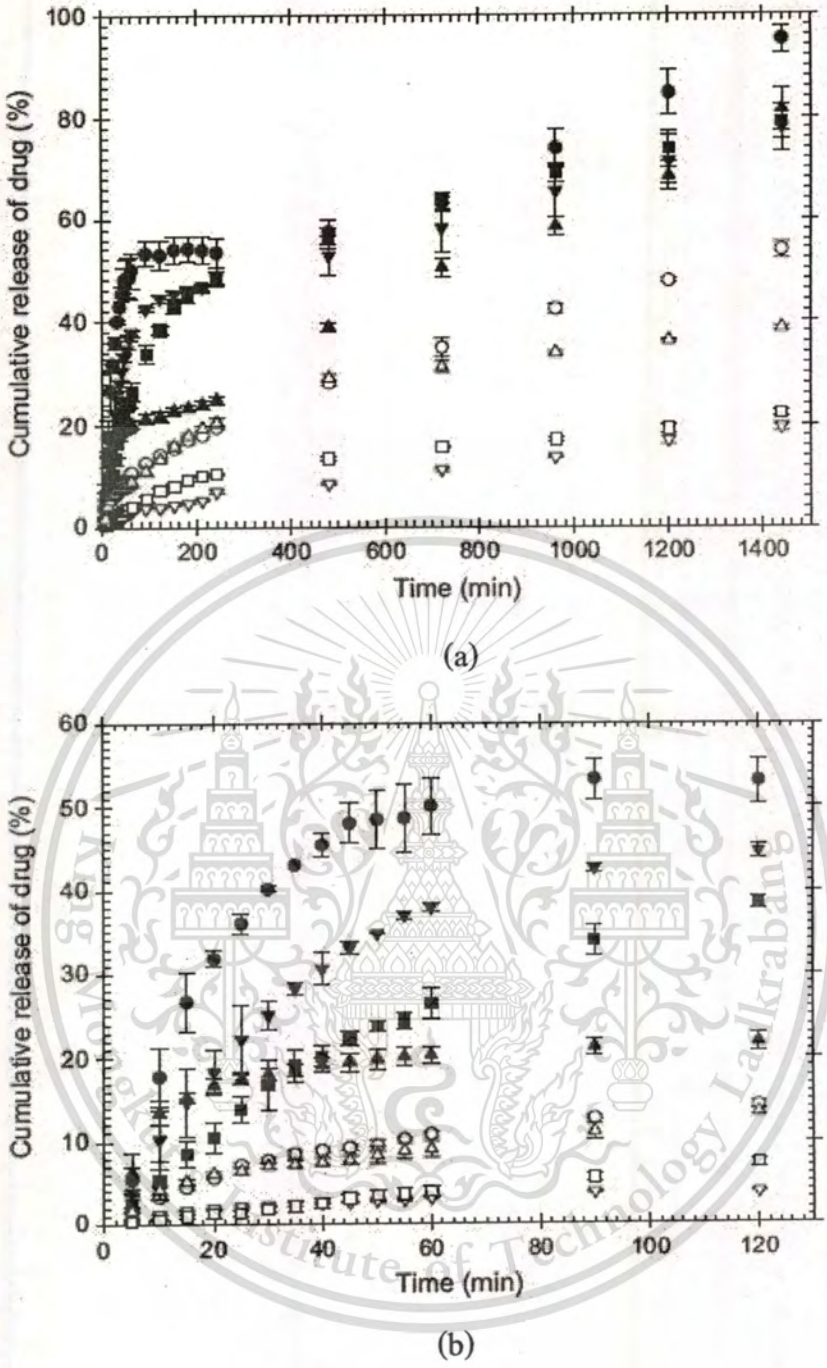

Figure 4.16 Cumulative release profiles of model drugs from (●) NAP-, (■) IND-, (▲) IBU-, and (▼) SUL-loaded electrospun CA fiber mats (closed symbols) and as-cast CA films (open symbols) by total immersion technique during (a) 0-1440 min and (b) 0-120 min.

Evidently, NAP released from the NAP-loaded electrospun CA fiber mat showed a burst release during the first 60 min, leveled off between 60 and 300 min after immersion, and monotonously increased to reach the maximum value at 24 hr (i.e., ~95%). The rapid release of NAP from the drug-loaded fiber mat was possibly due to the lack of interactions between the drug and the CA matrix and the high degree of swelling and the high solubility of the drug-loaded fiber mat in the testing medium (see Figures 4.14 and 4.15). The release of IND, IBU, and SUL from the corresponding drug-loaded electrospun CA fiber mats was relatively smoother (without the obvious presence of the plateau region), with the maximum release of the drugs at 24 hr being about 79, 81, and 78%, respectively. The maximum release of the drugs from the drug-loaded fiber mats could be ranked as follows: NAP- > IBU- > IND- > SUL-loaded electrospun CA fiber mats, while the molar mass of the drugs could be ranked as follows: IBU < NAP < SUL ≈ IND (see Table 4.5).

All of the drug-loaded as-cast CA films showed a monotonous and gradual increase in the amount of the drugs released with increasing the immersion time. In comparison with the drug-loaded electrospun CA fiber mats, the drugs released from the drug-loaded film counterparts were much slower and the maximum amount of the drugs released was also much lower. Specifically, the maximum release of NAP, IND, IBU, and SUL from the drug-loaded films at 24 hr was found to be about 54, 22, 39, and 19%, respectively. As a result, the maximum release of the drugs from the drug-loaded films could be ranked as follows: NAP- > IBU- > IND- > SUL-loaded as-cast films, which, obviously, are in the same order as that for the drug-loaded electrospun CA fiber mats. The much slower rates and the lower maximum amount of the drugs released from the drug-loaded films in comparison with those from the fiber mat counterparts could be due to the inability of the films to swell and to the lower weight loss in the testing medium (see Figures 4.14 and 4.15) as well as to the much lower specific surface area (cf. SEM images in Figures 4.9 and 4.10).

Prior to the drug release assay, all of the drug-loaded as-cast CA films exhibited some kinds of drug aggregates on their surfaces (see Figure 4.10), but, after the drug release assay at 24 hr, the surfaces of all of the drug-loaded films were as smooth as that of the neat one (i.e., Figure 4.10a). This led us to believe that the release of the drugs from the drug-loaded films was due mainly to the gradual dissolution of the drug aggregates on the film surfaces, while the diffusion of the drugs incorporated within the films occurred in a much lesser extent. On the contrary, since no presence of the drug aggregates was found on the surface of the drug-loaded fiber (see Figure 4.9), the release of the drugs from the drug-loaded fiber mats was mainly by the diffusion of the drugs from the fibers as the fiber mats could swell appreciably in the testing medium. While the fibrous morphology of the drug-loaded fiber mats after the drug release assay at 24 hr was still intact, the average diameter of the individual fibers of the mats was found to decrease slightly (results not shown).

The ability of a drug to release from a polymer matrix depends on many factors, e.g., the solubility of the drug in the polymer matrix, the solubility of the drug in the testing medium, the swelling ability and the solubility of the polymer matrix in the testing medium, the diffusion of the drug from the polymer matrix, etc. Among these, the swelling and the solubility of the drug in the polymer matrix are the main contributing factors. According to Figure 4.14, the swelling of all the drug-loaded electrospun CA fiber mats was inferior to that of the neat one. Among the various drug-loaded fiber mat samples, the one that contained IND showed the greatest swelling in the testing medium, while all others showed equivalent values. Based on the swelling studies, the ability for NAP to release from the NAP-loaded electrospun CA fiber mat should be the greatest, which is different from what was observed here. On the other hand, the results on the weight loss of both the drug-loaded fiber mats and films in the testing medium indicated that, for the drug-loaded fiber mats, NAP-loaded electrospun CA fiber mat should show the greatest release of NAP, followed by IBU-, SUL-, and IND-loaded ones, respectively, while for the drug-loaded films, NAP-

loaded as-cast CA film should, again, show the greatest release of NAP, followed by the rest of the materials as they showed equivalent values.

The solubility of the drug in the polymer matrix is controlled by the solubility parameters of both the drug and the polymer matrix [90, 91]. The solubility parameter (δ) relates directly to the cohesive energy density of a compound. Generally, the smaller the difference in the solubility parameters between the two components is, the greater their miscibility will be. The difference in the solubility parameters between a model drug and the polymer matrix is therefore a useful guide to determine the miscibility of the drug and the polymer matrix, and hence the ability of the drug to release from the polymer matrix. According to Table 4.5, the difference in the solubility parameters between CA [25.1 $(J\ cm^{-3})^{1/2}$] and SUL [24.8 $(J\ cm^{-3})^{1/2}$] was the smallest, followed by that between CA and IND [23.9 $(J\ cm^{-3})^{1/2}$], CA and NAP [21.0 $(J\ cm^{-3})^{1/2}$], and CA and IBU [19.1 $(J\ cm^{-3})^{1/2}$], respectively. Based on these values, the ability for the model drug to release from the CA matrix should fall in the following order: IBU > NAP > IND > SUL, which is slightly different from what was observed in this work.

<u>Part 3</u> Comparison the release of indomethacin from IND-loaded CA fiber mats in various methods

The procedure and conditions for the preparation of IND-loaded CA fiber mats were the same as above in Part 2. A selected SEM image of the obtained fibers is shown in Figure 4.17. Clearly, cross-sectionally round fibers with smooth surface were obtained. The average diameter of these fibers (n = 50) was determined to be 327 ± 31 nm. The release characteristics of the indomethacin from the IND-loaded as-spun CA fiber mats were carried out by 3 methods of the release assay, i.e., (1) the total immersion method with the addition of fresh medium, (2) without the addition of fresh medium and (3) with sequential dipping in fresh medium, respectively.

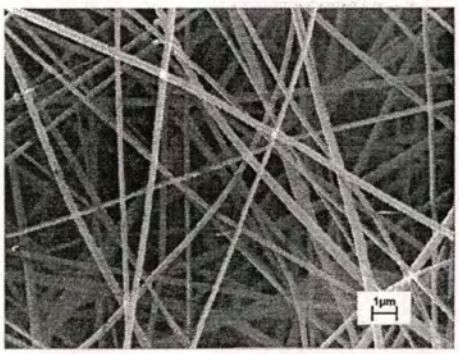

Figure 4.17 Selected scanning electron micrograph (5,000x) of electrospun fibers from 16% w/v CA solution in 2:1 v/v acetone:DMAc and the solutions containing indomethacin (IND) at a fixed amount of 20% by weight of CA. The electrostatic field strength was 12 kV/15 cm and the collection time was 10 min.

Prior to investigating the release characteristic of IND-loaded electrospun CA fiber mats, the actual amount of the drug within these samples was needed to determine. The actual amount of indomethacin within the electrospun fiber mats from the CA solution that contained the initial amount of indomethacin at 20 wt% was 90.1 ±2.58. The cumulative amount of the indomethacin released (reported as the percentage of the actual amount of indomethacin present in the IND-loaded samples) from the IND-loaded samples is illustrated in Figure 4.19. The results are shown in two ranges of the immersion time, i.e., 0-1440 and 0-160 min. The IND-loaded as-spun fiber mat samples in method 1 showed the burst release during the first 60 min and reached a steady increase at the maximum release of ~75% with further increase in the immersion time. On the other hand, the IND-loaded as spun fiber mat samples in method 2 showed a gradual increase in the cumulative release of indomethacin over the 24 hr testing period and the maximum amount of indomethacin released from the as-spun fiber mat samples was ~65%. The fact that the indomethacin released from method 1 exhibited the much greater release than method 2 was due possibly to

distinguish the diffusion between the drug which was encapsulated within the fibers and the medium buffer solution.

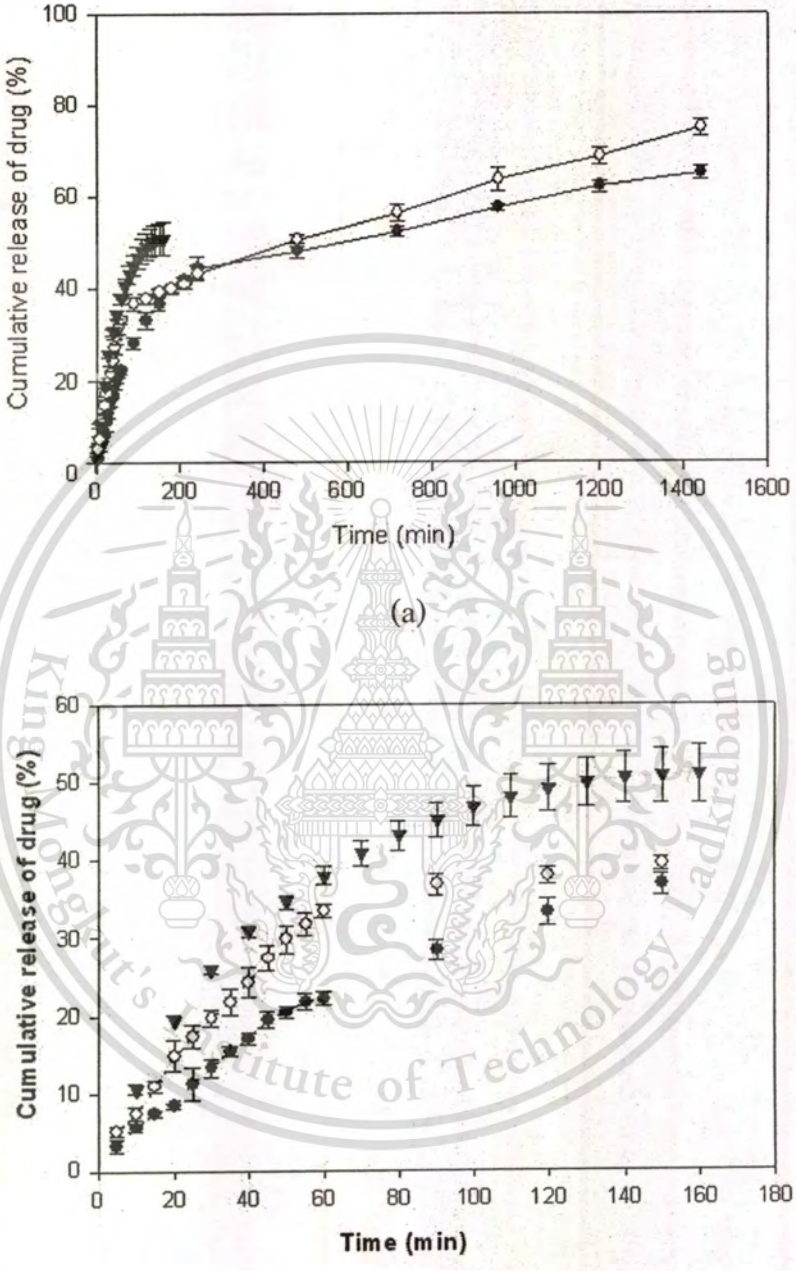

Figure 4.18 Cumulative release profiles of IND-loaded electrospun CA fiber mats from (○) with the addition of fresh buffer, (●) without the addition of fresh buffer during 0-1440 min, and (▼) with sequential dipping in fresh buffer during (a) 0-1440 min and (b) 0-160 min.

Generally, drug diffusion was transferred directly through the fiber membrane from a region of higher concentration to one of lower concentration in an aqueous medium solution. For the total immersion method in method 2, the amount of the drug released from the drug-loaded samples increased monotonically with diffusion time, but, over a longer immersion period, the rate of the drug released was much slower when compared with that in method 1. Due to, initially, the inner drug diffusion transfer could be continue until the outer drug concentration in buffer solution was more higher than within the fibers at the critical point which could be interrupted the ability of diffusion of drug to an aqueous medium. Comparatively, much lower diffusion time was observed for the study of the release characteristic of indomethacin in method 3 which showed an initial burst release and the maximum amount of IND released was ~51% after diffusion time at 160 min (see Figure 4.19b).

4.7 Release kinetics of model drugs from drug-loaded as-spun CA mats and as-cast CA films

The release kinetics of drug from a carrier is often characterized using the Ritger-Peppas equation [92-94]:

$$\frac{M_t}{M_\infty} = kt^n, \quad \text{for } \frac{M_t}{M_\infty} < 0.6, \tag{1}$$

where M_t is the accumulative amount of drugs released at an arbitrary time t, M_∞ is the accumulation amount of drugs released at an infinite time, n is an exponent characterizing the mechanism with which the release kinetics can be described, and k is the rate of release of the drugs that incorporates physical characteristics of the matrix/drug system as well as some physical contributions from the measurement methods.

For $n = 0.5$ the release mechanism can be described as Fickian diffusion [95]. For Fickian diffusion, a straight line is expected when the fractional accumulative amount of drug released (i.e. M_t / M_∞) is plotted as a function of $t^{0.5}$. It is also found

that the kinetic constant (k) from equation 1 was valid over an initial period of time and based on Fick's laws. The results from such analyses (i.e. parameter k and r^2, which signifies the goodness of the fit) are summarized in Table 4.8.

Table 4.8 Analyses of the release kinetics of the model drugs from drug-loaded as-spun CA mats and as-cast CA films based on the Fickian diffusion type of release mechanism.

Type of sample	Rate parameter k ($min^{-0.5}$)	r^2
Drug-loaded as-spun CA mats		
with 20 wt.% naproxen (NAP)	0.0845	0.9614
with 20 wt.% indomethacin (IND)	0.0510	0.9899
with 20 wt.% ibuprofen (IBU)	0.0254	0.8326
with 20 wt.% sulindac (SUL)	0.0805	0.9979
Drug-loaded as-cast CA films		
with 20 wt.% naproxen (NAP)	0.0247	0.9795
with 20 wt.% indomethacin (IND)	0.0383	0.9833
with 20 wt.% ibuprofen (IBU)	0.0340	0.9791
with 20 wt.% sulindac (SUL)	0.0213	0.9669
IND drug-loaded as-spun CA mats		
with the addition of fresh medium	0.0719	0.9897
without the addition of fresh medium	0.0533	0.9927
with sequential dipping in fresh medium	0.1265	0.9989

Apparently, the rate parameter k for all of the drug-loaded as-spun CA mats ranged between 0.0254 and 0.0845 $min^{-0.5}$, which that for all of the drug-loaded as-cast CA films ranged between 0.0213 and 0.0383 $min^{-0.5}$. In part 3, the kinetic rate release of the drugs (k) from the IND-loaded fiber mats could be ranked as follows: Method 3 > 1 > 2 (see Table 4.8).

CHAPTER 5

CONCLUSIONS

5.1 Conclusions

5.1.1 Effect of solvent system on morphology and fiber diameter

In this work the effects of solvent system and solution concentration on the morphological appearance and/or size of electrospun cellulose acetate (CA) products were prepared in a range of single-solvent systems (acetone, chloroform, *N,N*-dimethylformamide (DMF) , dichloromethane (DCM), methanol (MeOH), formic acid, and pyridine) and in a variety of mixed-solvent systems (acetone-DMAc, chloroform-MeOH, and DCM-MeOH). Some of the properties of the CA solutions i.e. shear viscosity, surface tension, and conductivity was measured. The morphological appearance and/or size of the as-spun products were/was investigated by use of scanning electron microscopy (SEM). Despite the solubility of CA in chloroform, DMF, DCM, MeOH, formic acid, and pyridine, electrospinning of the resulting solutions (5% w/v) resulted in the formation of discrete beads only whereas electrospinning of the 5% w/v solution of CA in acetone produced short and beaded fibers. Interestingly, at the same solution concentration, i.e. 5% w/v, electrospinning of solutions of CA in some chloroform-MeOH and DCM-MeOH mixtures produced beaded and smooth fibers. In particular, for both mixed-solvent systems at 4:1 (v/v) a large amount of fibers was obtained. The average diameters of the fibers obtained from the CA solutions in these mixed-solvent systems were in the ranges 0.79-1.09 μm for chloroform-MeOH and 0.67-1.06 μm for DCM-MeOH. For all solvent systems investigated smooth fibers were obtained from 16% w/v solutions of CA in 1:1, 2:1, and 3:1 v/v acetone-DMAc, 14-20% w/v solutions of CA in 2:1 acetone-DMAc, and 8-12% w/v solutions of CA in 4:1 v/v DCM-MeOH. For the as-spun fibers from solutions of CA in acetone-DMAc the average diameter ranged between 0.14 and 0.37

μm and for fibers prepared from solutions in DCM-MeOH it ranged between 0.48 and 1.58 μm.

5.1.2 Release of model drugs from drug-loaded CA fiber mats and films

Drug-loaded cellulose acetate (CA; acetyl content = 39.8%; *Mw* = 30000 Da) mats of electrospun fibers were successfully fabricated by an electrospinning technique from 16% w/v CA solutions in 2:1 v/v acetone-DMAc and were developed as transdermal drug delivery system. Four types of non-steroidal anti-inflammatory drugs (NSAIDs), i.e., naproxen (NAP), indomethacin (IND), ibuprofen (IBU), and sulindac (SUL) were incorporated in the electrospun CA fiber mats. These drugs are used in the symptomatic management of painful and inflammatory conditions. The amount of the drugs in the solutions was fixed at 20 wt.% based on the weight of CA powder. The morphology of the electrospun mats depended on the properties of the drugs containing polymer solutions which, in turn, were affected by the type of the model drugs incorporated. Three main factors that affected morphology of the electrospun fiber mats were viscosity, conductivity, and surface tension of the solutions. The drug-loaded electrospun CA fiber mats was cross-sectionally round fibers with smooth surface, with the average diameters of these fibers ranging between 263 and 297 nm. No presence of the drug aggregates of any kind was observed on the surfaces of these fibers, suggesting that the drugs were encapsulated well within the fibers. On the contrary, the corresponding drug-loaded solvent-cast CA films showed evidence of drug aggregates on their surfaces.

All of the drug-loaded electrospun CA fiber mats swelled very well after submersion in the acetate buffer solution at 37 °C for 24 hr (i.e., 570-630%), while the corresponding film counterparts did not swell at all in the same medium. While the percentage of weight loss for the neat fiber mats and films was low (i.e., 1.1 and 0.6%, respectively), that for the drug-loaded fiber mat and film samples was much greater (ranging from 8.7 to 18.8% for drug-loaded fiber mats and from 8.2 to 15.0% for drug-loaded films). The actual amount of the model drugs in the drug-loaded fiber mat and

film samples was determined to range between about 84 and 93% for the drug-loaded fiber mats and between about 81 and 90% for the drug-loaded films. Finally, the release characteristics of the model drugs from these samples (reported as the percentage of the weight of drugs divided by the actual weight of drugs in the fiber mat specimens) were carried out by the total immersion method in the acetate buffer solution at 37 °C. At any given immersion time point, the amount of the drugs released from the drug-loaded electrospun CA fiber mats was greater than that from the corresponding as-cast films. Since the electrospun fibers contain a very large surface to volume ratio and a short diffusion passage length, the drug release profiles of the electrospun membranes are very different from those of the bulk films with the same sample thickness. The unique nanostructure morphology of the membranes could provide several advantages for controlled delivery of drugs over the bulk films. The maximum release of the drugs from both the drug-loaded fiber mats and films was found in the following order: NAP > IBU > IND > SUL.

Indeed, replotting the IND-loaded as-spun release data in the form of M_t/M_∞ versus square root of time could be described with such an equation, indicating the Fickian diffusion type of the release mechanism of that drug. The kinetic rate release of the drugs (k) for all of the drug-loaded as-spun CA mats ranged between 0.0254 and 0.0845 $min^{-0.5}$, which that for all of the drug-loaded as-cast CA films ranged between 0.0213 and 0.0383 $min^{-0.5}$.

5.1.3 Comparison the release of indomethacin from IND-loaded CA fiber mats in various methods

The release characteristics of the indomethacin from the IND-loaded as-spun CA fiber mats were carried out by 3 methods of the release assay, i.e., (1) the total immersion method with the addition of fresh medium, (2) without the addition of fresh medium and (3) with sequential dipping in fresh medium, respectively. The total amount of the drug released from the IND-loaded as-spun CA fiber mats was about 75,

66, and 51% for method 1, 2, and 3, respectively. The kinetic rate release of the drugs (k) from the IND-loaded fiber mats could be ranked as follows: Method 3 > 1 > 2.

5.2 **Recommendations**

In this work, it must be noted that the electrospinning setup used only a conventional syringe which limited the feed rate of the solutions. The solutions should be delivered via syringe pump to control the mass flow rate.

It should be noted that the nature of both the drug and the polymer matrix could affect the release characteristic of the drug and the morphology appearance of the obtained fibers. In order to develop this contribution for a specific use of drug delivery system, the drug and the polymer matrix had to be appropriately chosen in order to achieve the suitable release characteristic for specific applications.

REFERENCES

[1.] Deitzel, J. M.; Kleinmeyer, J. D.; Hirvonen, J. K.; Beck Tan, N. C. Polymer **2001**, 42, 8163-8170.

[2.] Fong, H.; Reneker, D. H. Electrospinning and the formation of nanofibers; Hanser Gardner Publications: NY, **2001**.

[3.] Deitzel, J. M.; Kosik, W.; McKnight, S. H.; Tan, N. C. B.; DeSimone, J. M.; Crette, S. Polymer **2002**, 43, 1025-1029.

[4.] Buchko, C. J.; Chen, L. C.; Shen, Y.; Martin, D. C. Polymer **1999**, 40, 7397-7407.

[5.] Wang, X.; Kim, Y.-G.; Drew, C.; Ku, B.-C.; Kumar, J.; Samuelson, L. A. Nano Letters **2004**, 4, 331-334.

[6.] Jiang, H.; Fang, D.; Hsiao, B. S.; Chu, B.; Chen, W. Biomacromolecules **2004**, 5, 326-333.

[7.] Ding, B.; Kimura, E.; Sato, T.; Fujita, S.; Shiratori, S. Polymer **2004**, 45, 1895-1902.

[8.] Bognitzki, M.; Czado, W.; Frese, T.; Schaper, A.; Hellwig, M.; Steinhart, M.; Greiner, A.; Wendroff, J. H. Advanced Materials (Weinheim, Germany) **2001**, 13, 70-72.

[9.] Norris, I. D.; Shaker, M. M.; K., K. F.; MacDiarmid, A. G. Synthetic Metals **2000**, 109-114.

[10.] Ziabicki, A. In Fundamentals of Fiber Formation. Wiley Interscience: NY, **1976**.

[11.] Bose, G. M. Recheres sur la cause et sur la veritable theorie del'electricite: Wittenberg, **1745**.

[12.] Raleigh, L. London, Edinburgh, and Dublin Phil. Mag. J. **1882**, 44, 184-186.

[13.] Zeleny, Journal of Physical Review **1917**, 10, 1-6.

[14.] Vonnegut, B.; Neubauer, R. L. Journal of Colloid Science **1952**, 7, 616-622.

[15.] Taylor, G. I. Proceeedings of the Royal Society, London **1964**, 280, 383-397.

[16.] Michelson, D. Electrostatic Atomization: Bristol, UK, **1990**.

[17.] Formhals, A.US, 2,123,992, **1934**

[18.] Simons, H. L.US, 3,280,229, **1966**

[19.] Isakoff, L.US, 3, 593,074, **1971**

[20.] Fine, J.; Passaic, N. J.; Sigismondo, A. T.US, 4,223,101, **1980**

[21.] Guignard, C.US, 4,230,650, **1980**

[22.] Guignard, C.US, 4,287,139, **1981**

[23.] Martin, G. H.; Derek, I.US, 4,043,331, **1977**

[24.] Martin, G. H.; Derek, I.US, 4,044,404, **1977**

[25.] Bornat, A.US, 4,323,525, **1982**

[26.] Simm, W. L.; Claus, G. O.; Bonart, R. B.; Bela, V. F. G.US, 4,069,026, **1978**

[27.] Scardino, F. L.; Balonis, R. J.US, 6,106,913,, **2000**

[28.] Zarkoob, S.; Reneker, D. H.; Ertley, D.; Eby, R. K.; Hudson, S. D.US, 6,110, 590, **2000**

[29.] Baumgarten, P. K. J. Colloid Interface Sci. **1971**, 36, 71-79.

[30.] Larrondo, L.; Manley, R. S. J. Journal of Polymer Science: Polymer Physics **1981**, 19, 909- 919.

[31.] Larrondo, L.; Manley, R. S. J. Journal of Polymer Science: Polymer Physics **1981**, 19, 921-932.

[32.] Larrondo, L.; Manley, R. S. J. Journal of Polymer Science: Polymer Physics **1981**, 19, 933-940.

[33.] Doshi, J.; Reneker, D. H. Journal of Electrostatics **1995**, 35, 151-160.

[34.] Chun, I., Fine fibers spun by electrospinning process from polymer solutions and polymer melts in air and vacuum: characterization of structure and morphology on electrospun fibers and developing a new process model, University of Akron, OH, PhD Dissertation, **1995**

[35.] Spivak, A. F.; Dzenis, Y. A. Journal of Applied Mechanics **1999**, 66, 1026-1028.

[36.] Reneker, D. H.; Yarin, A. L.; Fong, H.; Koombhongse, S. Journal of Applied Physics **2000**, 87, 4531-4547.

[37.] Shin, Y. M.; Hohman, M. M.; Brenner, M. P.; Rutledge, G. C. Applied Physics Letters **2001**, 78, 1149-1151.

[38.] Reneker, D. H.; Kataphinan, W.; Theron, A.; Zussman, E.; Yarin, A. L. Polymer **2002**, 43, 6785-6794.

[39.] Fong, H.; Chun, I.; Reneker, D. H. Polymer **1999**, 40, 4585-4592.

[40.] Demir, M. M.; Yilgor, I.; Yilgor, E.; Erman, B. Polymer **2002**, 43, 3303-3309.

[41.] Deitzel, J. M.; Kleinmeyer, J.; Harris, D.; Beck Tan, N. C. Polymer **2000**, 42, 261-272.

[42.] Zhao, S.; Wu, X.; Wang, L.; Huang, Y. Journal of Applied Polymer Science **2004**, 91, 242-246.

[43.] Khil, M. S.; Kim, H. Y.; Kim, M. S.; Park, S. Y.; Lee, D.-R. Polymer **2004**, 45, 295-301.

[44.] Koski, A.; Yim, K.; Shivkumar, S. Materials Letters **2003**, 58, 493-497.

[45.] Jaeger, R.; Schonherr, H.; Vansco, G. J. Macromolecules **1996**, 29, 7634-7636.

[46.] Kattamuri, N.; Shawon, J.; Sung, C. Polymer Preprints (American Chemical Society, Division of Polymer Chemistry) **2003**, 44, 763-764.

[47.] McKee, M. G.; Wilkes, G. L.; Colby, R. H.; Long, T. E. Macromolecules **2004**, 37, 1760-1767.

[48.] Colby, R. H.; Fetters, L. J.; Funk, W. G.; Graessley, W. W. Macromolecules **1991**, 24, 3873-3882.

[49.] Colby, R. H.; Rubinstein, M.; Daoud, M. Journal de Physique II **1994**, 4, 1299-1310.

[50.] Colby, R. H.; Rubinstein, M.; Viovy, J. L. Macromolecules **1992**, 25, 996-998.

[51.] Lee, K. H.; Kim, H. Y.; La, Y. M.; Lee, D. R.; Sung, N. H. Journal of Polymer Science: Part B: polymer Physics **2002**, 40, 2259-2268.

[52.] Liu, H.; Hsieh, Y.-L. Journal of Polymer Science, Part B: Polymer Physics **2002**, 40, 2119-2129.

[53.] Kameoka, J.; Orth, R.; Yang, Y.; Czaplewski, D.; Mathers, R.; Coates, G. W.; Craighead, H. G. Nanotechnology **2003**, 14, 1124-1129.

[54.] Kameoka, J.; Craighead, H. G. Applied Physics Letters **2003**, 83, 371-373.

[55.] Czaplewski, D. A.; Kameoka, J.; Mathers, R.; Coates, G. W.; Craighead, H. G. Applied Physics Letters **2003**, 83, 4836-4838.

[56.] Zong, X.; Kim, K.; Fang, D.; Ran, S.; Hsiao, B. S.; Chu, B. Polymer **2002**, 43, 4403-4412.

[57.] Rangkupan, R.; Reneker, D. H. Journal of Metals, Materials and Minerals **2003**, 12, 81-87.

[58.] Kim, J.-S.; Reneker, D. H. Polymer Engineering and Science **1999**, 39, 849-854.

[59.] Bergshoef, M. M.; Vancso, G. J. Advanced Materials (Weinheim, Germany) **1999**, 11, 1362-1365.

[60.] Fong, H.; Liu, W.; Wang, C.-S.; Vaia, R. A. Polymer **2001**, 43, 775-780.

[61.] Gibson, P.; Schreuder-Gibson, H. MD American Society of Mechanical Engineers **2000**, 91, 45-61.

[62.] Gibson, P.; Schreuder-Gibson, H.; Rivin, D. Colloids and Surfaces, A: Physicochemical and Engineering Aspects **2001**, 187-188, 469-481.

[63.] Gibson, P.; Schreuder-Gibson, H.; Pentheny, C. Journal of Coated Fabrics **1998**, 28, 63-72.

[64.] Hajra, M. G.; Mehta, K.; Chase, G. G. Separation and Purification Technology **2003**, 30, 79-88.

[65.] Boland, E. D.; Wnek, G. E.; Simpson, D. G.; Pawlowski, K. J.; Bowlin, G. L. Journal of Macromolecular Science, Pure and Applied Chemistry **2001**, A38, 1231-1243.

[66.] Matthews, J. A.; Wnek, G. E.; Simpson, D. G.; Bowlin, G. L. Biomacromolecules **2002**, 3, 232-238.

[67.] Li, W.-J.; Laurencin Cato, T.; Caterson Edward, J.; Tuan Rocky, S.; Ko Frank, K. Journal of biomedical materials research **2002**, 60, 613-621.

[68.] Yoshimoto, H.; Shin, Y. M.; Terai, H.; Vacanti, J. P. Biomaterials **2003**, 24, 2077-2082.

[69.] Xu, C. Y.; Inai, R.; Kotaki, M.; Ramakrishna, S. Biomaterials **2004**, 25, 877-886.

[70.] Mo, X. M.; Xu, C. Y.; Kotaki, M.; Ramakrishna, S. Biomaterials **2004**, 25, 1883-1890.

[71.] Kenawy, E.-R.; Bowlin, G. L.; Mansfield, K.; Layman, J.; Sanders, E.; Simpson, D. G.; Wnek, G. E. Journal of Controlled Release **2002**, 81, 57-64.

[72.] Sanders, E. H.; Kloefkorn, R.; Bowlin, G. L.; Simpson, D. G.; Wnek, G. E. Macromolecules **2003**, 36, 3803-3805.

[73.] Kenawy, E.-R.; Abdel-Fattah, Y. R. Macromolecular Bioscience **2002**, 2, 261-266.

[74.] Taepaiboon, P.; Rungsardthong, U.; Supaphol, P. Nanotechnology **2006**, 17, 2317-2329.

[75.] Wang, F.J.; Yang, Y.Y.; Zhang, X.Z.; Zhu, X.; Chung, T.S.; Moochhala, S. Materials Science and Engineering C **2002**, 20, 93-100.

[76.] Zhou, H.Y.; Chen, X.G.; Liu, C.S.; Meng, X.H.; Liu, C.G.; Yu, L.J. Biochemical Engineering Journal **2006**, 31, 228-233.

[77.] Ma, D.; Mchuge, A.J. Journal of Membrane Science **2007**, 298, 156-168.

[78.] Morawetz, H. High Polymers, Vol. 21: Macromolecules in solution. 2nd Ed, **1975**.

[79.] Hager, B.L.; Berry, G.C. Journal of Polymer Science, Polymer Physics Edition **1982**, 20, 911-928

[80.] Flory, P.J. Principles of Polymer Chemistry, **1953**

[81.] Tanford, C. Physical Chemistry of Macromolecules, **1961**

[82.] Rai, P.; Rosen, S.L. Journal of Polymer Science, Part B: Polymer Physics **1997**, 35, 1985-1987

[83.] Adam, M.; Delsanti, M. Journal de Physique (Paris) **1982**, 43, 549-557

[84.] Adam, M.; Delsanti, M. Journal de Physique (Paris) **1983**, 44, 1185-1193

[85.] Takahashi, Y.; Isono, Y.; Noda, I.; Nagasawa, M. Macromolecules **1985**, 18, 1002-1008

[86.] Pearson, D.S. Rubber Chemistry and Technology **1987**, 60, 439-496

[87.] Colby, R.H.; Rubinstein, M. Macromolecules **1990**, 23, 2753-2757

[88.] Colby, R.H.; Fetters, L.J.; Funk, W.G.; Graessley, W.W. Macromolecules **1991**, 24, 3873-3882

[89.] Mozga, W. Physical properties of liquids.http://www.trimen.pl/witek/ciecze/liquids.html **2006**

[90.] Foster, A; Hempenstall, J; Tucker, I; Rades, T. International Journal of Pharmaceutical **2001**, 226, 147-161.

[91.] Jaeger, R.; Bergshoef, M.M.; Martin i Batlle, C.; Schoenherr, H.; Vansco, G.J. Macromolecular Symposium **1998**, 127, 141-150.

[92.] Venkatesh, S.; Hodgin, L.; Hanson, P.; Suryanarayanan, R. Journal of Control Release **1992**, 18, 13-18.

[93.] Ritger, P.L.; Peppas, N.A. Journal of Control Release **1987**, 5, 37-42.

[94.] Peppas, N.A.; Khare A.R. Advance Drug Delivery Review **1993**, 11, 1-35.

[95.] Verreck, G.; Chun, I.; Rosenblatt, J.; Peeters, J.; Van Dijck, A.; Mensch, J.; Noppe, M.; Brewster, M.E. Journal of Control Release **2003**, 92, 349-360.

APPENDICES

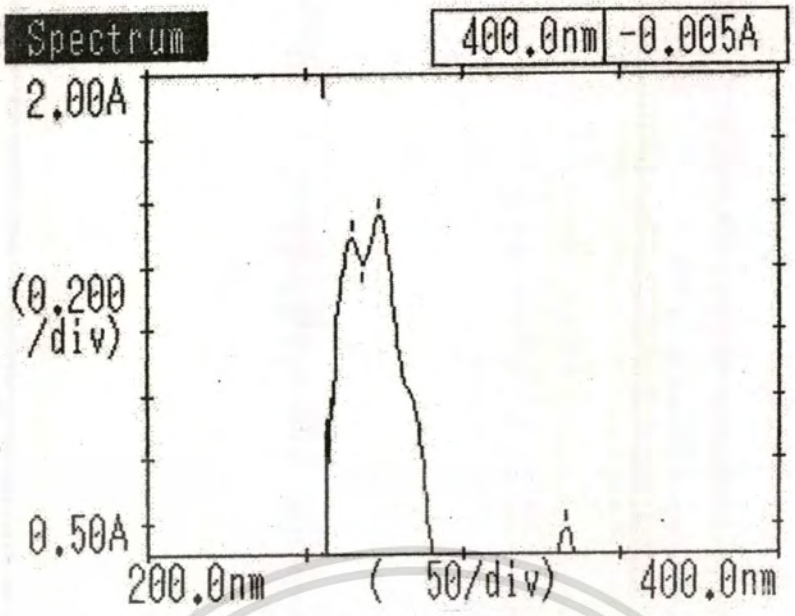

(a)

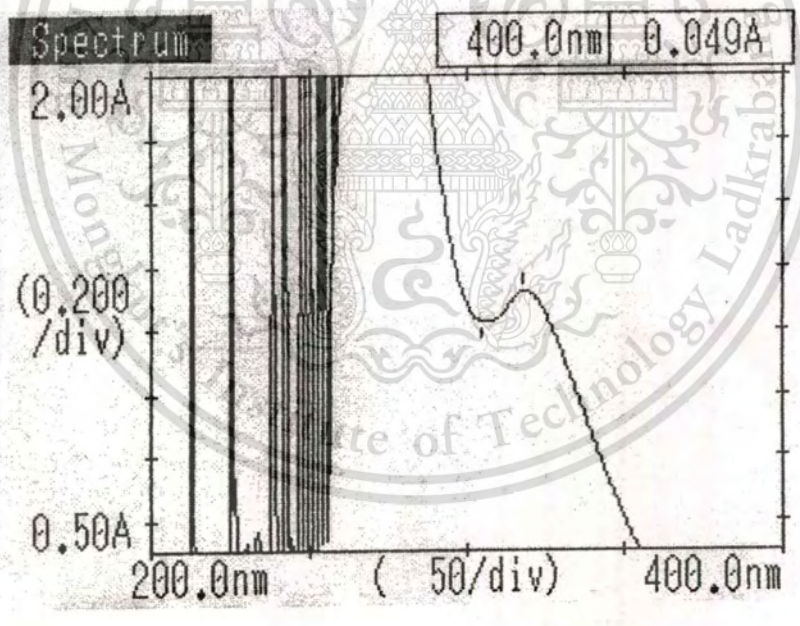

(b)

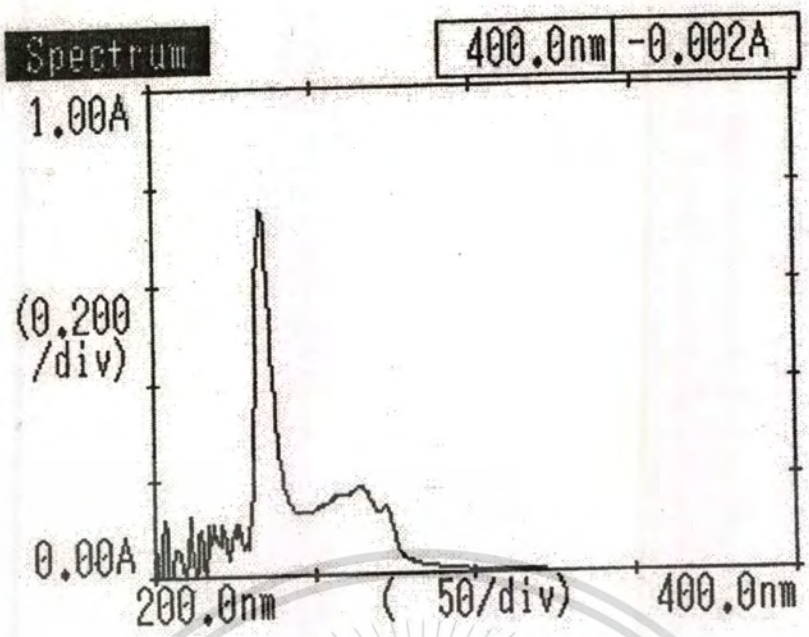

(c)

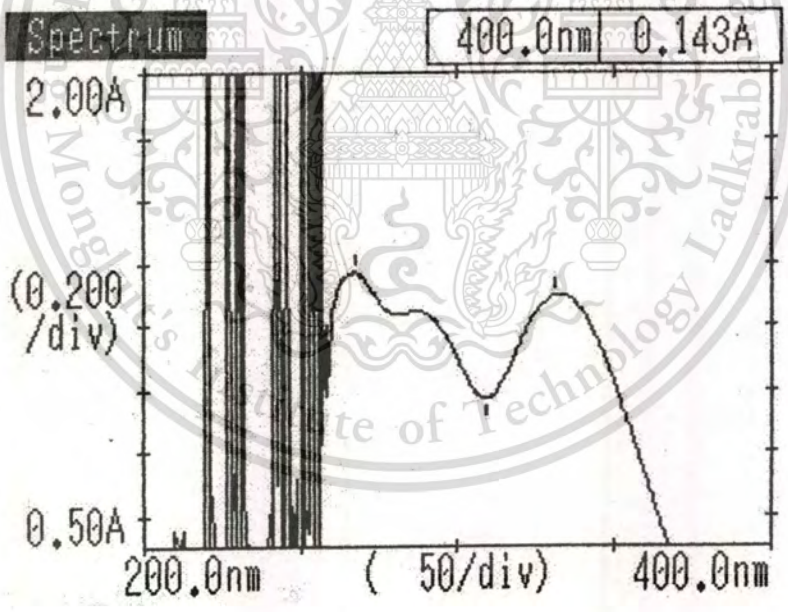

(d)

Appendix A UV-VIS spectra of (a) naproxen , (b) indomethacin, (c) ibuprofen , and (d) sulindac at a maximum absorbance peak (λ_{max}) at 274, 319, 232, and 327 nm, respectively.

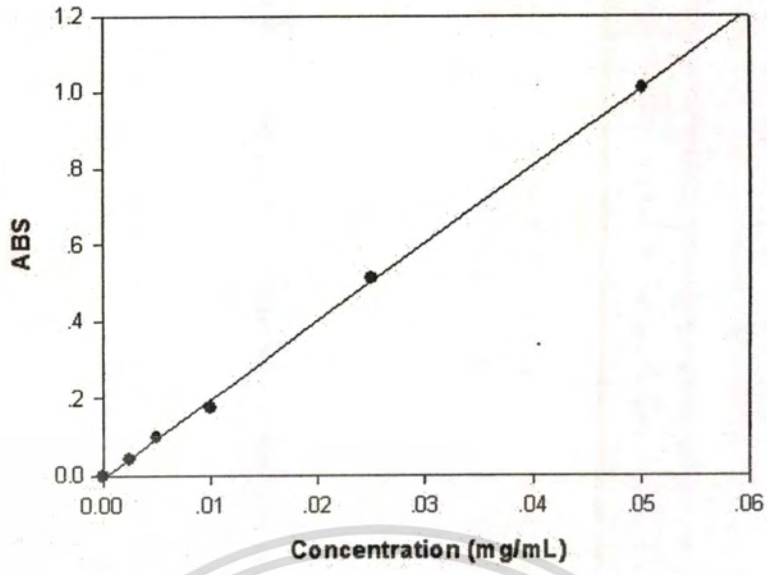

(a) NAP, ABS = 20.173C, $r^2 = 0.9987$

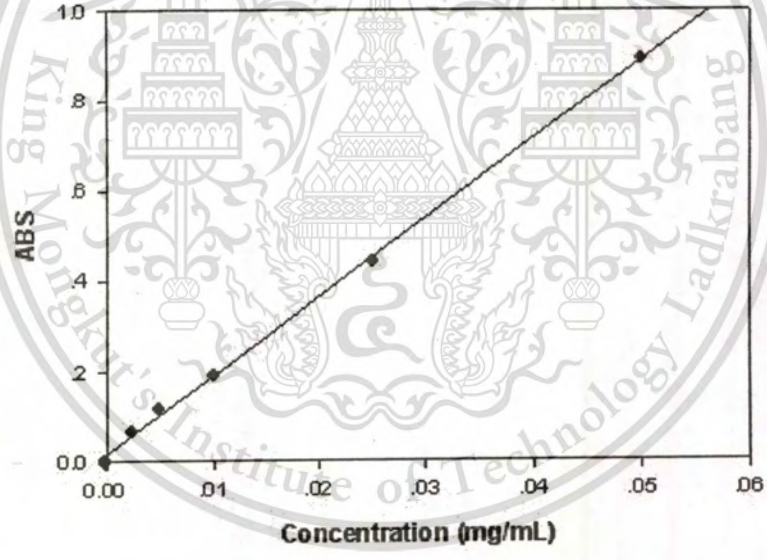

(b) IND, ABS = 17.917C, $r^2 = 0.9968$

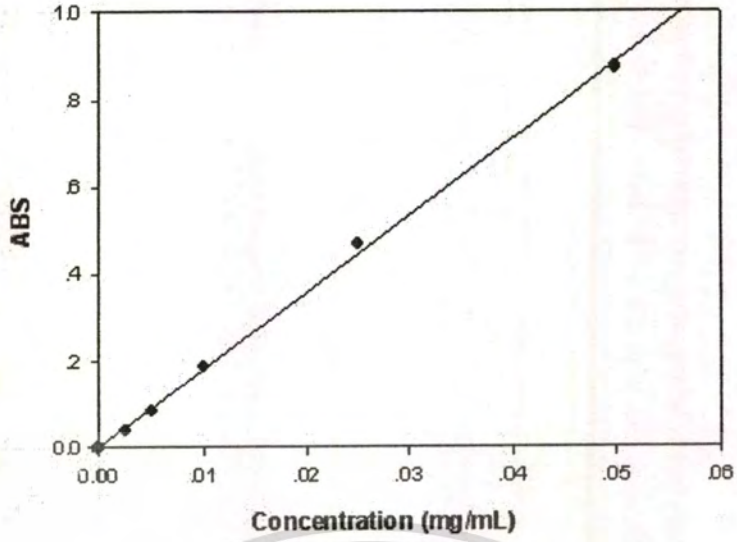

(c) IBU, ABS = 17.779C, $r^2 = 0.9981$

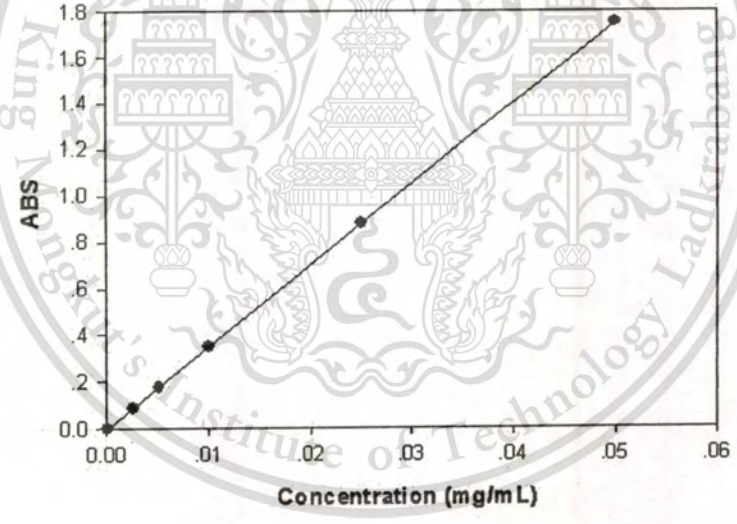

(d) SUL, ABS = 35.046C, $r^2 = 0.9996$

Appendix B The standard calibration plot of (a) naproxen (NAP), (b) indomethacin (IND), (c) ibuprofen (IBU), and (d) sulindac (SUL) in the concentration range of 0.0025-0.05 mg/mL.

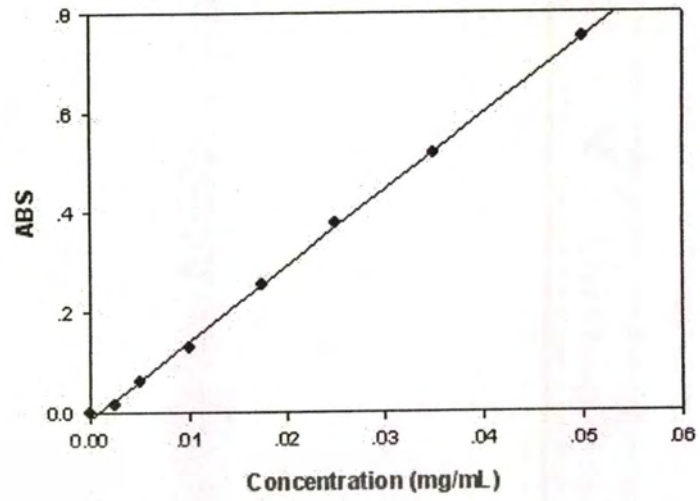

Appendix C The standard calibration plot of IND in the concentration range of 0.0025-0.05 mg/mL (for Part 3). The equation is ABS = 14.89C and $r^2 = 0.9981$.

Appendix D Cumulative release of NAP (%) from NAP-loaded electrospun CA fiber mats and NAP-loaded CA films by the total immersion technique

Time (min)	Cumulative release of NAP (%)									
	As-spun CA fiber mats					As-cast CA films				
	Test 1	Test 2	Test 3	Avg	SD	Test 1	Test 2	Test 3	Avg	SD
5	5.21	4.65	6.64	5.50	1.03	1.59	2.11	1.43	1.71	0.36
10	16.75	16.32	20.33	17.80	2.20	3.19	3.69	3.10	3.33	0.32
15	25.46	25.54	29.25	26.75	2.16	4.32	4.72	4.44	4.49	0.21
20	32.13	30.88	32.54	31.85	0.86	5.47	5.82	5.66	5.65	0.18
25	35.41	35.46	37.28	36.05	1.06	7.24	7.50	6.84	7.19	0.33
30	40.84	38.65	40.96	40.15	1.30	7.90	8.03	7.37	7.77	0.35
35	43.64	42.33	43.03	43.00	0.66	8.71	8.93	7.96	8.53	0.51
40	46.22	45.72	44.41	45.45	0.93	9.10	9.08	8.59	8.92	0.29
45	48.12	47.64	46.56	47.45	0.80	9.18	9.39	9.05	9.24	0.30
50	49.43	48.31	47.28	48.34	1.08	9.43	9.57	9.51	9.50	0.70
55	51.54	49.65	49.11	50.10	1.28	10.41	10.22	10.12	10.25	0.15
60	53.54	52.48	51.72	52.58	0.91	11.07	10.92	10.45	10.81	0.32
90	56.12	54.53	53.75	54.80	1.21	12.69	12.47	12.93	12.70	0.23
120	57.48	56.38	55.94	56.60	0.79	13.68	14.19	14.68	14.18	0.50
150	58.67	57.65	56.96	57.76	0.86	14.93	15.46	16.25	15.55	0.66
180	60.12	58.86	58.41	59.13	0.89	16.68	17.04	17.68	17.24	0.68
210	61.23	60.25	60.08	60.52	0.62	18.12	18.10	17.94	18.05	0.10
240	62.09	61.30	61.05	61.48	0.54	19.47	19.38	20.06	19.64	0.37
480	63.18	62.83	62.69	62.90	0.25	27.76	27.98	28.86	28.20	0.58
720	68.11	67.54	65.74	67.13	1.24	33.19	34.98	36.77	34.98	1.79
960	75.26	73.45	72.84	73.85	1.26	41.31	42.66	43.05	42.34	0.91
1200	86.47	84.29	83.49	84.75	1.54	47.33	47.97	47.83	47.71	0.34
1440	97.31	94.58	93.86	95.25	1.82	54.87	51.92	54.29	53.69	1.56

Appendix E Cumulative release of IND (%) from IND-loaded electrospun CA fiber mats and IND-loaded CA films by the total immersion technique

Time (min)	Cumulative release of IND (%)									
	As-spun CA fiber mats					As-cast CA films				
	Test 1	Test 2	Test 3	Avg	SD	Test 1	Test 2	Test 3	Avg	SD
5	1.7	3.2	2.5	2.47	0.75	0.39	0.31	0.32	0.34	0.04
10	3.1	5.2	7.7	5.33	2.30	0.65	0.45	0.43	0.51	0.12
15	6.7	9.8	8.9	8.47	1.59	1.34	0.83	0.66	0.94	0.35
20	9.0	10.1	12.5	10.53	1.79	1.75	1.08	0.90	1.24	0.45
25	12.4	15.4	13.7	13.83	1.50	1.81	1.23	1.17	1.40	0.35
30	13.6	19.5	17.4	16.83	3.00	2.27	1.46	1.54	1.76	0.45
35	18.1	21.4	18.0	19.17	1.93	2.89	1.68	1.90	2.16	0.64
40	19.8	21.6	19.4	20.27	1.17	3.00	1.90	2.89	2.60	0.61
45	23.0	22.6	21.4	22.33	0.83	3.65	2.62	3.11	3.13	0.52
50	23.2	24.2	24.3	23.90	0.61	4.12	2.81	3.36	3.43	0.66
55	23.4	25.2	24.6	24.40	0.92	4.20	2.91	3.70	3.60	0.65
60	24.8	26.4	28.4	26.53	1.80	4.40	3.36	4.04	3.93	0.53
90	32.4	36.0	33.3	33.90	1.87	6.12	5.01	5.58	5.57	0.56
120	37.6	39.0	38.8	38.47	0.76	7.63	6.59	7.57	7.26	0.58
150	43.1	44.4	41.8	43.10	1.30	8.25	7.75	8.45	8.15	0.36
180	47.0	44.8	43.9	45.23	1.59	9.21	9.06	9.21	9.16	0.09
210	47.6	46.0	46.3	46.63	0.85	10.38	9.84	9.93	10.05	0.29
240	50.8	48.0	47.3	48.70	1.85	10.58	10.12	10.29	10.33	0.23
480	57.6	53.7	57.3	56.20	2.17	13.39	13.20	14.02	13.54	0.43
720	62.0	65.2	63.4	63.53	1.60	15.49	15.60	15.92	15.67	0.22
960	67.7	71.0	68	68.90	1.82	17.16	16.79	17.39	17.11	0.30
1200	70.9	75.9	74.1	73.63	2.53	18.92	18.66	19.89	19.16	0.65
1440	77.5	83.0	76.4	78.97	3.53	21.74	22.29	22.75	22.26	0.51

Appendix F Cumulative release of IBU (%) from IBU-loaded electrospun CA fiber mats and IBU-loaded CA films by the total immersion technique

Time (min)	Cumulative release of IBU (%)									
	As-spun CA fiber mats					As-cast CA films				
	Test 1	Test 2	Test 3	Avg	SD	Test 1	Test 2	Test 3	Avg	SD
5	9.01	4.20	5.76	6.32	2.45	1.37	1.77	1.61	1.58	0.20
10	12.02	14.92	13.40	13.45	1.45	3.77	4.83	4.12	4.24	0.54
15	15.73	15.42	14.66	15.27	0.55	5.54	5.23	4.87	5.21	0.34
20	16.68	17.60	15.95	16.74	0.83	6.09	6.43	5.97	6.16	0.24
25	17.56	18.21	16.87	17.55	0.67	6.51	6.93	6.08	6.51	0.43
30	18.36	18.59	17.40	18.12	0.63	7.01	7.49	6.80	7.10	0.35
35	18.97	19.05	17.79	18.60	0.71	7.26	7.74	6.93	7.31	0.41
40	19.81	19.43	18.17	19.14	0.86	7.38	8.11	7.19	7.56	0.49
45	20.57	19.70	18.40	19.56	1.09	7.59	8.36	7.35	7.77	0.53
50	20.95	19.96	18.66	19.86	1.15	7.89	9.46	7.63	8.33	0.99
55	21.26	20.00	19.31	20.19	0.99	8.19	9.92	8.45	8.85	0.93
60	21.37	20.15	19.54	20.35	0.93	8.25	10.13	8.72	9.03	0.98
90	22.33	20.95	20.61	21.30	0.91	10.18	12.06	11.04	11.09	0.94
120	23.02	21.64	20.95	21.87	1.05	13.19	13.80	13.11	13.37	0.38
150	23.59	22.10	22.79	22.83	0.75	14.99	16.75	16.27	16.00	0.91
180	24.08	22.60	23.44	23.37	0.74	17.55	18.58	17.90	18.01	0.52
210	24.50	23.24	24.31	24.02	0.68	19.36	19.86	19.03	19.42	0.42
240	25.34	24.01	25.53	24.96	0.83	19.96	21.59	20.15	20.57	0.89
480	38.82	39.77	38.13	38.91	0.82	28.33	29.60	29.45	29.13	0.69
720	48.93	52.56	49.89	50.46	1.88	30.11	32.04	31.74	31.30	1.04
960	58.02	60.34	56.91	58.42	1.75	33.41	34.29	33.92	33.87	0.44
1200	68.28	69.81	66.64	68.24	1.59	35.96	36.47	36.20	36.21	0.26
1440	77.90	86.11	80.42	81.48	4.21	38.90	38.79	38.10	38.60	0.43

Appendix G Cumulative release of SUL (%) from SUL-loaded electrospun CA fiber mats and SUL-loaded CA films by the total immersion technique

Time (min)	Cumulative release of SUL (%)									
	As-spun CA fiber mats					As-cast CA films				
	Test 1	Test 2	Test 3	Avg	SD	Test 1	Test 2	Test 3	Avg	SD
5	4.2	3.6	4.2	4.00	0.35	0.48	0.55	0.62	0.55	0.07
10	14.4	8.7	7.9	10.33	3.54	1.23	1.23	1.32	1.26	0.05
15	19.6	12.5	12.3	14.80	4.16	1.75	1.73	1.49	1.66	0.14
20	21.4	16.3	17.4	18.37	2.68	1.86	1.96	1.89	1.90	0.05
25	26.5	18.7	21.7	22.30	3.93	2.01	2.30	2.05	2.12	0.16
30	27.2	24.4	23.8	25.13	1.81	2.10	2.47	2.26	2.28	0.19
35	29.0	27.7	28.1	28.27	0.67	2.25	2.62	2.38	2.42	0.19
40	32.8	29.9	29.2	30.63	1.91	2.40	2.67	2.53	2.53	0.14
45	33.9	33.1	32.4	33.13	0.75	2.49	2.71	2.59	2.60	0.11
50	34.9	34.7	34.8	34.80	0.10	2.55	2.85	2.92	2.77	0.20
55	37.1	36.4	37.5	37.00	0.56	2.66	2.99	3.00	2.88	0.19
60	37.4	38.0	38.4	37.93	0.50	3.05	3.11	3.15	3.10	0.05
90	42.5	43.1	42.2	42.60	0.46	3.68	3.82	3.75	3.75	0.07
120	43.5	45.2	45.0	44.57	0.93	3.78	3.85	3.92	3.85	0.05
150	44.5	46.1	45.7	45.43	0.83	4.44	4.27	4.25	4.32	0.10
180	45.8	46.3	46.2	46.10	0.26	4.79	4.62	4.53	4.65	0.13
210	46.4	46.6	47.3	46.77	0.47	5.26	5.32	5.22	5.27	0.05
240	47.2	48.8	49.6	48.53	1.22	7.29	6.67	6.90	6.95	0.31
480	49.4	52.0	57.2	52.87	3.97	8.64	8.26	8.49	8.46	0.19
720	54.6	56.1	63.7	58.13	4.88	11.58	10.92	11.25	11.25	0.33
960	62.0	62.9	71.2	65.37	5.07	13.90	13.53	13.58	13.67	0.20
1200	68.1	67.6	77.9	71.2	5.80	17.68	16.14	16.89	16.90	0.77
1440	76.7	74.0	83.0	77.90	4.62	19.89	18.53	19.77	19.40	0.75

Appendix H Cumulative release of IND (%) from IND-loaded electrospun CA fiber mats by the total immersion technique with and without the addition of fresh medium

Time (min)	Cumulative release of IND (%)									
	Added buffer					No added buffer				
	Test 1	Test 2	Test 3	Avg	SD	Test 1	Test 2	Test 3	Avg	SD
5	4.42	5.73	5.34	5.16	0.67	2.65	2.89	4.07	3.20	0.76
10	6.46	8.11	7.62	7.39	0.83	6.13	4.95	5.83	5.64	0.61
15	10.05	11.55	11.17	10.92	0.78	7.94	7.30	7.06	7.43	0.45
20	13.06	16.94	14.71	14.90	1.95	8.48	8.73	7.99	8.40	0.38
25	15.97	18.83	17.48	17.43	1.43	13.63	10.15	10.00	11.26	2.05
30	18.45	20.68	19.95	19.69	1.14	14.56	13.09	12.21	13.29	1.19
35	19.81	22.43	23.06	21.77	1.72	16.08	14.85	15.25	15.39	0.63
40	22.23	25.00	25.92	24.38	1.92	17.65	17.21	16.32	17.06	0.68
45	25.58	27.91	28.74	27.41	1.64	18.63	20.64	19.22	19.50	1.03
50	27.77	30.53	31.12	29.81	1.79	20.34	21.18	19.85	20.46	0.67
55	30.15	32.62	32.52	31.76	1.40	20.83	22.94	21.57	21.78	1.07
60	32.38	33.98	33.79	33.38	0.87	21.91	23.28	21.72	22.30	0.85
90	35.24	37.33	37.86	36.81	1.39	28.97	29.12	26.86	28.32	1.26
120	36.89	38.11	38.83	37.94	0.98	33.09	35.05	31.52	33.22	1.77
150	38.45	39.37	40.24	39.35	0.89	37.25	37.89	35.20	36.78	1.41
180	39.22	40.19	40.83	40.08	0.81	39.71	41.08	39.36	40.05	0.91
210	40.15	41.12	41.50	40.92	0.69	41.62	42.79	41.18	41.86	0.83
240	41.84	43.88	44.71	43.48	1.48	42.01	45.10	46.47	44.53	2.28
480	48.88	50.92	51.44	50.41	1.35	46.57	48.48	49.51	48.19	1.49
720	54.41	56.46	57.96	56.28	1.78	51.47	52.21	53.53	52.40	1.04
960	60.85	63.72	65.88	63.48	2.52	56.67	57.70	58.09	57.49	0.73
1200	66.70	68.74	70.57	68.67	1.94	60.69	62.25	63.14	62.03	1.24
1440	72.82	75.53	76.36	74.90	1.85	63.73	65.20	66.27	65.07	1.28

Appendix I Cumulative release of IND (%) from IND-loaded electrospun CA fiber mats by the total immersion technique with sequential dipping in fresh medium

Immersion Time (min)	Cumulative release of IND (%)				
	Test 1	Test 2	Test 3	Avg	SD
10	11.27	10.29	10.15	10.57	0.61
20	19.95	19.65	18.63	19.41	0.69
30	26.62	25.63	25.59	25.95	0.58
40	31.52	30.09	30.69	30.77	0.72
50	35.59	33.96	34.17	34.58	0.89
60	39.27	37.34	37.16	37.93	1.17
70	42.51	39.99	39.61	40.71	1.58
80	45.26	42.24	41.62	43.05	1.95
90	47.61	44.15	43.38	45.06	2.25
100	49.57	45.77	44.85	46.74	2.50
110	51.14	47.01	46.03	48.07	2.71
120	52.41	47.98	46.96	49.13	2.90
130	53.44	48.72	47.6	49.93	3.10
140	54.18	49.21	47.94	50.45	3.30
150	54.67	49.51	48.09	50.76	3.46
160	54.92	49.66	-	50.96	3.72

Appendix J Fractional release of drug (M_t/M_∞) plotted as a function of the square root of time for naproxen release

Time ($min^{1/2}$)	Fractional release of NAP (M_t/M_∞)									
	As-spun CA fiber mats					As-cast CA films				
	Test 1	Test 2	Test 3	Avg	SD	Test 1	Test 2	Test 3	Avg	SD
2.24	0.054	0.049	0.071	0.058	0.012	0.029	0.041	0.026	0.032	0.008
3.16	0.172	0.173	0.217	0.187	0.026	0.058	0.071	0.057	0.062	0.008
3.87	0.262	0.270	0.312	0.281	0.027	0.079	0.091	0.082	0.084	0.006
4.47	0.330	0.326	0.347	0.334	0.011	0.100	0.112	0.104	0.105	0.006
5.00	0.364	0.375	0.397	0.378	0.017	0.132	0.144	0.126	0.134	0.009
5.48	0.420	0.409	0.436	0.422	0.014	0.144	0.155	0.136	0.145	0.010
5.92	0.448	0.448	0.458	0.451	0.006	0.159	0.172	0.147	0.159	0.013
6.32	0.475	0.483	0.473	0.477	0.005	0.166	0.175	0.158	0.166	0.009
6.71	0.495	0.504	0.496	0.498	0.005	0.167	0.181	0.167	0.172	0.008
7.07	0.508	0.511	0.504	0.508	0.004	0.172	0.184	0.175	0.177	0.006
7.42	0.530	0.525	0.523	0.526	0.004	0.190	0.197	0.186	0.191	0.006
7.75	0.550	0.555	0.551	0.552	0.003	0.202	0.210	0.192	0.201	0.009
9.49	0.577	0.577	0.573	0.575	0.002	0.231	0.240	0.238	0.236	0.005
10.95	0.591	0.596	0.596	0.594	0.003	0.249	0.273	0.270	0.264	0.013
12.25	0.603	0.610	0.607	0.606	0.004	0.272	0.298	0.300	0.290	0.016
13.42	0.618	0.622	0.622	0.621	0.002	0.304	0.328	0.326	0.319	0.013

Appendix K Fractional release of drug (M_t/M_∞) plotted as a function of the square root of time for indomethacin release

Time ($min^{1/2}$)	Fractional release of IND (M_t/M_∞)									
	As-spun CA fiber mats					As-cast CA films				
	Test 1	Test 2	Test 3	Avg	SD	Test 1	Test 2	Test 3	Avg	SD
2.24	0.022	0.039	0.033	0.031	0.009	0.018	0.014	0.014	0.015	0.002
3.16	0.040	0.063	0.101	0.068	0.031	0.030	0.020	0.019	0.023	0.006
3.87	0.086	0.180	0.116	0.107	0.018	0.062	0.037	0.029	0.043	0.017
4.47	0.116	0.122	0.164	0.134	0.026	0.080	0.048	0.040	0.056	0.021
5.00	0.160	0.186	0.179	0.175	0.013	0.083	0.055	0.051	0.063	0.017
5.48	0.175	0.235	0.228	0.213	0.033	0.104	0.066	0.068	0.079	0.007
5.92	0.234	0.258	0.236	0.243	0.013	0.133	0.075	0.084	0.097	0.011
6.32	0.255	0.260	0.254	0.256	0.003	0.138	0.085	0.127	0.117	0.028
6.71	0.297	0.272	0.280	0.283	0.013	0.168	0.118	0.137	0.141	0.025
7.07	0.300	0.292	0.318	0.303	0.013	0.190	0.126	0.148	0.155	0.033
7.42	0.302	0.304	0.322	0.309	0.011	0.193	0.131	0.163	0.162	0.031
7.75	0.320	0.318	0.372	0.337	0.031	0.202	0.151	0.178	0.177	0.026
9.49	0.418	0.434	0.436	0.429	0.010	0.282	0.225	0.245	0.251	0.029
10.95	0.485	0.470	0.508	0.488	0.019	0.351	0.296	0.333	0.327	0.028
12.25	0.556	0.535	0.547	0.546	0.011	0.379	0.348	0.371	0.366	0.016
13.42	0.606	0.540	0.574	0.573	0.033	0.424	0.406	0.405	0.412	0.011

Appendix L Fractional release of drug (M_t/M_∞) plotted as a function of the square root of time for ibuprofen release

Time ($min^{1/2}$)	Fractional release of IBU (M_t/M_∞)									
	As-spun CA fiber mats					As-cast CA films				
	Test 1	Test 2	Test 3	Avg	SD	Test 1	Test 2	Test 3	Avg	SD
2.24	0.116	0.049	0.072	0.079	0.034	0.035	0.046	0.042	0.041	0.006
3.16	0.154	0.173	0.167	0.165	0.010	0.097	0.125	0.108	0.110	0.014
3.87	0.202	0.179	0.182	0.188	0.013	0.142	0.135	0.128	0.135	0.007
4.47	0.214	0.204	0.198	0.205	0.008	0.157	0.166	0.157	0.160	0.005
5.00	0.225	0.211	0.210	0.215	0.008	0.167	0.179	0.160	0.169	0.010
5.48	0.236	0.216	0.216	0.223	0.012	0.180	0.193	0.178	0.184	0.008
5.92	0.244	0.221	0.221	0.229	0.013	0.187	0.199	0.182	0.189	0.009
6.32	0.254	0.226	0.226	0.235	0.016	0.190	0.209	0.189	0.196	0.011
6.71	0.264	0.229	0.229	0.241	0.020	0.195	0.216	0.193	0.201	0.013
7.07	0.269	0.232	0.232	0.244	0.021	0.203	0.244	0.200	0.216	0.025
7.42	0.273	0.232	0.240	0.248	0.022	0.211	0.256	0.222	0.230	0.018
7.75	0.274	0.234	0.243	0.250	0.021	0.212	0.261	0.229	0.234	0.025
9.49	0.287	0.243	0.256	0.262	0.023	0.262	0.311	0.290	0.288	0.025
10.95	0.296	0.251	0.261	0.269	0.024	0.339	0.356	0.344	0.346	0.009
12.25	0.303	0.257	0.283	0.281	0.023	0.385	0.432	0.427	0.415	0.026
13.42	0.309	0.262	0.291	0.287	0.024	0.451	0.479	0.470	0.467	0.014

Appendix M Fractional release of drug (M_t/M_∞) plotted as a function of the square root of time for sulindac release

Time ($min^{1/2}$)	Fractional release of SUL (M_t/M_∞)									
	As-spun CA fiber mats					As-cast CA films				
	Test 1	Test 2	Test 3	Avg	SD	Test 1	Test 2	Test 3	Avg	SD
2.24	0.055	0.049	0.051	0.052	0.003	0.024	0.030	0.031	0.028	0.004
3.16	0.188	0.118	0.095	0.133	0.048	0.062	0.066	0.067	0.065	0.003
3.87	0.256	0.169	0.148	0.190	0.057	0.088	0.093	0.075	0.085	0.009
4.47	0.279	0.220	0.210	0.236	0.037	0.094	0.106	0.096	0.099	0.006
5.00	0.346	0.253	0.261	0.286	0.052	0.101	0.124	0.104	0.110	0.013
5.48	0.355	0.330	0.287	0.323	0.034	0.106	0.133	0.114	0.118	0.014
5.92	0.378	0.374	0.339	0.363	0.021	0.113	0.141	0.120	0.125	0.015
6.32	0.428	0.404	0.352	0.393	0.039	0.121	0.144	0.128	0.130	0.012
6.71	0.442	0.447	0.390	0.425	0.032	0.125	0.146	0.131	0.134	0.011
7.07	0.455	0.469	0.419	0.447	0.026	0.128	0.154	0.148	0.143	0.014
7.42	0.484	0.492	0.452	0.475	0.021	0.134	0.161	0.152	0.148	0.014
7.75	0.488	0.514	0.463	0.487	0.026	0.153	0.168	0.159	0.160	0.008
9.49	0.554	0.582	0.508	0.547	0.037	0.185	0.206	0.190	0.193	0.011
10.95	0.567	0.611	0.542	0.572	0.035	0.190	0.208	0.198	0.198	0.009
12.25	0.580	0.623	0.551	0.585	0.036	0.223	0.230	0.215	0.223	0.008
13.42	0.597	0.626	0.557	0.593	0.035	0.264	0.250	0.230	0.240	0.010

Appendix N Fractional release of drug (M_t/M_∞) plotted as a function of the square root of time for IND release with and without the addition of fresh medium

Time ($min^{1/2}$)	Fractional release of IND (M_t/M_∞)									
	Added buffer					No added buffer				
	Test 1	Test 2	Test 3	Avg	SD	Test 1	Test 2	Test 3	Avg	SD
2.24	0.061	0.076	0.070	0.069	0.008	0.042	0.044	0.061	0.049	0.010
3.16	0.089	0.107	0.100	0.099	0.009	0.096	0.076	0.088	0.087	0.010
3.87	0.138	0.153	0.146	0.146	0.008	0.125	0.112	0.107	0.115	0.009
4.47	0.179	0.224	0.193	0.199	0.023	0.133	0.133	0.121	0.129	0.007
5.00	0.219	0.249	0.229	0.232	0.015	0.214	0.156	0.151	0.174	0.035
5.48	0.253	0.274	0.261	0.263	0.011	0.228	0.201	0.184	0.204	0.022
5.92	0.272	0.297	0.302	0.290	0.016	0.252	0.228	0.230	0.237	0.013
6.32	0.305	0.331	0.339	0.325	0.018	0.277	0.264	0.246	0.262	0.016
6.71	0.351	0.370	0.376	0.366	0.013	0.292	0.317	0.290	0.300	0.015
7.07	0.381	0.404	0.408	0.398	0.015	0.319	0.325	0.300	0.315	0.013
7.42	0.414	0.432	0.426	0.424	0.009	0.327	0.352	0.325	0.335	0.015
7.75	0.445	0.450	0.443	0.446	0.004	0.344	0.357	0.328	0.343	0.015
9.49	0.484	0.494	0.496	0.491	0.006	0.455	0.447	0.405	0.436	0.027
10.95	0.507	0.505	0.509	0.507	0.002	0.519	0.538	0.476	0.511	0.032
12.25	0.528	0.521	0.527	0.525	0.004	0.584	0.581	0.531	0.565	0.030
13.42	0.539	0.532	0.535	0.535	0.004	0.623	0.630	0.594	0.616	0.019

Appendix O Fractional release of drug (M_t/M_∞) plotted as a function of the square root of time for IND release with sequential dipping in fresh medium

Time ($min^{1/2}$)	Fractional release of IND (M_t/M_∞)				
	Test 1	Test 2	Test 3	Avg	SD
3.16	0.205	0.207	0.211	0.208	0.003
4.47	0.363	0.396	0.387	0.382	0.017
5.48	0.485	0.516	0.532	0.511	0.024
6.32	0.574	0.606	0.638	0.606	0.032
7.07	0.648	0.684	0.711	0.681	0.032

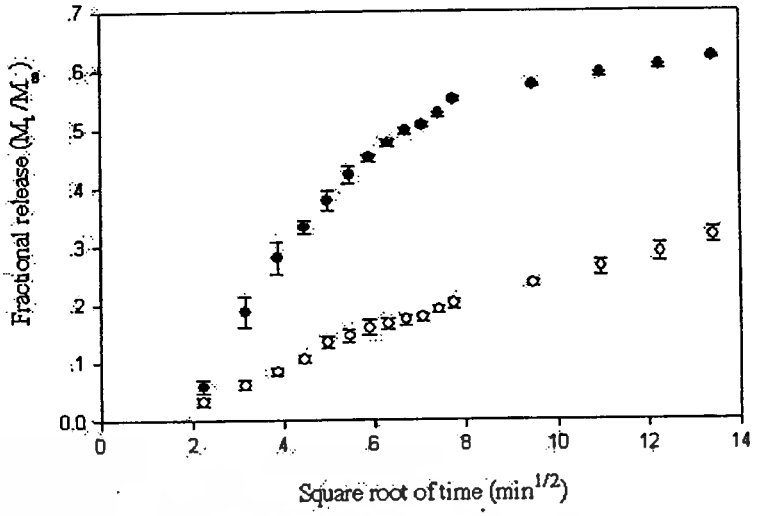

(a)

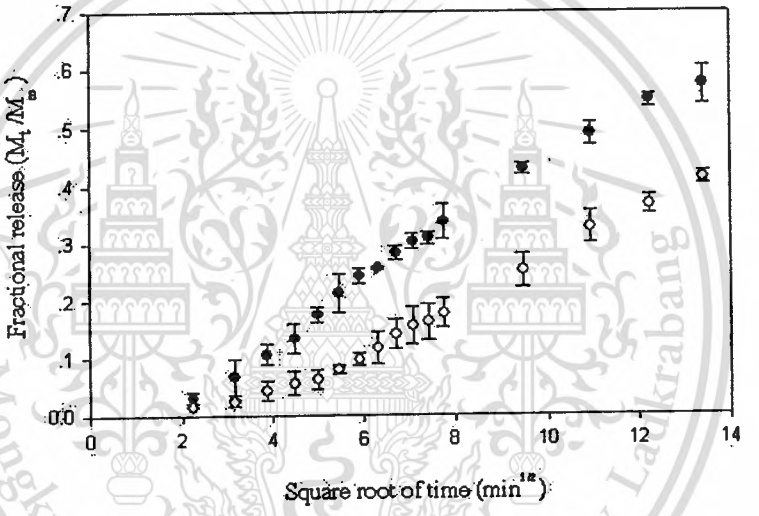

(b)

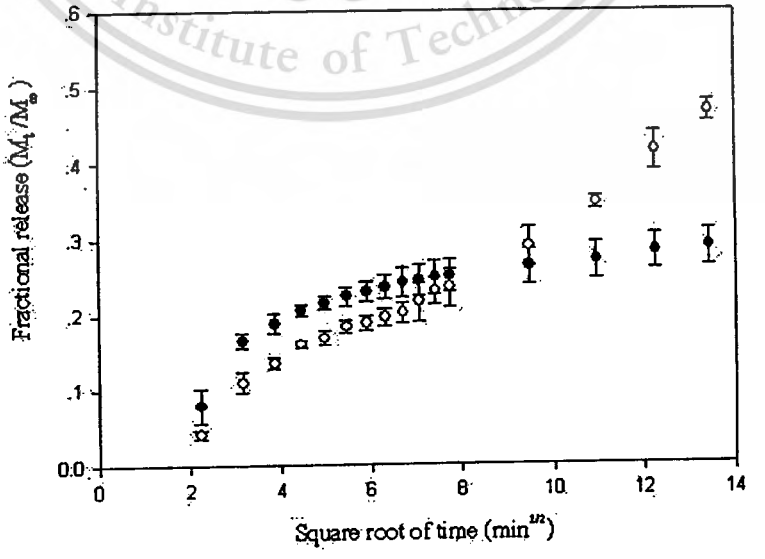

(c)

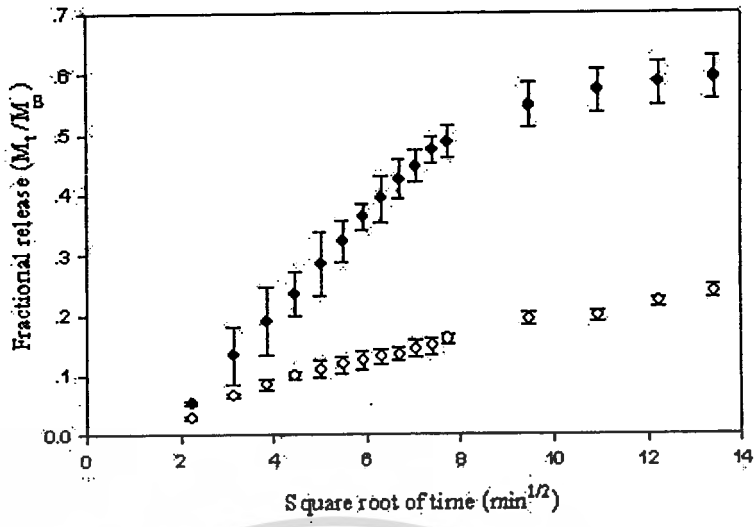

(d)

Appendix P Fractional release profiles of drug (M_t/M_∞) plotted as a function of the square root of time from (a) NAP, (b) IND, (c) IBU, and (d) SUL (● for drug-loaded electrospun CA fiber mats, o for drug-loaded as-cast CA films) during 0-180 min

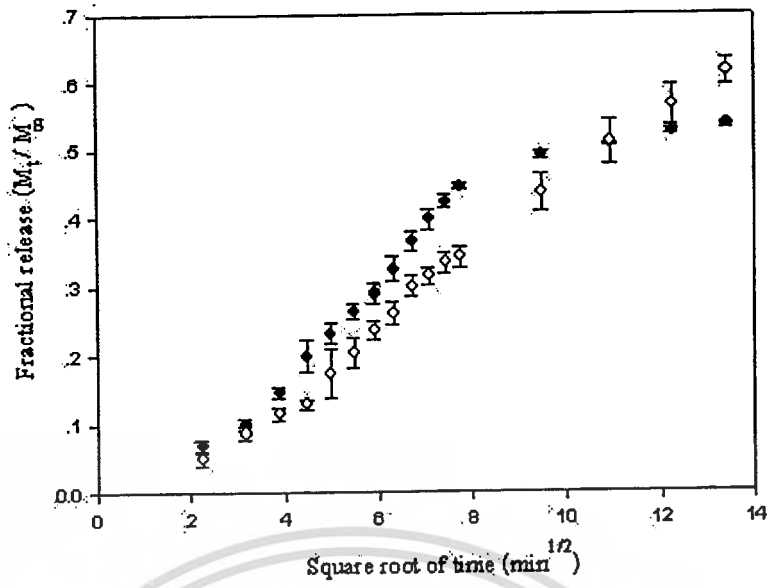

(a)

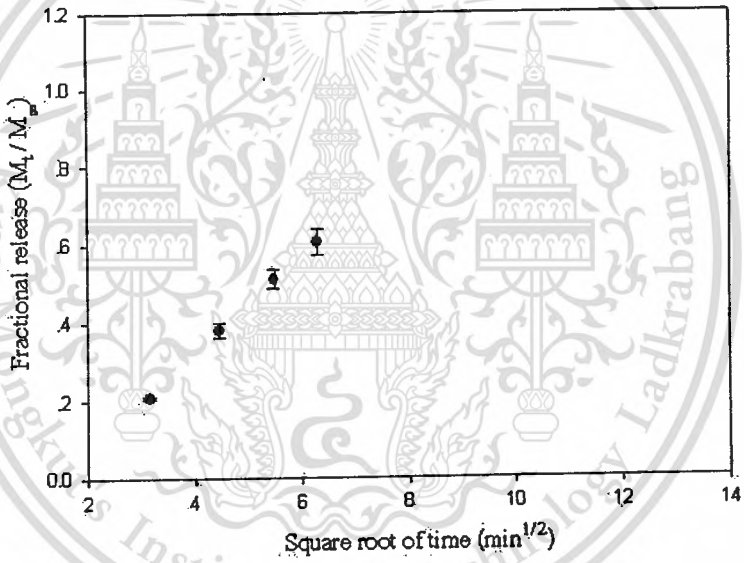

(b)

Appendix Q Fractional release profiles of drug (M_t/M_∞) plotted as a function of the square root of time for (a) with and without the addition of fresh buffer and (b) with sequential dipping in fresh medium

AUTHOR BIOGRAPHY

Name: Mr. Santi Tungprapa

Date of Birth: November 10, 1974

Nationality: Thai

University Education:

1993-1996 Bachelor Degree of Chemistry, Faculty of Science, Chulalongkorn University, Bangkok, Thailand

1997-1999 Master Degree of Organic Chemistry, Faculty of Science, Chulalongkorn University, Bangkok, Thailand

Publications :

1. Tungprapa, S., Jangchud, I., Supaphol, P., and Meechaisue, C. Electrospun methacrylate-based copolymer fibers: effect of mixed-solvent system on morphology appearance of as-spun fibers, in preparation.
2. Tungprapa, S., Weerasombut, M., Puangparn, T., Jangchud, I., Fakum, P., Semongkhol, S., Meechaisue, C., and Supaphol, P. (2007) Electrospun cellulose acetate fibers: effect of solvent system on morphology and fiber diameter. Cellulose, 14(6), 563-575.
3. Tungprapa, S., Jangchud, I., and Supaphol, P. (2007) Release characteristics of four model drugs from drug-loaded electrospun cellulose acetate fiber mats. Polymer, 48(17), 5030-5041.
4. Tungprapa, S., Jangchud, I., Ngamdee, P., Rutnakornpituk, M., and Supaphol, P. (2006) Ultrafine electrospun poly(ethylene glycol) – polydimethylsiloxane - poly(ethylene glycol) triblock copolymer / poly(ethylene oxide) blend fibers. Materials Letters, 60(24), 2920-2924.

Presentation:

1. Tungprapa, S., Jangchud, I., and Supaphol, P. (2006, November 7-10) Release characteristics of four model drugs from drug-loaded electrospun cellulose acetate fiber mats. Paper presented at The Sixth Asian BioCeramics Symposium, Bangkok, Thailand.